RI 9049

Bureau of Mines Report of Investigations/1987

Fracture Geometries in Three Ore Bodies Mined by Undercut Caving as Determined From Oriented Drill Core and Scanline Mapping

By Louis A. Panek and Michael T. Melvin

UNITED STATES DEPARTMENT OF THE INTERIOR

Report of Investigations 9049

Fracture Geometries in Three Ore Bodies Mined by Undercut Caving as Determined From Oriented Drill Core and Scanline Mapping

By Louis A. Panek and Michael T. Melvin

UNITED STATES DEPARTMENT OF THE INTERIOR
William P. Clark, Secretary

BUREAU OF MINES
Donald Paul Hodel, Secretary

Library of Congress Cataloging-in-Publication Data

Panek, Louis Anthony, 1919–
Fracture geometries in three ore bodies mined by undercut caving as determined from oriented drill core and scanline mapping.

(Report of investigations; 9049)

Bibliography: p. 82.

Supt. of Docs. no.: I 28.23:9049.

1. Rock deformation–Arizona. 2. Rock deformation–Colorado. 3. Ore-deposits–Arizona. 4. Ore-deposits–Colorado. 5. Mining engineering–Arizona. 6. Mining engineering–Colorado. I. Melvin, Michael T. II. Title. III. Series: Reports of investigations (United States. Bureau of Mines); 9049.

TN23.U43 [QE604] 622 s [551.8] 86-600180

CONTENTS

ILLUSTRATIONS

ILLUSTRATIONS—Continued

TABLES

UNIT OF MEASURE ABBREVIATIONS USED IN THIS REPORT

ft	foot	pct	percent
in	inch	psi	pound (force) per square inch
lb	pound		

FRACTURE GEOMETRIES IN THREE ORE BODIES MINED BY UNDERCUT CAVING AS DETERMINED FROM ORIENTED DRILL CORE AND SCANLINE MAPPING

By Louis A. Panek[1] and Michael T. Melvin[2]

ABSTRACT

Block caving, a low-cost method of mining large low-grade deposits, has the potential for application to a larger class of mineral deposits than has been attempted heretofore, provided that quantitative methods can be developed to predict the span required to induce caving and the size distribution of the caved fragments. Prerequisite to employing a numerical method of structural analysis to evaluate the stability or failure of the rock mass in the vicinity of an excavation are the specifications of rock mass strength and fracturing (jointing). This Bureau of Mines report characterizes the fracturing geometries in three ore bodies that are mined by undercut-cave methods, utilizing data that were generated by measurements on oriented diamond drill cores and along multiple scanlines on underground exposures. Procedures employed for data acquisition and for data analysis are described in detail. Numerous polar equal-area plots of fracture orientation and histograms of fracture spacing, obtained by Bureau-developed codes FRACTAN and GDIST, are presented. Fracture-trace-length estimates are derived from the multiple-scanline mapping measurements, a new procedure.

[1]Mining engineer, Denver Research Center, Bureau of Mines, Denver, CO (retired) currently J. S. Westwater professor of Mining Engineering, Michigan Technological University, Houghton, MI.

[2]Mathematical statistician, Denver Research Center, Bureau of Mines, Denver, CO (now with Minerals Management Service, U.S. Department of the Interior, Denver, CO).

INTRODUCTION

The stability of an excavation in a rock mass may be analyzed as a function of the strength characteristics of the intact rock and the rock mass defects. The defects may be the more or less planar separations parallel to the stratification in sedimentary rocks, or fracture cleavage, or the joints and faults that are found in igneous rock bodies. Rock mass defects are commonly observed to be systematic in that they tend to parallel two or three well-defined orientations. Some stability analyses have therefore treated the rock mass as a stack of prisms completely separated by joints (*23*);[3] others have analyzed a failure surface that passes partly through intact material and partly along joint surfaces (*21*).

A comprehensive approach to analyzing the stability of open pit slopes, taking account of the natural statistical variability of the rock mass structural parameters, including the jointing, was recently developed under a Bureau of Mines contract (*9-16*).

Many structural analyses have been published that take into account some aspect of the jointing in a hypothetical rock mass, but few of them have presented a quantitative characterization of an actual rock body. Stability analyses too often incorporate the implicit assumption that rock jointing characteristics observed in the more competent rocks that are typically penetrated by water and highway tunnels are also representative of mineral deposits. If we are to develop capability to account for the influence of rock fractures in structural analyses of mine excavations, we need to specify the geometry of fracturing as actually observed in some representative mineral deposits so that analyses may incorporate realistic fracture geometries rather than grossly inaccurate, hypothetical characteristics.

A limited effort is made at many metal mines to collect rock jointing data. The time available for such work is very limited for the practical reason that very limited direct use has been found for the data. Practical applications for rock fracture data require that correlations be established between rock fracturing parameters and rock mass strength and fragmentation parameters, which can be derived only from a systematically established data base.

Block caving is a low-cost, high-volume method of extracting large, deep, economically marginal mineral deposits. The present report summarizes part of an investigation that is aimed at developing a rationale for predicting quantitatively the cavability characteristics of a mineral deposit prior to mining, so that the undercut-cave method may be extended to a much wider range of physical characteristics than has been heretofore attempted. An overview of the entire investigation was recently published (*27*).

The rock mass fracture system is also a significant consideration with respect to the extraction of metals by in-place leaching of an ore deposit, since the permeability of the ore body is a function of the attitude, spacing, and extent of the preexisting fractures.

[3]Italic numbers in parentheses refer to items in the list of references preceding the appendix at the end of this report.

The ultimate objectives of the present analysis of rock mass fracturing are to predict the minimum open span required for sustained caving and the size distribution of the caved ore fragments, which are expected to be functions also of various strength parameters. An intermediate objective of the cavability investigation was to generate the necessary data base by determining these characteristics at three mines that represent a spectrum of rock mass competence from weak to strong, all of them employing an undercut-cave method of mining. The San Manuel Mine ore can be considered a typical porphyry copper deposit, a strong but well-fractured granitic rock mass. The relatively incompetent copper oxide ore body of the Lakeshore Mine differs chiefly in being highly altered and more intensely fractured, whereas the Henderson Mine ore, a competent molybdenite-bearing granitic rock mass, is far less intensively fractured. The foregoing are gross characteristics that would be perceived on examination of exploration drill cores or visits to underground tunnels.

The measurements of rock fracturing were generated by the two methods most readily available at a mine site, namely, mapping of exposed drift walls and logging of drill cores. Thus, if cavability is found to depend in a quantitative, predictable manner on the measurable parameters of fracturing in the ore body, then a justification exists for generating more detailed data to characterize the fracturing. The two methods were to be compared as to reliability, efficacy, etc., enabling the prospective mapper to form a judgment as to the method or combination of methods that best fits his or her objectives.

A population of fractures can be quantified by specifying their orientations (dip and azimuth of dip are used herein), spacings, and extents. Time was not available to deal with secondary characteristics such as joint infilling materials and roughness of joint surfaces. Up to 1,000 ft of 1.87-in-diam drill core at each mine was oriented on recovery from the drill holes so that fracture orientations could be determined; fracture extent is difficult to determine from an individual drill core. To facilitate comparisons with measurements obtained from cores, a scanline method was employed for mapping on drift wall exposures. Mapping on parallel multiple scanlines permitted a limited evaluation of fracture extent.

The general procedure employed in data analysis was first to perform a cluster analysis to identify separate sets of fractures having similar orientations. Based on the indicated clusters, some pooling of data was then done to reduce the total number of data groups. Within each such group, the distribution of fracture spacings was determined along the axis of the core or the scanline, both for the unclustered data and within fracture families having like orientation. Analysis of fracture trace length was made for the multiple-scanline mapping.

This report describes the methods of data acquisition and presents all the rock fracture data generated for the three study mines.

ACKNOWLEDGMENTS

The fieldwork described herein was conducted at the Lakeshore Mine, Casa Grande, AZ, under agreements with the Hecla Mining Co. and Noranda Lakeshore Mines, Inc.; at the San Manuel Mine, Inc., San Manuel, AZ, under an agreement with the San Manuel Division, Magma Copper Co.; and at the Henderson Mine, Empire, CO, under an agreement with the Climax Molybdenum Co. Division of AMAX, Inc. The assistance rendered by the respective mine staffs is gratefully acknowledged.

Scanline mapping was performed mainly by R. R. Pulse, physical scientist, Denver Research Center, Bureau of Mines; J. W. Carter, geologist, Denver Research Center, contributed substantially to this task at the Lakeshore Mine. Pulse and Carter performed the borescope measurements that were necessary to orient half of the drill cores at the Lakeshore Mine. Orienting of recovered core was performed by the drill crews, about two-thirds of the drilling being done by contractors and the rest by Denver Research Center technicians E. B. Wimer, H. C. Farley, and R. D. Wilton. Fracture orientation was measured on oriented drill cores by R. R. Pulse for the Lakeshore Mine, by K. E. Bastow, geological engineer, Denver Research Center, for the San Manuel Mine, and by the mine geological staff for the Henderson Mine. Computer processing of the data, working from the field notes and using the FRACTAN and GDIST codes, was performed by M. T. Melvin, statistician, Denver Research Center.

RATIONALE

The rock mass is presumed to contain planar (or subplanar) defects, discontinuities or "planes" of weakness, with cohesive strengths ranging from zero to 100 psi or more. If the planes of weakness occur at 100-ft intervals, the spacing may be too great to assist the caving process, considering a typical stope of 100- to 200-ft span. If the planes of weakness are spaced at 10-ft intervals, the caving may be technically acceptable, but the caved fragments may be considered excessively large for handling by presently available equipment. If the planes of weakness are spaced at 0.1-ft intervals, easy caving may be assured, but the development openings may tend to cave also, i.e., ground support is likely to be a problem.

At some stage in a successful caving process, the undercut ore becomes subdivided into what may be thought of as a set of blocks, closely fitting but essentially detached from one another. Although the formation of these blocks may be initiated along the preexisting zero-strength fractures, the complete separation of most blocks requires that some degree of bonding be overcome along planes of weakness. The greater the number of zero-strength fractures, the less the need to develop or extend fractures to interconnect between preexisting fractures, and thus the weaker the rock mass. Block formation obviously is facilitated by the presence of at least three different families of fractures, with attitudes such that a series of parallelepipeds is delineated. The thicknesses of the blocks depend largely on the distances between fractures of the same family, i.e., those having nearly the same attitude, as specified by their dip and dip azimuth.

This implies the need to orient core that is recovered for the purpose of characterizing the fracturing, so that the number and orientation of the distinct families can be identified. The ease of formation of blocks and the block sizes are important in determining the span required to be undercut to initiate sustained caving and the size distribution of the resulting caved ore fragments. The caving span can be analyzed by modern methods of theoretical structural analysis, given the pattern of fracturing and the strength parameters. The size of caved fragments is important to the design of openings through which the ore must flow, the selection of equipment to transfer the fragmented ore to the main transport system, and the main haulage system.

Characterizing the fracture geometry in a rock mass is one of the first large data-acquisition tasks that is a prerequisite to design of an undercut-cave system of mining based on quantifiable mechanical properties of the in-place ore body. A complete specification of the fracture geometry in a rock mass would require the determination of the size or extent of each fracture, its attitude in space, and the distances to its neighbors. If access to the fracturing is via drill hole or drill core, the sample consists of all fractures that intersect the line of the drill hole; attitude in space can be determined from drill core whose orientation is established when it is removed from the drill hole, or by measuring fracture attitude inside the drill hole. Information as to fracture spacing is limited to measurements along the core or drill hole; information as to fracture extent is virtually nil.

If access to the fracturing is via exposed rock surface, such as the wall of a drift, the sampling may consist of all fractures that intersect a line on the wall, in which case the information obtainable is essentially the same as for a drill hole. Or, the sample may consist of all fractures that lie within a specified area, such as a 6-ft circle. Mapping of an exposed surface provides some information as to fracture extent, but not complete information, since a large proportion of fractures do not terminate within the field of observation; furthermore, a surface usually does not exhibit the full size of a fracture, but instead cuts across the fracture at a random distance from its diameter.

Thus, complete specification of fracturing is not possible, either by core drilling or by mapping of exposures. The approach taken by the present investigation was to employ both methods, attempting to extract a maximum of information, by simple procedures, systematically applied, and to compare the results achieved by the two methods. The procedures for data acquisition and data interpretation that are developed in the investigation will thus tend to be practically useful to the typical mine staff, rather than primarily research tools.

The fracture-related information generated by visual observation of exposed rock mass surfaces or drill cores may be as brief as that required to broadly characterize the rock mass competence, such as strong-blocky, weak-friable, etc., or it may include detailed information such as petrographic type, phenocryst size, degree of argillification or silicification, joint attitude, joint spacing, joint filling minerals, joint surface roughness, etc. In general, the greater the uncertainty as to the ultimate uses of the data, the more will be collected, within the limitations imposed by time and cost.

Some rather detailed rock mass classification schemes have been devised in recent years (*3-4, 7*), primarily to predict the support problems that will be encountered in driving a tunnel through rock. A classification scheme is essentially intended to provide approximate estimates of excavation stability and support requrements, earlier and at less cost than by performing and evaluating strength tests.

For the present investigation, however, since one major goal is to precalculate by structural analysis methods the minimum unsupported span required to achieve sustained caving, testing is clearly required to develop a set of quantitative measures of rock mass resistance to breakdown under specified combinations of stress. In any event, the objective is not to develop a classification scheme suitable for predicting cavability (*24*), but rather to analyze the caving process as a mechanical failure phenomenon, inquiring as to the potential contribution that might be derived from specifications as the the intensity of fracturing in the rock mass, i.e., the orientation, spacing, and extent of the fractures. Considering the data that can be generated by readily available techniques without expensive apparatus, one would like to know which categories are most significant.

A presumption of the present investigation is that more data concerning fracture geometry could be generated at operating mines, if its importance to design could be substantiated, because measurements of joint spacing and orientation can be generated relatively easily and lend themselves to computerized data processing. On the other hand, quantifying surface texture and planarity, joint-filling minerals, etc., is quite time consuming. Cost-benefit considerations favor the creating of strength test data in preference to more detailed descriptive data.

In the context of strength, which implies resistance to separation, a rock mass can be considered to consist of two phases: (1) intact rock and (2) discrete, planar (or subplanar) surfaces of separation, surfaces along which the tensile strength is zero. All zero-tensile-strength surfaces are categorized herein as fractures. In geological terms, most of these fractures would be called joints because of the lack of obvious sliding along their surfaces of contact.

Inspection of surfaces of freshly broken intact rock revealed that it commonly also contains planar defects, the strength along which is presumably less than that of the bulk of the intact rock. On the other hand, planar features resembling joints may be recemented or silicified to the degree that their tensile strength exceeds that of the bulk of the intact rock.[4] Thus, as defined herein, all planar fractures are discontinuities, but all visually apparent discontinuities are not fractures. Consequently, only separation surfaces were logged as fractures, since there was no simple procedure for dealing with non-zero-strength defects. To include the latter in an analysis, the true strength of each would have to be determined by a mechanical test; testing is outside the scope of this report.

These distinctions are important with respect to the measurement procedure and the interpretation of the measurements. Fracture measuring on an exposure included any exposed planar surface that intersected the scanline; any such surface may have been a non-zero-strength planar defect before the drift was driven (blasted). Drill core logging included as a fracture every surface of separation that was believed to be not caused by man but doubtless included some fractures that were created in the core drilling procedure. These sources of ambiguity, which are necessarily present in geologic logging data, may severely limit the correlations that can be established from such data

The fracturing within a rock mass can be characterized in terms of fracture orientation, size, and location. Fracture orientation is herein specified by the dip and azimuth of dip. Provided that the diamond drill core orientation is determined when the core is recovered from the drill hole, the fracture measurements obtainable from the core consist of the dip and dip azimuth of each fracture, and the distance from the collar of the hole to the fracture along the axis of the core; fracture extent cannot practically be determined from a 1.87-in-diam core. To acquire as nearly as possible the equivalent information from drift exposures as from drill cores, fractures were mapped along horizontal straight-line segments usually 50 ft long; in addition, estimates of fracture extent were obtainable by mapping along a grid of four or five parallel line segments. The general plan was, in each study mine, to recover oriented core from about six 100-ft-long holes and to map a dozen 50-ft-long segments of drift wall.

To facilitate correlating the fracture data with determinations of the rock strength and of the size distribution of caved ore fragments, the sampling was concentrated in one or two areas of each mine. The data obtained in each mine can be regarded as typical, but not necessarily representative of the entire ore body.

[4]The lowest, sulfide (tactite) portion of the Lakeshore ore body was visibly banded, with spacings of about 1 in; the inference was that measurements of jointing would not be feasible in such an intensely jointed rock mass. This ore proved difficult to cave, because these joints were recemented—they were not separation surfaces. Similarly the Henderson ore exhibits silicified molybdenite bands along which the rock mass does not readily break.

DATA ACQUISITION

PRODUCING ORIENTED DRILL CORES

Consideration was given to several methods of recovering and orienting diamond drill cores. The objective was to work toward a system that would lend itself to frequent use at a mine, which implies simplicity and low cost, even if 100 pct of the core cannot be successfully oriented.

Exploratory core drilling is ordinarily done with a 5- or 10-ft-long single-tube core barrel. After the core barrel is removed from the drill hole, the core is slid out of the tilted tube into the core box. If the core does not readily come out, the barrel is hammered to loosen the core; this tends to break up the core and is unsatisfactory for preserving core orientation.

Drilling trials had been conducted earlier with a triple-tube core barrel, which is intended to provide superior core recovery capability. However, the system characteristics make for slow drilling progress, because, whenever the core breaks away from the solid, the water feed to the bit is automatically interrupted, which immediately forces the driller to recover the core and reset the spring-loaded water valve. The split inner (third) tube is pumped in and out of the second tube by hand, which takes time. Core quality was not greatly improved over the results achieved with the double-tube barrel.

Virtually all the oriented core was consequently recovered by the wireline method, using a commercially available 5-ft-long double-tube core barrel. The inner tube is split in half lengthwise so that one half of the tube can be lifted off, exposing the full length of core, which can then be carefully lifted into the core box. Two such inner barrels were employed, one being loaded into the drill hole as soon as the other was removed, to minimize drilling delays.

In one commercially available system, the core orientation is established by making three continuous grooves (with carbide tools) along the core. An Eastman multishot camera is used to make occasional photographs that show the groove azimuth and inclination. In 1976, when this investigation was initiated, the cost per foot for drilling oriented core was about four times as much by this method as by using the impression technique. Also, subsequent experience suggests that the three-continuous-scribe-line procedure would break off the friable cores as badly as the three-initial-scribe procedure, which was tried with poor results.

The drilling contract for the first mine permitted the contractor to select the core-orienting procedure, and hence the Lakeshore cores were oriented by scribing (with carbide tools) only the stump of core remaining in the hole after recovery of each length of drilled core. An Eastman single-shot camera was then used to produce a photograph of the carbide cutters superimposed on a compass and pendulum. This method was slow and required manual labor; thus the driller tended to minimize orientation sessions, which resulted in long sections of core that could not be oriented because of breaks between successive oriented segments. The scribing often destroyed the core stump, which caused lost orientation and lost drilling time in performing the orientation operation.

Only 20 ft of the core from the first 100-ft hole was successfully oriented, partly because th 10-ft-long single-tube core barrel permitted uncontrollable movements of fragments within the barrel. Nearly 100-pct recovery was achieved from the remaining five 100-ft holes by changing to a 5-ft-long split, double-tube core barrel, but even so, only 55 pct of the 600 ft of core was successfully oriented. The conclusion was that a well-fractured, altered rock mass could be completely recovered with wireline equipment and split, double-tube core barrel, but that a core scribing method would not produce acceptable orientation results.

All subsequent core orienting, at the San Manuel and Henderson Mines, was consequently performed by the impression method that had been experimented with earlier. PVC pipe, with common household caulking compound stuck in the end (fig. 1), was inserted in the hole, through the drill rods, and pressed against the stump of core at the end of the hole; the impression of the stump was withdrawn from the hole (fig. 2) and, by matching the appropriate core end, used to orient the length of core just recovered from the hole and/or the next length of core recovered (fig. 3). Since the stump was sometimes broken in the next drilling, the safer procedure is to try to orient all recovered core before continuing with the drilling. Accuracy depends on maintaining the orientation along the PVC pipe as successive sections are attached. For holes longer than about 100 ft, orientation of the far end of the pipe can be assured by using an attached mercury switch to activate a battery-powered light outside the drill hole. The impression method has limitations but is cheap and simple.

FIGURE 1.—Preparing to insert the impression device into the drill hole. Caulking is in place on end of caulking holder, which is attached to the first length of PVC pipe.

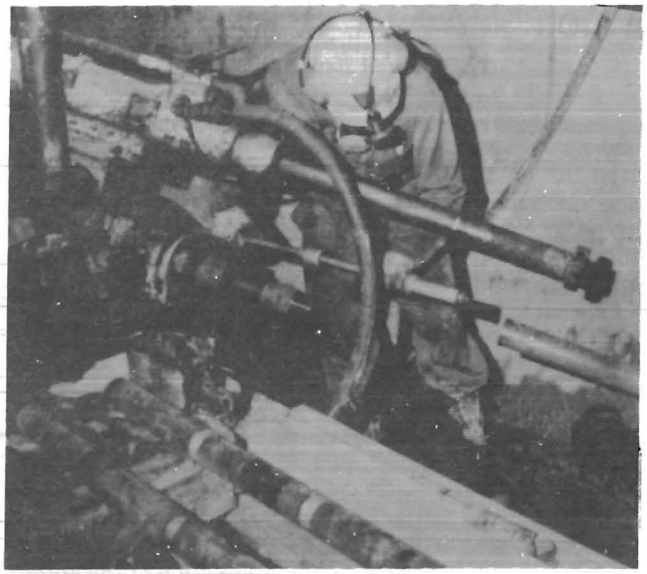

FIGURE 2.—Removing impression of the stump of core from the drill hole.

FIGURE 3.—Impression taken of stump of core in drill hole is oriented to match fracture surface on end of recovered core.

The apparatus used to obtain an impression included a number of 10-ft lengths of ½-in-diam, schedule 80 PVC pipe, two caulking holders, and a supply of caulking material. A 1.5-in-ID aluminum-tube caulking holder with an outer, sliding, centering ring was attachable by a set screw to any of the lengths of PVC pipe; two holders were provided so that one impression could be saved for subsequent matching while the next one was being made.

The caulking material picks up rock particles and must be replaced often. One pipe coupling was glued to each length of PVC pipe in advance so that the pipe was ready for quick assembly and disassembly in the mine; Teflon lubricant was helpful. Breakage of couplings was frequent in use, requiring an extra supply of pipe, fittings, and PVC glue, plus vise-grip pliers and a hacksaw. Orientation was provided by an axial scribe line on each coupling, created by a hacksaw or bandsaw; the scribe line was filled with paint to enhance its visibility. As each length of pipe was attached to those in the drill hole, it was aligned with them by means of the scribe line on its coupling.

The plastic pipe is light enough in weight that it has been pushed 300 ft up a 45° inclined drill hole, which is about the limit. The pipe, being actually too flexible, assumes an S-shape, bearing against the side of the hole; with increasing total length of pipe in the hole, the total frictional resistance increases, eventually causing the pipe to jam. Consequently 100 ft is a reasonable limit on the length of an upward-inclined hole in which the impression device can be raised by PVC pipe.

After the orientation was determined for each successive 5-ft length of recovered drill core, one half of the split core barrel was removed, (fig. 4) and, after observing the precaution that all fragments fit together without gaps, a felt-tip, waterproof marker was used to stripe the core along the side that was originally uppermost in the drill hole (fig. 5). (The stripe should be placed on the south side of the core from a hole drilled vertically upward, and on the north side for a hole drilled vertically downward, to facilitate later data processing operations.)

The distance from the collar of the hole to the end of each length of core recovered, as well as the distance to any shattered zone, was marked on a wooden spacer block or (better) on the core. An arrow indicating the drilling direction was marked on many core fragments to facilitate replacing them in proper orientation in the core box after any later removal for examination or measurement.

The core was transferred to a core box, and the two halves of the split core barrel were rejoined with wrappings of glass filament tape (fig. 6). Each core box was numbered and marked in sequence. Paperboard cartons are adequate for core boxes, provided they are protected at all times against moisture. Plastic core boxes are lightweight and can be reused indefinitely if not stored in the sun. Boxed drill cores were transported out of the mine to the core shack at intervals. (If allowed to accumulate underground, they risk being disturbed by specimen seekers.)

For logging, the core was placed in a long wooden trough made of 2-by-4-inch lumber. A 100-ft cloth tape marked in feet and tenths was thumbtacked to the trough to show the distance from the collar of the hole to any fracture. This distance and the fracture orientation were the principal items recorded. The Lakeshore Mine drill cores were supported in the same geographic orientation as they originally occupied in place (fig. 7), which was not difficult since all six holes were inclined at 30°. Values of dip and dip azimuth, which were measured with the Cocla device, were consequently the true values, requiring no corrections. Nevertheless the logging was slowed by the extra steps that had to be taken to prevent the core from sliding down the trough.

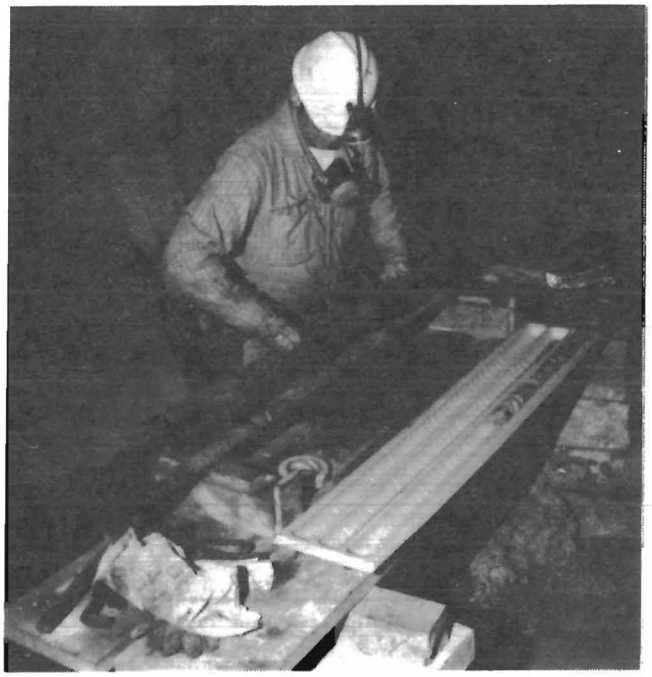

FIGURE 4.—Removing half of the split core barrel to expose the recovered drill core.

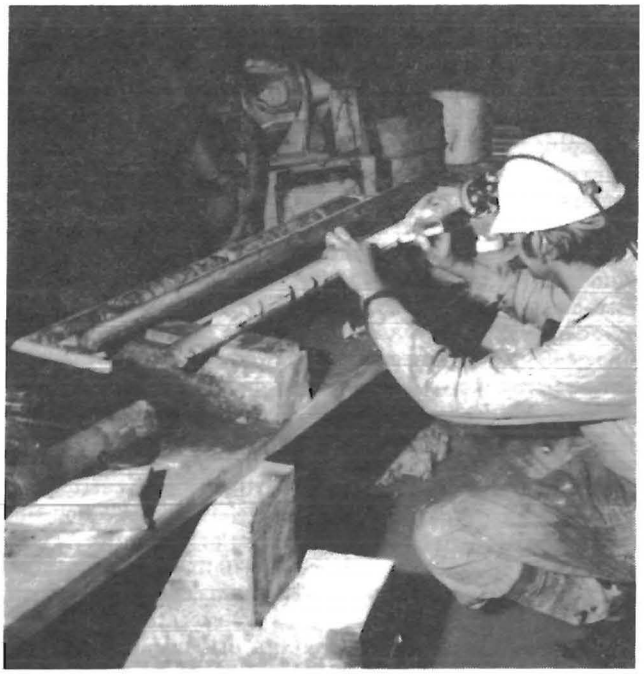

FIGURE 5.—Marking the orientation stripe on the recovered core.

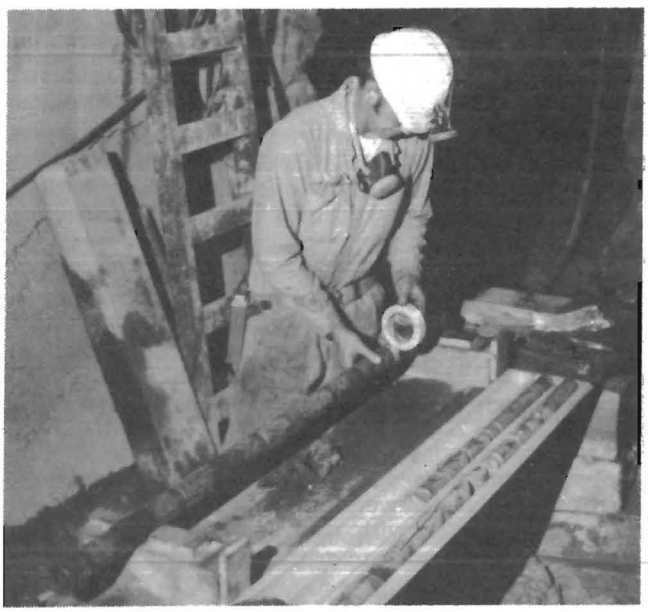

FIGURE 6.—Rejoining halves of the split barrel by wrapping at four points with glass filament tape.

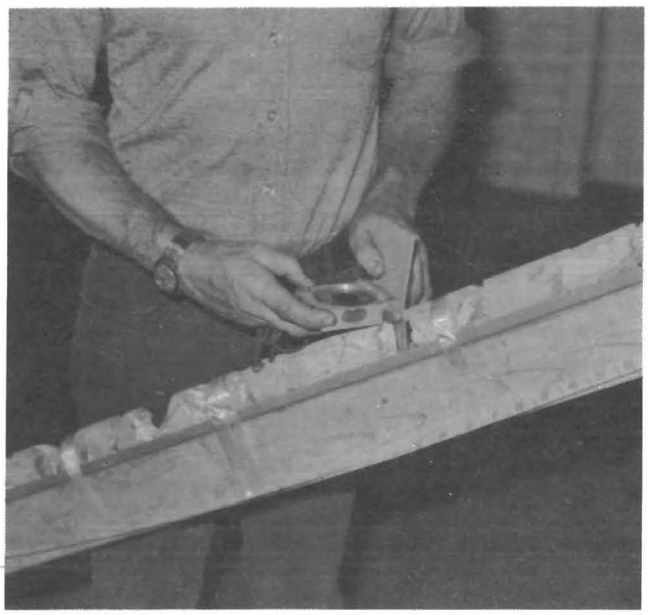

FIGURE 7.—Measuring dip and dip azimuth of a fracture in oriented core that is supported at 30° inclination. Cocla compass is held against an aluminum guide oriented parallel to the fracture surface. Core is taped at intervals to the supporting trough to prevent it from sliding down.

The drill cores from the other two mines were laid out for logging in a long horizontal trough, orientation stripe on top; the direction of drilling, indicated by the arrows on the core, was arbitrarily designated north. The as-logged fracture orientations were later converted to the true geographic orientations.

Fractures in the oriented drill cores recovered at the Henderson Mine were measured in the mine core shack, where the structural steel of the building caused a variable attraction for a magnetic compass. A special nonmagnetic goniometer (fig 8), incorporating two plastic protractors, was designed by D. R. Stewart, head geological engineer, AMAX Climax Molybdenum Co., for use by the mine geological engineering staff, who made the measurements.

Owing to the poor success at Lakeshore in orienting drill core by the scribing method as it was recovered from the hole, half of the 600 ft of core had to be oriented by borescope observations in the six drill holes. In sections of unoriented core, easily observable features (such as contacts with lenses of chrysocolla or hematite) were recorded by distance from the collar, 20 to 30 such features being selected in the unoriented portions of core from each drill hole. Each of these features was located (borescope viewing) in the drill hole and its attitude determined, from which the corresponding section of drill core was oriented. Each recovered length of core had been striped black to indicate continuity within the 5-ft segment, whether or not the orientation was subsequently determined by the driller, as indicated by a blue stripe. Although the technique of determining the attitudes of planar features via borescope in a drill hole had been established earlier (*25*), this was a tedious, time-consuming task for a two-man team. The earlier experience had indicated that measuring fracture attitudes on drill cores was much faster than by borehole observations. In the borehole the 400-lb weight of the 1.5-in-diam borescope was supported by a length of steel aircraft cable (3/32-in-diam, 7 × 19 construction), which passed over a pulley anchored at the end of the hole (*28*, p. 90); the other end of the cable was fastened outside the borehole to a post-mounted boat winch. This arrangement facilitated the many raising and lowering adjustments of the borescope position.

FIGURE 8.—Measuring with AMAX goniometer the orientations of fracture planes in oriented drill core laid in a horizontal position.

In the borehole logging procedure, the borescope was first winched to the end of the drill hole and then slowly withdrawn, with the viewing head oriented upward. Measurement of distance from the collar was made as any notable planar feature was crossed. The viewing head was then rotated to the horizontal, left-hand position, and the distance from the collar to the planar feature was again recorded. The operation was repeated for the horizontal, right-hand position. Dip and dip azimuth were calculated by the program given in IC 8615 (*25*). Later, to orient the core for measurements of fractures, the same features on the core (as were measured in the boreholes) were oriented to the calculated dip and dip azimuth. With the combined techniques 100 pct of the core was oriented.

MAPPING FRACTURES ALONG MULTIPLE SCANLINES

Attempts were made to map fractures on the undercutting level, to better sample the ore that would be caved. However, interference from blasting, timber obstructions, potential rock falls, and very limited time availability of such sites led to early abandonment of this procedure in favor of mapping on the next lower level, the production level, which was in ore at all three mines. Even so, any segment of a production drift was ordinarily exposed for only a few weeks after the drift was driven and until it was lined with concrete. Consequently, data acquisition by mapping in drifts was conducted intermittently over several months as sites became available.

Directional bias occurred in site selection, since most drifts in the production area have the same orientation.

The influence of this bias was expected to be minor, because the rough wall surfaces created by blasting tend to expose fracture surfaces that would not be measured on a perfectly flat wall. Several square inches of exposed fracture surface was needed to properly orient the measuring instrument, which in almost all instances was a Cocla geological stratum compass. A Brunton compass was briefly employed, but found to be much slower. Note that if the compass-indicated azimuth of a drift does not consistently deviate from the map azimuth by the same angle, a variable magnetic influence is present; this would necessitate the use of the USBM DRAP device (*5*) to measure fracture orientations.

Each scanline was established by a string stretched between nails hammered into fractures. Except for one vertical mapping site in a raise, scanlines were horizontal. In mapping along a scanline, the geologist measures only the fractures that intersect the line. For each fracture three measurements were recorded: angle of dip, azimuth of dip, and distance (feet and tenths) from the zero reference point to the point where the fracture would intersect the string line. In case of overbreak the fracture plane was projected, using a straight stick, to establish the point of intersection on the string line.

At the Lakeshore Mine each mapping unit consisted of four parallel scanlines 50 ft long, spaced 1.33 ft apart vertically, on the wall of a drift. The 50-ft length of drift was divided into 10-ft mapping intervals. Mapping of each 10-ft interval was completed along all four scanlines before proceeding to the next 10-ft interval, to facilitate identification of fractures that crossed more than one scanline.

The procedure for mapping a 10-ft interval was as follows: Sketch the attitudes of the fractures to be measured, numbering each fracture in sequence 1, 2, 3, . . ., as in figure 9. Measure and enter on the record sheet the distance to the fracture and its azimuth and dip. For any fracture that crosses more than one line, make separate measurements at each scanline. At Lakeshore measurements were made along scanline B only for those fractures that were long enough to intersect at least one other scanline.

At the San Manuel and Henderson Mines, the scanline mapping unit was usually 50 ft long, but five parallel scanlines were employed, spaced 1 ft apart; distance, azimuth, and dip were measured for every fracture that intersected every scanline.

The fracture information generated by the present study is quite different from that produced by the usual structural mapping procedure employed in a mine, typified by Wilson's maps (*36-37*), because the objectives are different. The mine geologist ordinarily maps all drifts as they are exposed, and, lacking the time to measure all the fractures, measures only the most prominent ones, those that seem to have the greatest continuities or the greatest apertures or the greatest numbers. Mapping a fractional sample of the footage of the mine openings is not acceptable, because portions of the major geologic structure would inevitably be missed. The mine geologist maps as much structural detail as can be conveniently shown graphically on a plan map of the mine openings. Typical mine structural maps show five or six fractures per inch of map along the wall of a drift. Since the mapping is ordinarily done to a scale of 40 or 50 ft to the inch, the density of mapped fractures is about one for every 7 to 10 ft. A casual inspection of line mapping sketches generated in the present study commonly reveals 20 or more fractures intercepted by the multiple scanlines within a 10-ft mapping segment, no account being taken of fracture traces too short to be intercepted by a scanline. Thus the mine geologist samples far fewer than 10 pct of all the fractures actually present and selects the sample subjectively. This information identifies the orientations of the most prominent fracture families, but it cannot be used to develop quantitative data on fracture intensity (such as fracture spacing, fracture extent, or fracture area per unit of volume of the rock mass), which is essential to a quantitative evaluation of mine excavation stability.

The scanline mapping employed in the present study provided concentrated samples from 50-ft lengths of drift wall at locations that were distributed over a representative area of the mine. After a 50-ft mapping site was chosen, the mapper presumably had no more options in regard to the sampling, because every fracture crossing every prescribed scanline was required to be measured, provided only that a few square inches of fracture surface was exposed to hold the Cocla compass against. The geologist's judgment nevertheless can be expected to influence the data significantly, because comparative trials show that the number of joints mapped on the same scanline by different individuals ordinarily varies by a factor of 1.5 to 3.8 (*18*).

The multiple-scanline procedure was devised to provide measurements related to fracture extent and also to speed the mapping. Much time can be expended in hunting for the ends of fracture traces under the usual mine conditions of poor visibility. (Illumination was by the observer's cap lamp.) Many fractures terminate beyond the limits of the exposure. Decision making is eliminated when the mapper needs only to deal with the fracture surfaces that intersect the scanlines.

Although fracture fillings and fracture apertures were recorded during the early part of the data acquisition phase, these factors did not seem to vary enough to warrant the expenditure of the additional time to evaluate them, and hence this procedure was discontinued.

Scanline mapping was performed intermittently as a one-person task, independent of other activities. A 50-ft interval could be mapped in two to three work shifts; placing string lines and other site preparation chores usually consumed one-half shift.

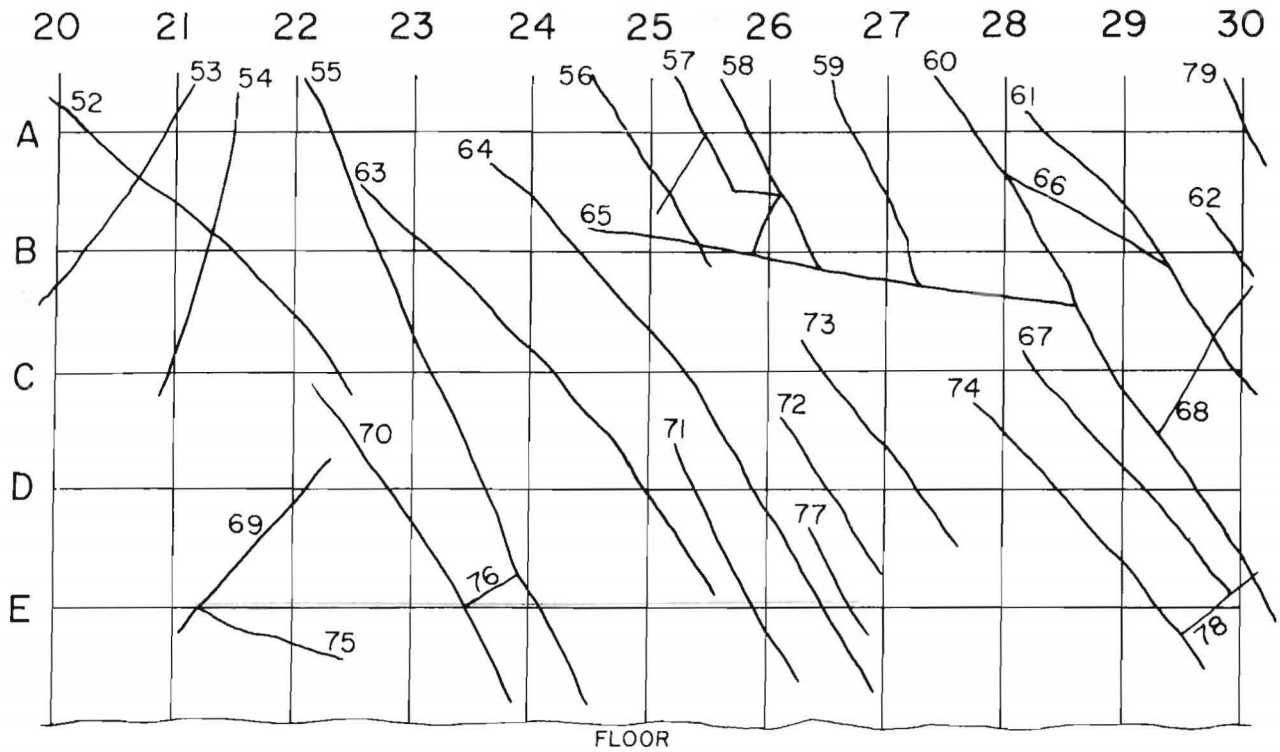

Frac	Distance, ft					Dip / Dip azimuth				
	A	B	C	D	E	A	B	C	D	E
52	20.2	21.5	22.3			45/314	45/315	45/320		
53	20.9	20.3				80/55	80/55			
54	21.4	21.3	21.0			74/295	75/295	74/295		
55	22.2	22.7	23.1	23.6	24.1	55/300	55/306	58/305	60/305	62/305
56	24.8	25.4				80/44	80/44			
57	25.4					70/300				
58	25.8	26.4				55/295	55/295			
59	26.7	27.2				86/60	85/60			
60	27.6	28.3	28.8	29.6	30.2	62/325	60/328	62/325	68/328	70/328
61	28.3	29.3	29.9	30.3		86/60	85/65	75/68	78/62	
62		29.9	30.3	30.6			65/300	68/306	70/310	
63		23.1	24.1	24.9			75/50	78/48	74/45	

Frac	Distance, ft					Dip / Dip azimuth				
	A	B	C	D	E	A	B	C	D	E
64		24.3	25.2	25.8	26.4		56/314	55/315	56/315	56/315
65		25.9					55/235			
66		29.1					38/310			
67			28.3	29.1				88/295	88/295	
68			29.6					55/235		
69				22.1	21.2				84/225	85/225
70				22.7	23.4				76/298	75/295
71				25.3	25.8				80/300	80/300
72				26.5					62/52	
73			26.5	27.3				62/325	62/325	
74				28.4	29.3				88/300	85/300
75					21.1					62/235

FIGURE 9.—Sample field sheets for five-scanline mapping. Top, Numbered fracture traces crossing scanlines A to E, 20 to 30 ft from the zero reference; bottom, recorded fracture measurements. Note that whereas the tabled values are measured on the rock exposure at the mine, the sketch is only a guide to the interpretation of the field measurements; it is not an exact reproduction.

DATA REDUCTION

Measurements of fracture orientation and location along a line were followed by a series of data reduction operations, most of which were performed by computer, not because of their complexity, but primarily to save time and to avoid introducing human error. Since essentially the same operations were performed on the data from each mine, the procedures are collected here for convenience of reference, to be followed by the presentation of results.

FRACTURE ORIENTATION

The approach taken was to analyze each set of data, i.e., each 50-ft unit of scanline mapping and the oriented core from each drill hole, to determine first the orientations of the individual fracture families and then the spacing and extent characteristics.

The orientations of a set of fracture planes can be visualized by considering their normals to be radii of a unit sphere. Each fracture-plane normal (pole) is represented by the point of intersection of the respective radius with the surface of the upper half of the sphere. Thus, a horizontal fracture plane is represented by the zenith point on the sphere; a vertical fracture is represented by a point on the equator. The upper hemisphere includes all possible values of fracture-plane dip angle (0 to 90° below the horizontal) and azimuth of dip (0 to 360°, reckoned clockwise from north) for the fracture-plane poles; the lower hemisphere intersections, diametrically opposite to those on the upper hemisphere, are disregarded since they duplicate the same information.

A plot of all fracture-plane poles on an equal-area projection of the hemisphere, referred to as a polar equal-area (PEA) diagram, is the least distorted graphical representation of a set of measurements of dip and dip azimuth. Upper hemisphere plots are convenient in that pole intersections are plotted in the first quadrant for northeast-dipping fractures, in the second quadrant for northwest-dipping fractures, etc.

For two of the mines the core fracture orientations had been measured with the core axis horizontal, pointing to an arbitrary north azimuth. The as-logged fracture orientations were converted to the true geographic orientations by two transformations: (1) The first step in effect rotated the north-south core axis about a horizontal east-west axis to make the core axis inclination equal to that of the drill hole axis; (2) the second step in effect rotated the inclined core about a vertical axis to make its azimuth coincide with that of the drill hole. Computer-calculated orientations were spot-checked graphically via stereographic projection (*33*, p. 67) as follows: Plot the fracture-plane pole orientation on an overlay sheet, rotate the overlay so that its east-west axis coincides with north-south on the stereographic net, translate the pole point northward on the overlay along its small-circle path ("latitude" coordinate) by the number of degrees of drill hole inclination above the horizontal (translate the pole point southward for a drill hole inclined below the horizontal), and read off the dip and dip azimuth of the rotated fracture plane. In effect the core axis is now inclined at the same angle as the drill hole, but with north azimuth, and hence the final step consists only of adding the drill hole azimuth angle to the new dip azimuth of the fracture plane. Accuracy of dip and dip azimuth within about 1° can be achieved by this method when using a 6-in-diam stereographic net.

The customary data presentation, in which the individual poles are replaced by isopleths (contours) indicating the density of poles (per incremental area of the hemisphere), is misleading because it emphasizes the concentrations of poles and may delete many poles in areas of low density. Furthermore, unless all the density values have been appropriately weighted, the distribution of pole densities is necessarily distorted by the bias that is introduced by the sampling scheme (*31*). For example, if the poles of a given fracture family are not parallel to the drill hole axis but deviate from it by an angle δ (fig. 10), then the number of fractures of that family observed along a given length of core will be reduced on the average to cos δ times the number of fractures that would be observed if the drill hole crossed the fractures at right angles. If $\delta >$ 60°, the density of fractures of a given family is reduced to 50 pct or less of the true value; this expected band of large underrepresentation is shown on all PEA plots for oriented core, so that one may form a more accurate impression of the distribution of the fracture orientations. Although the same principle might seem to apply to scanline data, the roughness of the drift walls reduces this sort of bias substantially.

CLUSTER ANALYSIS

The points of intersection of the fracture-plane poles with the upper hemisphere surface may tend to cluster about a few preferred locations, representing fracture families that have similar orientations. The computer code FRACTAN (*30*) was used to classify each set of observed fracture-plane orientations, whether obtained by

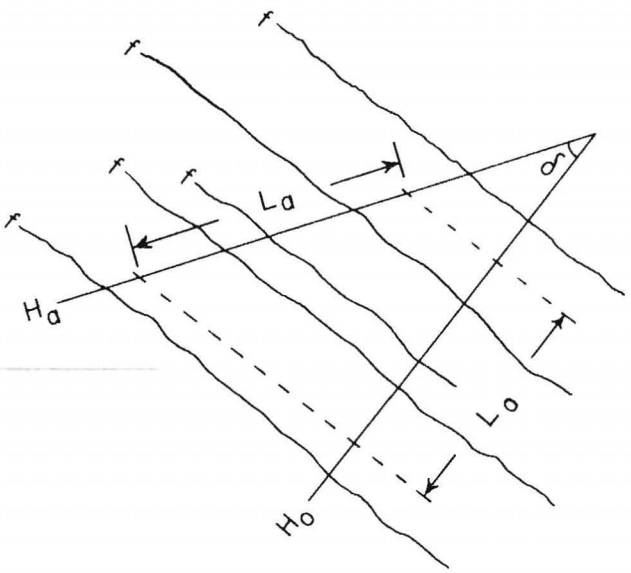

FIGURE 10.—Scanline or drill hole H_o crosses a family of fractures f at right angles; δ = 0. Scanline or drill hole H_a deviates by δ from the fracture-pole orientation. The same number of fractures N is intercepted by both scanlines between the dotted lines. Since $L_a = L_o/\cos \delta$, therefore $N/L_a = (N/L_o) \cos \delta$.

scanline mapping or from drill cores, into a collection of distinct subsets (referred to as clusters or families). To initiate the numerical computer program operations, the analyst specifies a value of r (degrees), the radius of the counting circle that is used in partitioning the fracture-plane pole points into clusters.

After partitioning the data into clusters, the FRACTAN program calculates the dip and dip azimuth for the mean axis of each cluster, i.e., the average orientation of each fracture-plane family. For each selected value of r, the FRACTAN printout also includes a PEA plot of all the poles in the data set, a PEA plot of the dense points, and a PEA plot of the poles in each cluster. These plots, produced by line printer, are convenient for rapidly evaluating data when the analyst already is familiar with the essential fracture characteristics of a particular ore body. Owing to the usual line printer limitations, only one character (fracture-plane pole) can be printed in each incremental area of the diagram, irrespective of the actual number or location of the poles that lie within that area; hence many poles are omitted in the areas of higher concentration.

To exhibit all the data points, the PEA plots shown herein were produced by a Tektronix 4054 Graphic Computing System unit, transferring directly from the computer the results of the FRACTAN dense-point analysis and cluster analysis. The plotting position of a fracture-pole point on a PEA projection (upper hemisphere) is given by the coordinates

$$x = R\,(1 - \cos\phi)^{1/2} \sin\theta$$

and $$y = R\,(1 - \cos\phi)^{1/2} \cos\theta$$

where R = radius of the plotting circle,

ϕ = dip angle of the fracture plane, 0 to 90°,

and θ = azimuth of dip of the fracture plane, 0 to 360°.

As will be seen, the fracture-plane poles contained in any of the present data sets have a wide range of orientations, and consequently the scatter within any cluster is substantially dependent on the number of clusters into which the data set is subdivided. A within-between type of variance analysis reflecting this relationship is incorporated into FRACTAN, which calculates the total variability F among the set of fracture-plane orientations, as follows:

F = (sum of squares of deviations of the individual pole orientations from their cluster mean orientations)
+ (sum of squares of deviations of the cluster means from each other).

Selecting a larger numnber of clusters decreases the first component of F but increases the second component; F has a minimum at or near the best partition. By making about five trial FRACTAN partitioning solutions with selected values of the screening parameter r (e.g., r = 9, 9.5, 10, 10.5, 11) the analyst usually can find one or two partitions that produce a near-minimum value of F, and one of these solutions will ordinarily satisfy also the criteria that the clusters identified are (1) moderate in number and (2) logically representative of the PEA plots of fracture plane poles and of dense points. Neither F nor the partitioning is critically sensitive to the value of r.

The best (in the sense defined above) FRACTAN partitioning solution is depicted herein by a PEA plot for each 50-ft scanline mapping unit and for the oriented core from each drill hole. The value of r is given for each solution, but the value of F is omitted because F increases with the number of observations in the data set; i.e., F values can be compared only for different values of r within the same data set.

Since earlier investigations (and this one as well) showed that the dispersion of fracture-plane pole points on the hemisphere is usually better described by an elliptical distribution than by a circular distribution, FRACTAN computes a pair of elliptical dispersion parameters. Whether the distribution is circular or elliptical, however, the usual distribution function presumes an exponential decrease of fracture frequency with increasing deviation of the fracture planes from the family mean orientation. If all the fracture orientations in each set of data were tightly clustered about two or three mean axes, the scatter about a cluster mean axis would be unambiguous. Each of the present data sets, however, exhibits numerous fracture orientations, with substantial overlap of one family on another because of the considerable scatter of orientations within each family. In the PEA plots of the actual data, one can see relatively little open space that is unoccupied by pole points (other than the underrepresented zones created by sampling bias), which would be indicative of the limit of dispersion of a fracture family.

The FRACTAN method of cluster analysis establishes a boundary between two clusters that is ambiguous in that each cluster probably contains a few fractures that are some of the most deviant members of the adjoining cluster; also, the denser of two adjoining clusters may tend to include more members of the less dense cluster than it contributes to the latter. In any event the angular range of a cluster is necessarily truncated, and hence any ordinary dispersion parameter underestimates the true dispersion. Even if there were no overlap between adjoining distributions, calculation of valid dispersion parameters would require that the deviation of each fracture plane with respect to its family mean axis be weighted to compensate for the geometric bias introduced in sampling. Formulating meaningful interpretations of the usual calculated dispersion parameters is thus seen to be subject to several difficulties. The actual dispersions are of course visually apparent on the PEA diagrams, which show the individual poles within each cluster and the mean axis of each cluster.

For the sake of completeness, despite the difficulties with respect to interpretation, each FRACTAN solution tabulated herein includes a listing of the eigenvalues W1 ≤ W2 ≤ W3 (*30, 35*) of the orientation matrix M (*35*) for each cluster. The sum of the eigenvalues is equal to n, the number of fracture-plane poles in the cluster. If the two lesser eigenvalues, W1 and W2, are of equal size, the pole points have a circular distribution (on the reference hemisphere) about the mean orientation. If all the poles in the cluster have the same orientation, then W3 = n. Thus, the ratio W3/n, given in the tables herein, is a measure of the tightness of the cluster.

To eliminate the restrictive feature of FRACTAN that requires every fracture-plane pole to be assigned to a cluster, Mahtab and Yegulalp (*26*) devised a procedure, based on Chauvenet's criterion, for rejecting extremal pole points, i.e., those that might be considered to fall between clusters. Implementing this procedure would delete observed data from the least dense areas of a PEA plot, thus reducing the scatter within clusters. However, if the

low density of poles in certain orientations correlates with increase of δ (sampling geometry bias), as generally seems to be the case for the oriented core, at least, discarding the weak data would exacerbate the problem.

As pointed out by Terzaghi (*31*, pp. 297, 298, 301), one approach is to create a weighted pole-density plot, and the best practical approach is to base the analysis on pooled data sets generated for several different orientations of the mapped exposures or the drill holes.

In summarizing the fracture orientation analysis for the individual scanline sites and drill holes, since so many fracture families were identified, consideration was given to rejecting all small clusters on grounds of insufficient observations. However, calculating an estimated number of fractures = the observed number of fractures in each family divided by cos δ, where δ is the angle of deviation of the family mean axis from the scanline or drill hole (this estimate is listed in each PEA diagram), seemed to make little change in the ranking of families by number of observed fractures, although the smaller fracture families were commonly the most increased in size by this weighting. Ultimately, rejection of data played little part in the summarizing.

The decrease in number of observed fractures for $\delta > 60°$, which is especially notable in the PEA plots for the drill core data, suggests the desirability of pooling several data sets to obtain a better cluster solution, since a family that is greatly underrepresented in one drill hole may be compensated by similar underrepresentation of the other families in other drill holes at the same site.

On the other hand, if analysis is made of pooled data derived from sites that are truly different, e.g., because of relative rotational movements of large blocks of the ore body delineated by faults, the cluster solution will tend to exhibit a substantially greater number of clusters than are found in a single mining block, with mean axis orientations that are distributed all over the hemisphere, which may be a totally false picture of the fracturing that exists within any single mining block. To illustrate this concept, let us suppose that every 100-ft cube of an ore body exhibits good cavability and that every 100-ft cube contains a different set of fracture families—a cluster solution for fracture orientations derived from a pooling of the data from three such 100-ft cubes would not be a valid basis for explaining the cavability. Consequently, one must exercise caution in interpreting any solution or average obtained from pooled data if the result is inconsistent with the solutions obtained from the individual data sets. Results are presented herein for a number of poolings, mainly to reflect average results within a limited portion of a mine.

FRACTURE SPACING

After the FRACTAN processing to determine the fracture families, various sets of data were processed by the computer code GDIST (*1*) to analyze (1) the distances between fractures as originally measured parallel to the scanline or the drill hole axis, without regard to clusters, and (2) the orthogonal distances between successive fractures of the same family.

GDIST calculates the statistics of an observed distribution (mean, median, standard deviation, relative frequency, etc.) and tests the observed distribution for fit to six common statistical distributions: normal, lognormal, exponential, chi square, gamma, and uniform.

If the distances from the zero reference to successive fractures, as measured along a drill core or along a scanline, are, for example, a_1, a_2, b_1, c_1, a_3, c_2, b_2, . . ., where a, b, and c designate three fracture families or fracture orientations, then the spacings of the nonclustered fractures are the differences a_2-a_1, b_1-a_2, c_1-b_1, a_3-c_1, . . ., and the spacings within individual fracture families (clustered data) are the differences a_2-a_1, a_3-a_2, . . ., b_2-b_1, . . ., c_2-c_1, . . ., etc.

To avoid measuring the distances to fractures along drill cores, investigations have widely experimented with various core recovery indices; these include the percentage of core recovered, the percentage of the total length of recovered core that consists of intact pieces at least 4 in long, and the percentage of the total drilled length that consists of intact pieces at least Q inches long (Q selected by the user). The latter two are referred to as rock quality designations, RQD. A poor correlation has generally been found between RQD values and rock mass behavior parameters. An RQD value of course utilizes information concerning only one point of the distribution of fracture spacings. Since the present analyses provide far more information, RQD was not explicitly determined. Furthermore, as has been shown, the expected value of RQD can be computed, given the form and the parameters of the distribution of fracture spacings (*20*), all of which are presented herein.

Much attention has been given in the technical literature to fracture spacings in nonclustered drill core data, because relatively few oriented drill core data have been available. However, the distribution of spacing within fracture families that have similar orientations is more directly usable for deriving quantitative inferences concerning the geometry of the fracture system in a rock mass. The as-measured (apparent) distances between successive members of a cluster were converted to orthogonal spacings (perpendicular to the mean fracture orientation) by (fig. 10)—

$$\text{Orthogonal spacing} = (\cos \delta)(\text{apparent spacing}), \quad (1)$$

where δ was determined from the equal-angle stereographic projection. The analyses of spacing distributions were not performed for every cluster in every individual drill hole or scanline site, because a very large number of results would be produced, probably widely divergent owing to the number of spacings in most clusters being too small to provide good estimates. Instead, the GDIST analyses were performed on pooled sets of data, groups of drill holes or scanlines that were located near each other in the mine. Moreover, this procedure is consistent with the generalization, developed from studies of the FRACTAN cluster analyses, that the best overall view of the rock mass characteristics at any site is obtained from a pooling of the data. Consistent treatment of the data is achieved by using cluster orientations that were determined by best FRACTAN solutions for the pooled data.

Histograms are plotted for all data that were analyzed by GDIST. Without exception, the greatest concentration of spacings is in the smallest-spacing class interval, which tends to favor a lognormal or a negative exponential distribution. The calculated values of the common parameters are tabulated below the corresponding histograms, including the mean and standard deviation of the logarithms of the observations, which pertain to the lognormal distribution.

A negative exponential distribution has two parameters, a location parameter a that corresponds to the minimum observed spacing (which is virtually identical to the arbitrarily imposed truncation point, 0.15 or 0.20 ft) and a shape parameter σ, the probability density being expressed by—

$$f(s) = \sigma^{-1} \exp [-(s-a)/\sigma], \quad (s>a, \sigma>0), \qquad (2)$$

where s is the fracture spacing, σ is the standard deviation, and the mean is equal to a + σ. Details concerning the other distributions appear in IC 8731 (*1*).

With regard to the fit of the observed data to the several hypothetical distributions, each distribution is listed as acceptable unless the chi-squared goodness-of-fit test indicates that the observed set of spacings would be obtained less than 5 pct of the time if that distribution were the true one. The distribution having the highest probability is listed as the best fit. For data sets of less than 50 observations, where the chi-squared test is weak, the simpler Kolmogorov-Smirnov one-sample test was used, instead of the options available in GDIST, to judge the acceptability of fit and the distribution of best fit.

FRACTURE TRACE LENGTH

The final data processing was to analyze fracture trace length, which is a significant factor for evaluating the fracturing intensity in a rock mass. Trace length is a function of fracture size and shape. Fracture size or extent has been observed to be finite; moreover, the greater the fracture size, the fewer the fractures observed. The limited data available on fracture shapes (*9*, pp. 7-9) suggest that fractures may be approximately represented by circular or elliptical disks, the diameters of which are specified by a statistical distribution. To infer fracture sizes from fracture trace lengths, account must be taken of the sources of bias that arise from several geometric probability relationships (*2*). For example, the probability that a given fracture intersects the mapped exposure is proportional to the square root of the area of that fracture, and the probability that the fracture on the exposure intersects a given scanline is proportional to the length of the fracture trace.

With respect to fracture trace length on an exposure, arguments and evidence have appeared in the literature (*9, 12*) in support of two candidate distributions, the lognormal and the negative exponential. The mapping limitation of the present investigation, that fracture traces of about 3 in or less were neglected because fracture attitude could not be determined, increases the likelihood that the truncated distributions of mapped trace lengths will appear to be acceptable fits to both the lognormal and the exponential. Also, the number of fractures observed in any family is too small to permit one to discriminate between the two distributions with high confidence. Furthermore, the trace lengths were determined only to within a 1.33- or 1-ft interval (the scanline spacing). Because there are convenient estimation expressions for the exponential distribution, the present approach is to treat the fracture trace lengths as if they are samples from exponential distributions. Calculations based on alternative assumptions can readily be made subsequently from the observed data, which are tabulated herein.

Two potential sources of bias in estimating fracture trace length are those due to truncation and to censoring, both of which have been analyzed for an exponential distribution. With respect to the present measurements, truncation refers to the aforementioned lower limit of about 3 in for measurable traces. The effect of this bias is no more than about 20 pct if the mean trace length is at least 4 times the truncation length (*2*), which is the case for the present data. Censoring refers to the indeterminate lengths of fracture traces that extend beyond the mapping limits on the exposure. The chief objective in what follows is to develop appropriate expressions from which to calculate estimates of mean trace length from the censored determinations that were made in the three study mines.

The probability density fuction for the two-parameter negative exponential distribution is of the form—

$$f(x) = \theta^{-1} \exp [-(x-x_o)/\theta], \quad (x>x_o, \theta>0) \qquad (3)$$

where x = observed fracture trace length,

x_o = a constant,

$\mu = x_o + \theta$ = mean observed trace length,

and θ = standard deviation of the distribution.

The probability that a random observation selected from this distribution takes a value between x_o and x_c is given by—

$$F(x_c) = \int_{x_o}^{x_o+x_c} f(x)\, dx = 1 - \exp(-x_c/\theta). \qquad (4)$$

The probability that $x > x_c$ is equal to $1-F(x_c) = \exp(-x_c/\theta)$. The sample estimate of $Pr(x>x_c)$ is $(N-N_c)/N$, where N is the total number of fracture traces that are intersected by a specified scanline and $N-N_c$ is the number of these observed traces that are longer than x_c. It follows that—

$$N - N_c = N \exp(-x_c/\theta), \qquad (5)$$

and hence, as pointed out by Epstein (*17*), if the exponential assumption holds, log $(N-N_c)$ will plot linearly against x_c and the slope of the graph will equal $-1/\theta$.

For the four-scanline mapping scheme employed at the Lakeshore Mine, nine classes of data can be defined, classes 1 to 9 in figure 11, with respect to any family of fractures. Attitude and location were measured for all fractures that crossed line A, all that crossed line C, and all that crossed line D; measurements at intersections along line B were made only for fracture traces that crossed at least one of lines A, C, or D. Initially at San Manuel a 4-scanline scheme was employed in which all 10 classes of figure 11 were determined, because all fractures that crossed all 4 scanlines were measured. For the 5-scanline scheme employed at the San Manuel and Henderson Mines, 15 classes of data are defined (fig. 12), because attitude and location were measured for all fractures that crossed every one of the five scanlines.

In this type of mapping, classes always occur for which at least one end of the fracture trace is undetermined; in figure 11 these are classes 3 to 9; in figure 12 these are classes 5 to 13. Fracture traces are said to be censored when they are of indeterminate length, extending beyond the mapping limits.

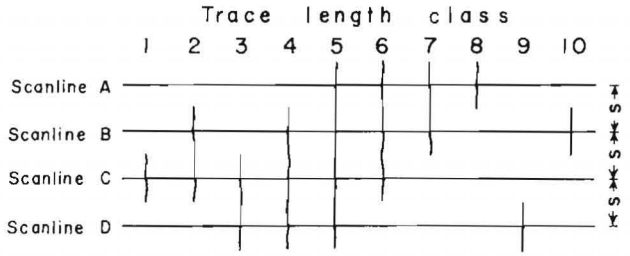

FIGURE 11. Fracture trace length classes, four-scanline scheme.

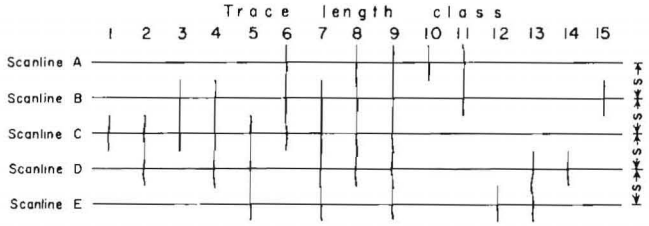

FIGURE 12.—Fracture trace length classes, five-scanline scheme.

TABLE 1.—Equations used to calculate estimated mean half-length of intersected fracture traces

Half-lengths extend-	x_c	$(\hat{\theta}'/s)\sin\alpha$	Equation
		4 SCANLINES, FIGURE 11	
Down from line A	$3s/\sin\alpha$	$\frac{0.5N_8 + 1.5N_7 + 2.5N_6 + 3N_5}{N_8 + N_7 + N_6}$	9
Down from line B	$2s/\sin\alpha$	$\frac{0.5(N_7 + N_{10}) + 1.5(N_2 + N_6) + 2(N_4 + N_5)}{N_7 + N_{10} + N_2 + N_6}$	10
Up from line C	$2s/\sin\alpha$	$\frac{0.5(N_1 + N_3) + 1.5(N_2 + N_4) + 2(N_5 + N_6)}{N_1 + N_3 + N_2 + N_4}$	11
Up from line D	$3s/\sin\alpha$	$\frac{0.5N_9 + 1.5N_3 + 2.5N_4 + 3N_5}{N_9 + N_3 + N_4}$	12
		5 SCANLINES, FIGURE 12	
Down from line A	$4s/\sin\alpha$	$\frac{0.5N_{10} + 1.5N_{11} + 2.5N_6 + 3.5N_8 + 4N_9}{N_{10} + N_{11} + N_6 + N_8}$	13
Down from line B	$3s/\sin\alpha$	$\frac{0.5(N_{11} + N_{15}) + 1.5(N_3 + N_6) + 2.5(N_4 + N_8) + 3(N_7 + N_9)}{N_{11} + N_{15} + N_3 + N_6 + N_4 + N_8}$	14
Down from line C	$2s/\sin\alpha$	$\frac{0.5(N_1 + N_3 + N_6) + 1.5(N_2 + N_4 + N_8) + 2(N_5 + N_7 + N_9)}{N_1 + N_3 + N_6 + N_2 + N_4 + N_8}$	15
Up from line C	$2s/\sin\alpha$	$\frac{0.5(N_1 + N_2 + N_5) + 1.5(N_3 + N_4 + N_7) + 2(N_6 + N_8 + N_9)}{N_1 + N_2 + N_5 + N_3 + N_4 + N_7}$	16
Up from line D	$3s/\sin\alpha$	$\frac{0.5(N_{13} + N_{14}) + 1.5(N_2 + N_5) + 2.5(N_4 + N_7) + 3(N_8 + N_9)}{N_{13} + N_{14} + N_2 + N_5 + N_4 + N_7}$	17
Up from line E	$4s/\sin\alpha$	$\frac{0.5N_{12} + 1.5N_{13} + 2.5N_5 + 3.5N_7 + 4N_9}{N_{12} + N_{13} + N_5 + N_7}$	18

Assuming an exponential distribution, the best estimate of mean intersected trace length for a family of vertical fractures censored at a distance x_c from a specified scanline is given by (*6*)—

$$\hat{\theta} = T_c/N_c, \tag{6}$$

where T_c is the sum of the lengths of the N intersected fracture traces of a specified fracture family up to the censoring length x_c, and N_c is the number of uncensored traces. T_c can also be expressed as

$$T_c = \Sigma\, t_i, \qquad (i = 1 \text{ to } N), \tag{7}$$

where t_i is the lesser of x_c or the observed trace length for the ith fracture of the specified family.

If the mean orientation of the fracture family is not vertical, equation 6 becomes—

$$\hat{\theta} = T_c/N_c \sin\alpha, \tag{6a}$$

where α is the apparent dip of the mean fracture-plane orientation on the wall of the drift; α was determined by stereonet as the inclination of the line of intersection of the drift wall with the mean fracture-plane orientation of the specified fracture family.

A characteristic of the multiple-scanline system is that each class of intersected trace lengths extends over two or more scanline spacing intervals. In figure 12, the lengths of the traces in class 1 are greater than zero and less than two scanline intervals; the lengths of the traces in classes 2 and 3 are greater than one and less than three scanline intervals; the lengths of the traces in class 4 are greater than two and less than four intervals. (One scanline interval = s if the fractures are vertical, s/sin α otherwise).

For example, analyzing the sample consisting of all the vertical fracture traces that intersect line C of figure 12 with respect to the censoring at $x_c = 2$ scanline intervals, the trace lengths of class 1, ranging from 0 to 2 intervals, are uncensored and their total trace length is sN_1, the midpoint of the range being at one scanline interval; the trace lengths of class 2, ranging from one to three intervals, have a total length $2sN_2$, the midpoint of

the range being at two scanline intervals; and so on. The foregoing information provides one data point for the semilog plot of equation 5, since $x_c = 2s$ and $(N\text{-}N_c) = N_5 + N_6 + N_7 + N_8 + N_9$. It also provides one estimate of the mean intersected trace length via equation 6, since—

$$\frac{\hat{\theta}}{s} = \frac{N_1 + 2(N_2+N_3)+3N_4+2.5(N_5+N_6)+3.5(N_7+N_8)+4N_9}{N_c = N_1 + N_2 + N_3 + N_4} \quad (8)$$

These estimates of mean trace length have low efficiency, because only four of the nine pertinent data classes comprise known (uncensored) trace lengths. A similar pair of estimates could be calculated for all vertical fracture traces that cross scanline B, and a third pair for all that cross line D; the second and third estimates are even less efficient, because only three of the eight pertinent data classes comprise uncensored lengths. The situation is even more restrictive if one attempts to analyze the sample consisting of all fracture traces that intersect line C of figure 11, where only two of the six pertinent data classes comprise uncensored lengths.

Many more estimates of mean trace length are calculable if one analyzes the half lengths of the traces instead of the full lengths, and these estimates are more efficient because two-thirds to four-fifths of the pertinent data classes comprise uncensored data. For example, considering only the traces that intersect line A of figure 12, the expected value of the portions of those traces that extend below line A is one-half the mean length of the traces crossing line A. For the censoring at $x_c = 4$ scanline intervals, an estimate of the *mean half-length* $\hat{\theta}'$ of the traces intersected by line A is given by equation 12, table 1 (obtained from equation 6).

Table 1 gives six equations for calculating mean half-lengths of traces for a five-scanline scheme and four equations for a four-scanline scheme, all of which are obtained from equation 6. (The method of equation 6 is used herein, rather than the method of equation 5, because it provides a more direct route to estimates of $\hat{\theta}'$.) One may observe that in each of these 10 equations, unlike equation 8, most of the measured trace length classes appear explicitly in the uncensored set of traces, where their specific different lengths can influence the calculated value of $\hat{\theta}'$.

For each of the three mines, there are tabulated herein for each fracture family the number of observed fracture traces in each of the separate classes shown in figures 11 and 12, along with the estimates $\hat{\theta}'$ calculated by the equations given in table 1; these are unbiased estimates of the means of the actual full trace lengths on the exposures, because the trace-length bias due to scanline sampling exactly nullifies the bias caused by the use of trace half-length determinations (*29*). Assuming that the fractures are of circular shape and that their diameters follow an exponential distribution, fracture size can be estimated from (*8*)—

$$\text{Fracture mean diameter} = (2/\pi)(\text{fracture mean trace length}, \quad (19)$$

which incorporates a correction for the bias due to fracture size.

The rationale and procedures for analysis that have been described in this section were applied to the measurement data for all three mines, which are presented in the next three sections. For each mine the sequence of data presentation is as follows:

I. Oriented Core
   - A. Analyses of fracture orientations (partitioning into clusters)
     1. Each drill hole individually.
     2. Groups of drill holes, pooled by drilling site in the mine.
   - B. Analyses of fracture spacings (without regard for fracture families)
     1. Along each drill core individually.
     2. Groups of drill cores, pooled by drilling site in the mine.
   - C. Analyses of fracture spacings within fracture families, for groups of drill holes, using the partitions established in I. A. 2. Results expressed as orthogonal spacings, taking account of cos δ.

II. Scanline Mapping
   - A. Analyses of fracture orientations (partitioning into clusters)
     1. Each mapping site individually.
     2. Groups of mapping sites, pooled by study area in the mine.
   - B. Analyses of fracture spacings (without regard for clusters)
     1. Along scanlines at each mapping site individually.
     2. Groups of mapping sites, pooled by study area in the mine.
   - C. Analyses of fracture spacings within clusters, for groups of mapping sites, using the partitions established in II. A. 2. Results expressed as orthogonal spacings, taking account of cos δ.
   - D. Analyses of fracture trace lengths within clusters using the partitions established in II. A. 2. or II. A. 1.

EXPLANATION OF PEA DIAGRAMS

For each mine a set of PEA (polar equal-area) diagrams is presented (*33*). These diagrams show the orientations of the individual fracture plane poles (normals) for each drill hole and each scanline mapping site, so that the reader can visualize the scatter in real-world data, its influence on the statistical measures, which are tabulated below the plots, and the contributions of each drill hole or mapping site to the results for the pooled sets of data.

Pooled data are represented in two forms, the FRACTAN-calculated "dense points" (*30*) and the individual fracture plane poles, to reveal the nature of the interpretation provided by the dense points. To portray the global sampling coverage achieved by the set of drill holes at each study site, one diagram gives the locus of fracture plane poles that deviate 60° or less from each of the drill hole orientations (since most of the poles lie within that locus).

In the PEA diagrams the following conventions are used:

1. To represent on the upper-hemisphere stereoplot the attitude of any axis, such as a drill hole, a scanline, or a pole, one plots a point with coordinates (a) the azimuth value corresponding to the upward-inclined direction of the axis and (b) the angle of inclination of the axis above the horizontal (0° plots on the circumference, 90° at the center).

2. Numerals corresponding to the cluster number represent the poles of the joint planes.

3. For oriented core, a large circled numeral denotes the orientation of the drill hole axis, which occupies a central orientation with respect to the poles found in that core. A dotted line indicates the zone in which all poles deviate 60° or less from the drill hole axis.

4. For scanline mapping, S denotes the scanline orientation. For a horizontal scanline on a vertical exposure (the usual case), S appears on the circumference (0° inclination) at the azimuth of that scanline. For a vertical scanline (San Manuel site 24) S appears at the center of the diagram.

5. For both oriented core and scanline mapping, 0 is plotted at the mean orientation of each cluster; the estimated number of fractures = observed number ÷ cos δ.

All the PEA plots for each mine are grouped at the end of the discussion of that mine, along with the relevant GDIST analyses.

LAKESHORE MINE DATA

The Lakeshore Mine is a porphyry-type copper deposit about 28 miles south of Casa Grande, AZ. Principal host rocks for the copper mineralization are andesite, porphyry (varying from quartz diorite to quartz monzonite), and metasediments, all of which are extensively shattered and moderately to strongly altered (*19*). The ore body is bounded on the east by the Lakeshore Fault, which dips westerly about 60°.

The ore body is shaped like a cap, the vertical dimension being the smallest, and pitches gently toward the northwest. The lower portion is a zone of primary mineralization. The upper portion of the ore body, the site of the present investigation, is disseminated oxide. Because of the chrysocolla and plentiful iron oxides present in the numerous fractures, the oxide ore mass is quite friable.

When the present data acquisition began, the oxide mine had just started into production, operating from the 1100 level, approximately 670 ft below the surface. No other underground workings existed that could have influenced the ground conditions at our data acquisition sites, although sulfide ore extraction had also begun, about 1,500 ft to the south. The oxide ore was developed for undercut-cave mining by successive blocks, progressing toward the northeast. The ore, undercut 15 ft above, dropped by gravity to the scraping drifts on the 1100 level, which is shown in plan view in figure 13.

Mapping of fractures on exposed drift walls, indicated as sites 1 to 15, was performed in January and May, 1976. The configuration of 50-ft-long mapping units essentially reflects the best area coverage that could be achieved from the exposures that were available in those periods, which were necessarily in the next block northeast of the then currently producing blocks.

Drilling to recover oriented cores, shown in figure 14, was conducted from October 26 to December 10, 1976; six holes were drilled 3 in in diameter and 100 ft long, all inclined 30° above the horizontal. A 17-ft-long section of the drift was left unconcreted temporarily to provide greater clearance for drilling, the bare drift measuring about 9 ft high by 12 ft wide. Drilling rates were 30 to 40 ft per shift. Hole 1 was drilled with a single-tube core barrel,

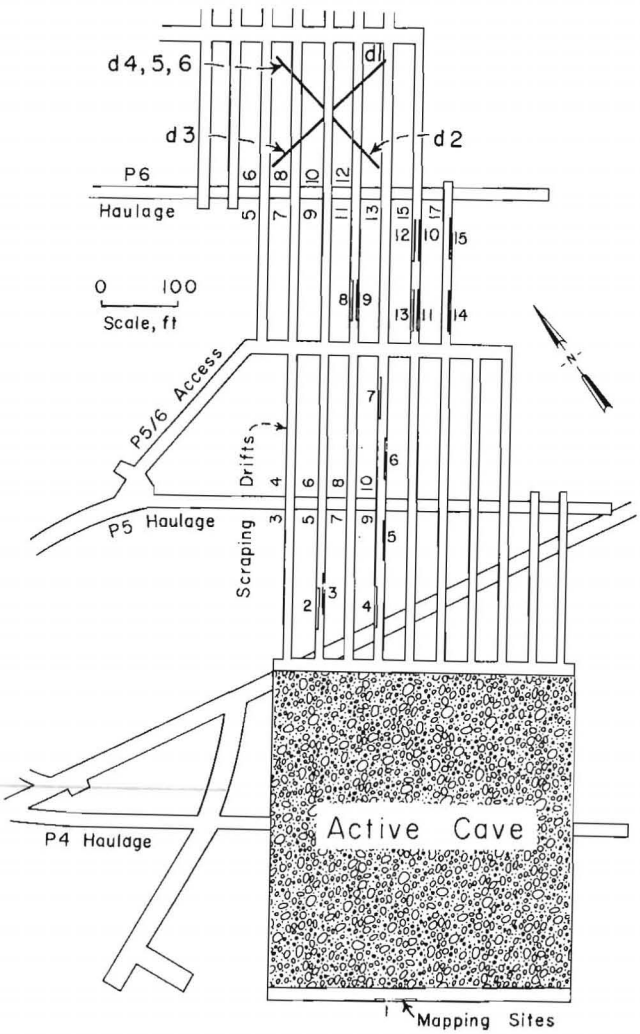

FIGURE 13.—Lakeshore Mine: Plan view of 1100 level showing scanline mapping sites 1 to 15 and diamond drill holes d1 to d6 for oriented core.

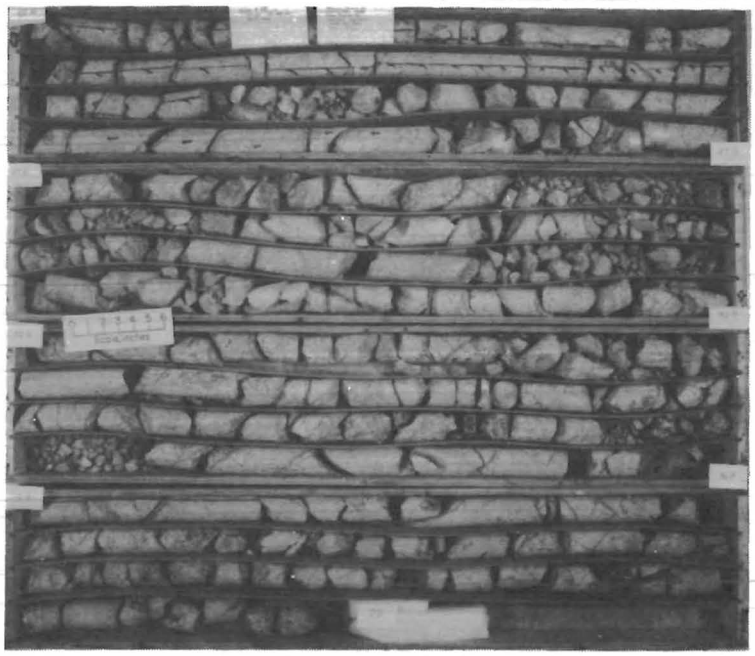

HOLE 1, 2 TO 62 FT

HOLE 5, 15 TO 56 FT

HOLE 2, 43 TO 100 FT

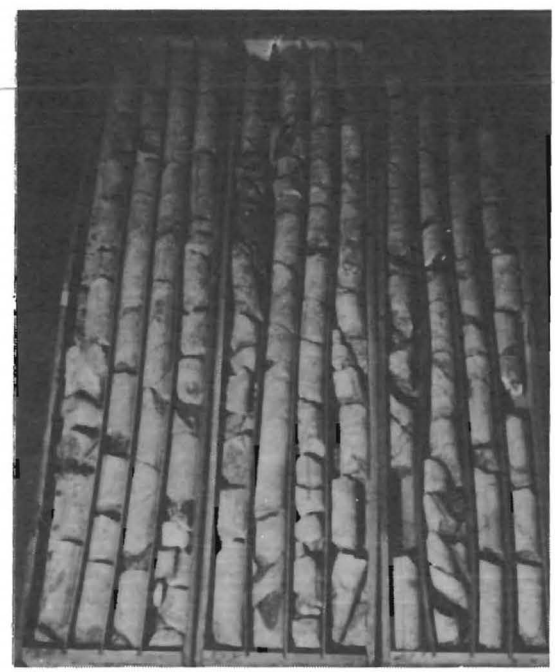

HOLE 6, 16 TO 62 FT

FIGURE 14.—Lakeshore Mine oriented diamond drill cores.

employing apparatus to scribe the core stump remaining in the drill hole. Results quickly showed that major changes were required to improve core recovery and especially core orientation. The use of a split, double-tube core barrel was then instituted, along with the impression method of core orienting, and this combination became the standard method for all subsequent oriented-core production. Holes 1 to 4 were drilled in vertical, mutually

perpendicular planes. Holes 5 and 6 were drilled parallel to hole 4, in a triangular configuration spaced at distances of 16, 30, and 34 in, with the objective of providing data to evaluate the reproducibility of results and the extents of the fractures intercepted, since otherwise there was no means of determining fracture extent from the drill hole data. However, the extent determinations could not be accepted with confidence because of the numerous difficulties encountered in attempting to correlate fractures between holes.

LAKESHORE ORIENTED CORE

Fracture Orientation

All the fracture orientations determined from the drill cores are presented in PEA diagrams, one for each drill hole, in figures 15 and 16. The best FRACTAN cluster solution is indicated by using the cluster number as the plotting symbol for each fracture-plane pole point. For each of the individual drill holes, the fracture-plane normals are concentrated within 60° of the drill hole axis. Because of this directional bias, the fracture patterns appear to be different for the four drilling directions which penetrate four octants of a 100-ft-radius sphere. Two alternative interpretations were considered: (1) Each of the four octants comprises a different population, or (2) each drill hole provides a different view of the same population. The latter explanation seems more acceptable, chiefly because of (1) the apparent underrepresentation of fracture-plane poles that deviate from the drill hole axis by more than 60° and (2) the evidence for commonality of fracture families in the several sets of data.

In addition to the cluster analyses for the six individual drill holes, FRACTAN partitions were made for the pooled data from parallel holes 4, 5, and 6 and for the pooled data from all six holes. The plotted results are shown in figures 17 and 18, respectively. To conserve space, PEA plots of dense points are shown only for pooled sets of data. The plots of the dense points are helpful in identifying significant clusters that are poorly represented in the data because they lie in the zones for which $\delta > 60°$.

Comparison of the mean orientations of the fracture families, as indicated by these eight analyses, reveal approximate correspondences at seven orientations, as listed by columns in table 2. Families whose orientations differ by 20° or more are commonly grouped together, which reflects in part the desire to identify similarities even if blocks of the rock mass may have been subjected to physical rotations in the geologic past, and in part the recognition of the large scatter in the data. Not only do the PEA plots for individual holes drilled in different directions exhibit substantial scatter about each mean fracture orientation, but the results obtained from the three parallel holes exhibit a similar variation, one from another. For example, of the four major clusters identified in hole 4 (clusters 2 and 5 are essentially one), two are not identified in holes 5 or 6; of the three clusters identified in hole 5, one is not identified in either hole 4 or hole 6; and of the five clusters identified in hole 6, three are not identified in either hole 4 or hole 5.

Nevertheless, the four fracture families obtained from the pooling of holes 4, 5, and 6 are identified on the average 58 pct of the time in holes 1, 2, and 3, the six families obtained from the all-holes-pooled data are identified on the average 58 pct of the time in holes 1 through 6, and any single hole exhibited on the average four of the seven correlatable cluster orientations. Figure 18*B*, which shows the 60° zones about the four drill hole orientations, helps to explain why fractures with certain orientations can be expected to be underrepresented in the data. This consistency as to fracture families among individual holes and pooled holes, given the occasional deviation of 20° to 30° between orientations for subsets of the same family, justifies the interpretation that all six holes are samples from the same population, and that the fracture pattern in the vicinity of the drilling location is best described in terms of the six families that are identified from the combined measurements in all six drill holes. These six families have relatively steep dips, to NE, ENE, SSW, SW, W, and NNW, four being 60° or more. A family of flat-dipping fractures may exist, having been identified in holes 2, 3, and 6, but apparently these fractures were not sufficiently numerous to be identifiable as a family in the all-holes-pooled data. The most prominent fracture orientation, exhibited in all six holes, dips steeply NNW.

TABLE 2.—Lakeshore oriented core: Mean dip and dip azimuth (dipaz) of clusters as determined by FRACTAN analysis

(Fracture families grouped to show correlations; below each dip, dipaz pair is given the corresponding W3/n)

Drill hole	Dip direction, deg							
	0-360 Flat	30-46 NE	60-70 ENE	181-209 SSW	229-254 SW	267-292 W	337-2 NNW	Not correlated
1	—	60, 35 45/55	51, 60 34/39	—	86, 254 39/42	62, 275 24/28	78, 316 14/15	60, 113 155/228
2	6, 166 13/13	88, 46 28/30	—	72, 181 232/348	—	—	84, 311 15/16	35, 106 36/39
3	21, 171 25/28	—	—	52, 209 22/23	—	68, 275 340/500	61, 337 10/10	—
4	—	—	58, 60 32/34	58, 204 62/68	86, 230 45/48	—	66, 351 268/402 63, 339 21/21	—
5	—	—	84, 68 21/23	—	—	66, 292 22/24	69, 2 236/332	—
6	9, 285 26/29	89, 32 86/100	55, 62 27/31	—	—	—	72, 344 141/166	39, 14 21/22
4+5+6	6, 314 52/57	—	58, 63 80/87	—	86, 236 74/79	—	72, 357 741/1077	—
1+2+3+4+5+6	—	72, 30 337/387	48, 70 236/280	39, 201 131/150	60, 229 98/104	71, 267 376/452	80, 338 892/1318	—

— No appropriate cluster identified.

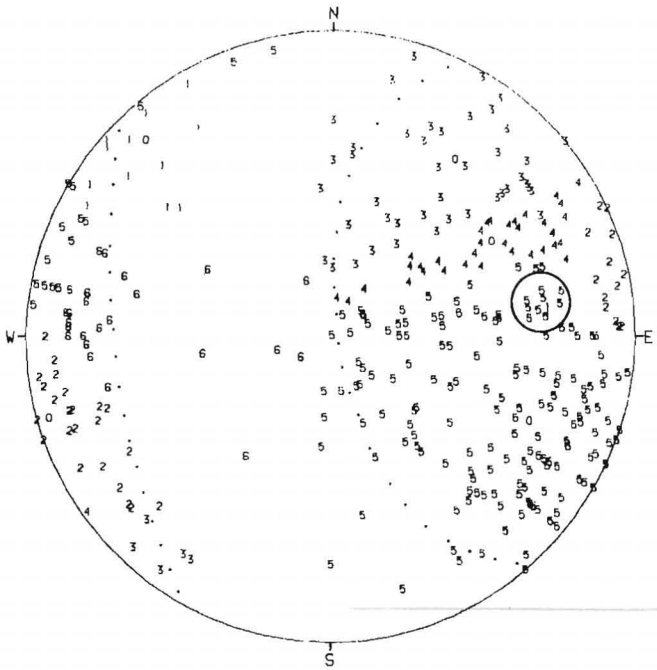

HOLE 1

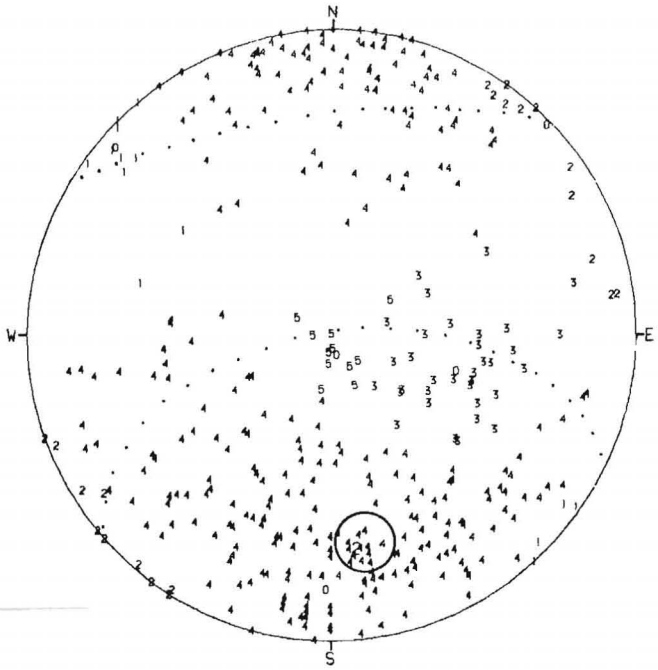

HOLE 2

FRACTAN r	Clusters					Eigenvalues		
	No.	Obs	Est	Dip	Az	W1	W2	W3
				HOLE 1 (INCL +29, AZ 83)				
9.00	1	15	36	78	316	0	1	14
	2	42	51	86	254	1	2	39
	3	55	73	60	35	2	8	45
	4	39	42	51	60	0	5	34
	5	205	228	60	113	17	34	155
	6	28	53	62	275	1	3	24
				HOLE 2 (INCL +30, AZ 173)				
10.50	1	16	27	84	311	0	1	15
	2	30	58	88	46	0	2	28
	3	39	65	35	106	1	2	36
	4	348	358	72	181	51	65	232
	5	13	22	6	166	0	0	13
				HOLE 3 (INCL +28, AZ 263)				
10.00	1	10	23	61	337	0	0	10
	2	23	33	52	209	0	1	22
	3	28	66	21	171	1	2	25
	4	500	513	68	275	77	83	340

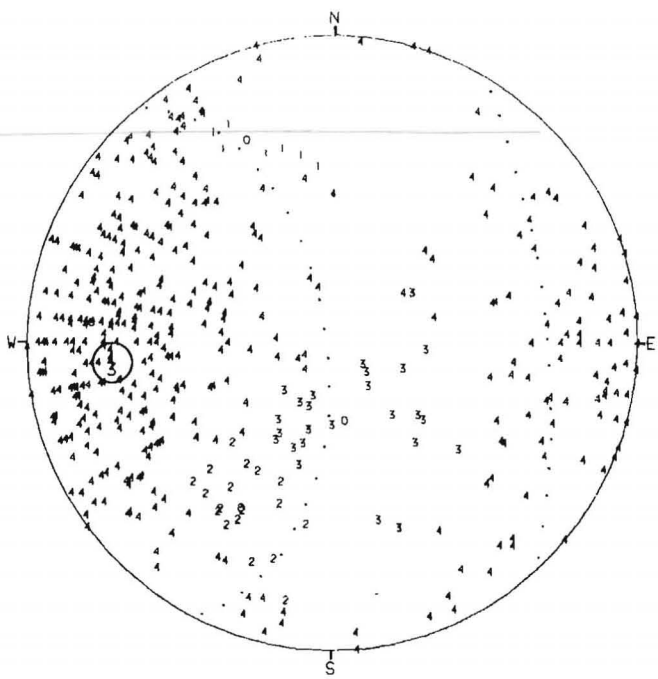

HOLE 3

FIGURE 15.—Lakeshore Mine oriented core, holes 1, 2, and 3, polar equal-area plots, upper hemisphere.

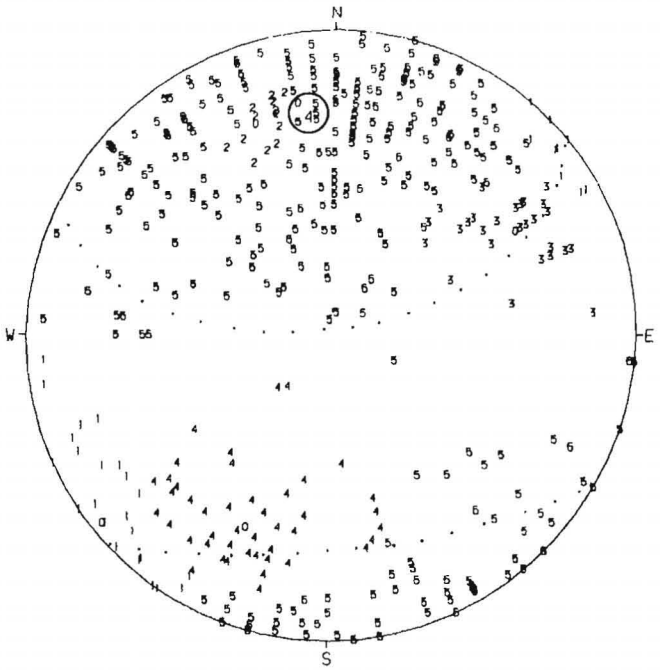

HOLE 4

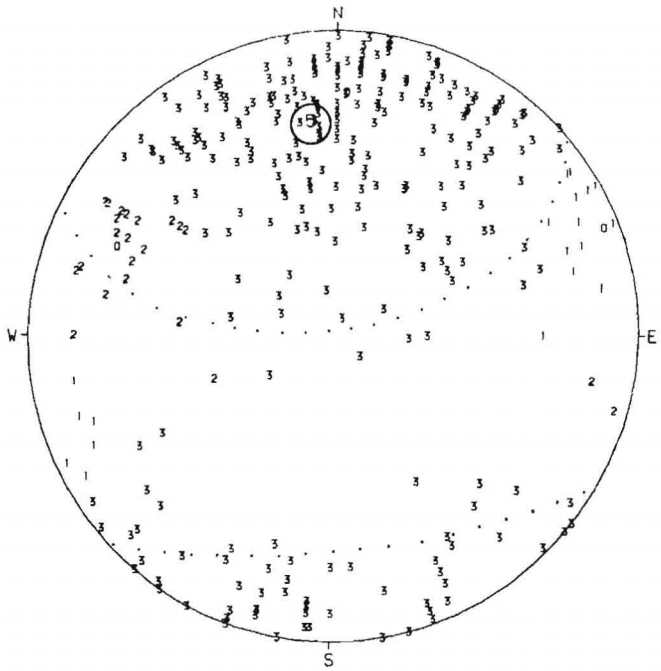

HOLE 5

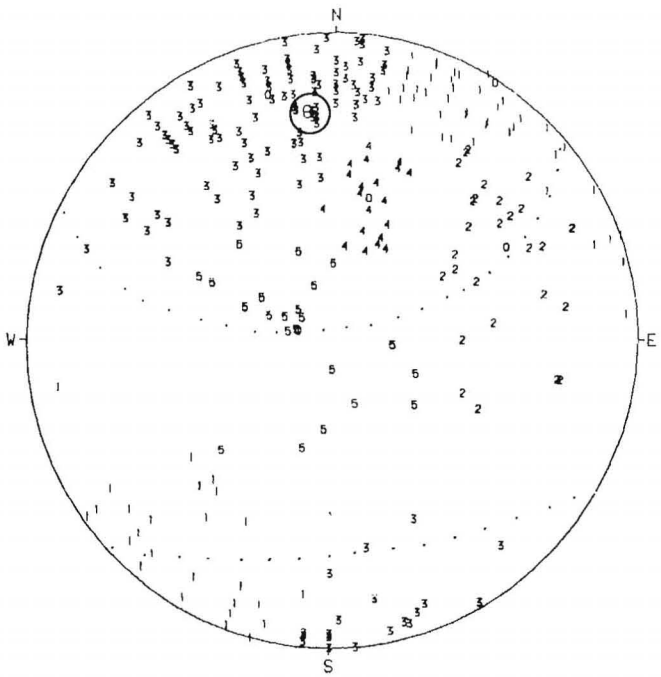

HOLE 6

FRACTAN r	Clusters					Eigenvalues		
	No.	Obs	Est	Dip	Az	W1	W2	W3
			HOLE 4 (INCL +29, AZ 353)					
9.00	1	48	110	86	230	1	2	45
	2	21	22	63	339	0	0	21
	3	34	61	58	60	1	1	32
	4	68	182	58	204	2	3	62
	5	402	404	66	351	59	75	268
			HOLE 5 (INCL +30, AZ 353)					
10.50	1	23	83	84	68	1	1	21
	2	24	40	66	292	1	1	22
	3	332	339	69	2	45	51	236
			HOLE 6 (INCL +26, AZ 353)					
11.00	1	100	144	89	32	6	8	86
	2	31	59	55	62	1	3	27
	3	166	170	72	344	9	16	141
	4	22	25	39	14	0	1	21
	5	29	60	9	285	1	3	26

FIGURE 16.—Lakeshore Mine oriented core, holes 4, 5, and 6, polar equal-area plots, upper hemisphere.

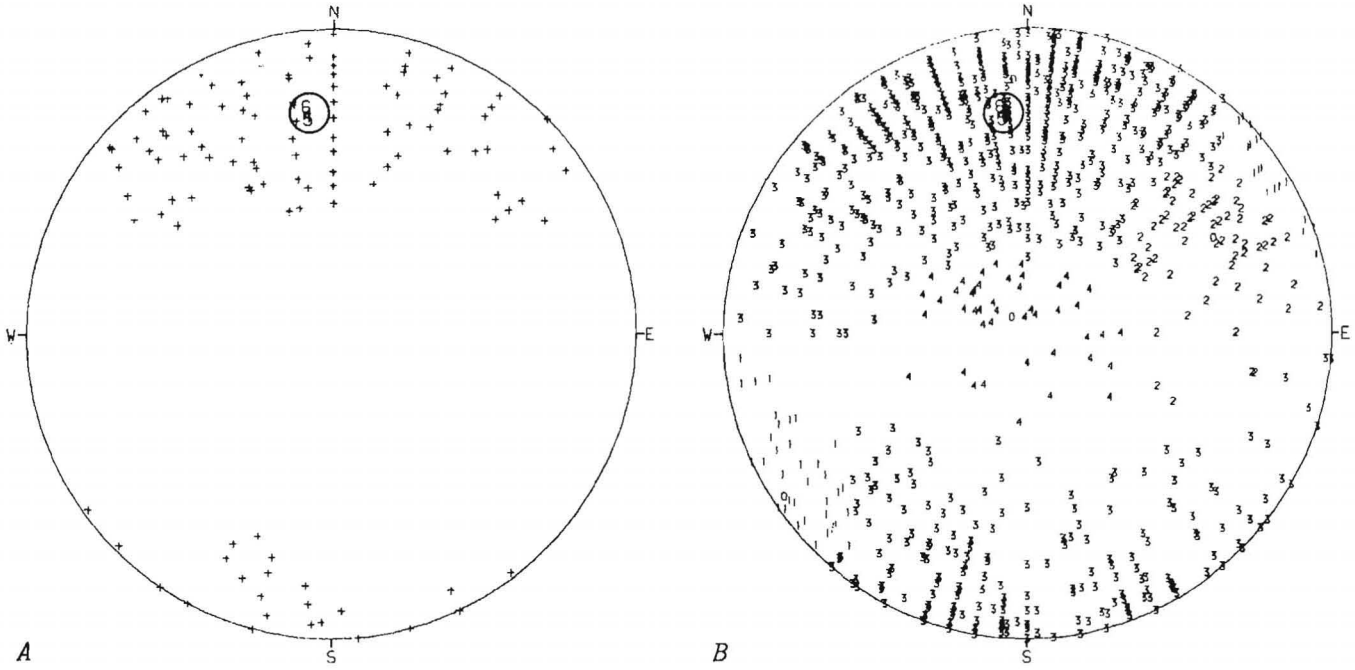

FRACTAN r	Clusters				Eigenvalues		
	No.	Obs	Dip	Az	W1	W2	W3
HOLES 4 + 5 + 6 POOLED							
9.00	1	79	86	236	2	3	74
	2	87	58	63	3	4	80
	3	1077	72	357	128	208	741
	4	57	6	314	1	3	52

FIGURE 17.—Lakeshore Mine oriented core, pooled holes 4 + 5 + 6, polar equal-area plots, upper hemisphere. *A*, Dense points determined by FRACTAN cluster solution; *B*, numerals corresponding to the cluster numbers denote the poles of the joint planes.

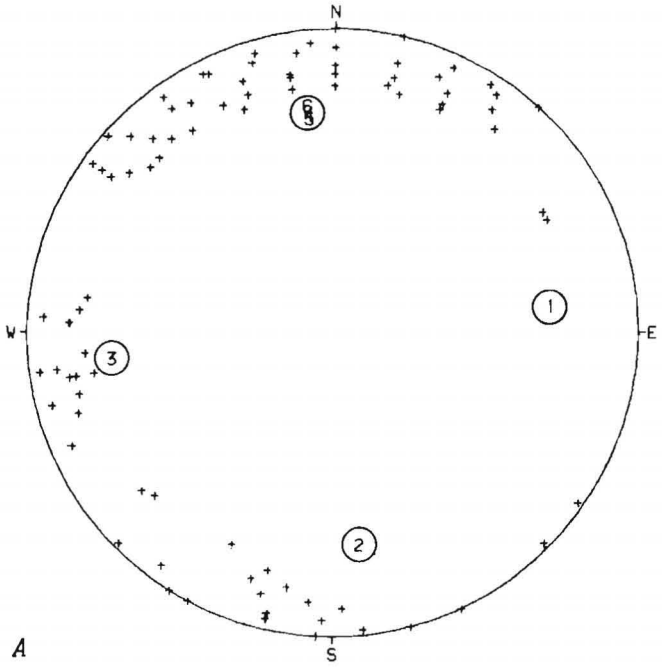

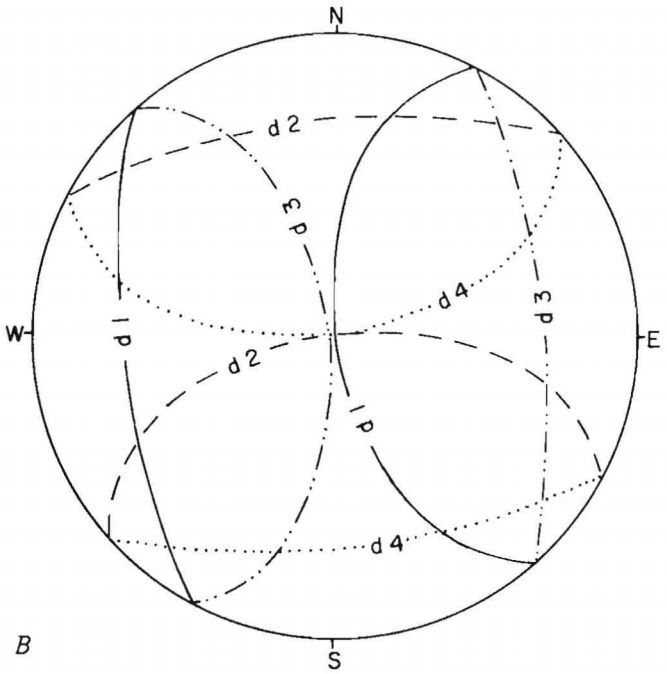

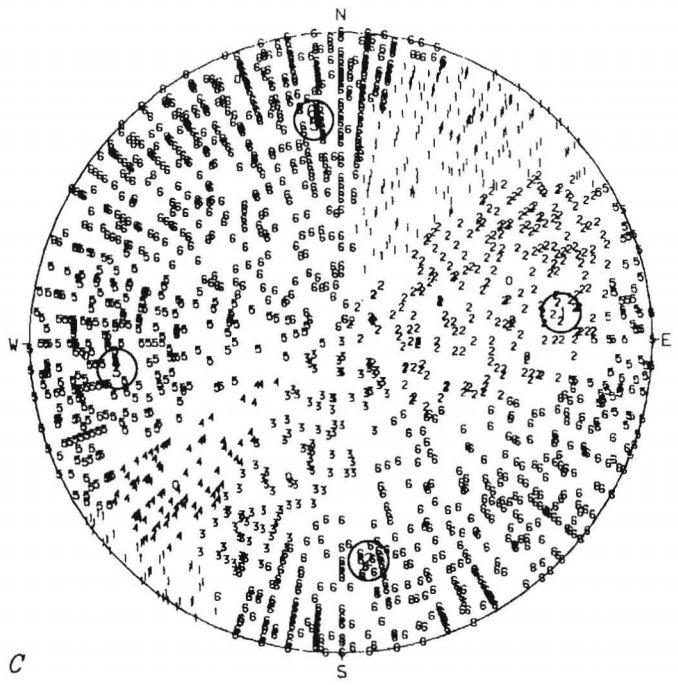

FRACTAN r	Clusters				Eigenvalues		
	No.	Obs	Dip	Az	W1	W2	W3
HOLES 1+2+3+4+5+6 POOLED							
9.50	1	387	72	30	10	40	337
	2	280	48	70	12	32	236
	3	150	39	201	2	18	131
	4	104	60	229	1	5	98
	5	452	71	267	20	56	376
	6	1318	80	338	185	242	892

FIGURE 18.—Lakeshore Mine oriented core, pooled holes 1 + 2 + 3 + 4 + 5 + 6, polar equal-area plots, upper hemisphere. *A*, Dense points determined by FRACTAN cluster solution; *B*, 60° cones about the four drill hole directions; *C*, numerals corresponding to the cluster numbers denote the poles of the joint planes.

Fracture Spacing

The spacings between successive fractures along the drill cores, without regard for fracture families, are shown in figure 19. The spacings, best describable by an exponential distribution, are quite small in all four directions, the median spacing ranging from 0.25 to 0.31 ft.

The spacings between successive fractures of similar orientation are shown in figure 20. These results were obtained from the pooled data for all six drill holes, as follows: The FRACTAN cluster analysis, figure 18, partitioned the fractures into six clusters. For each drill hole the orthogonal fracture spacings within a given cluster were computed by equation 1, using the appropriate value of δ corresponding to the mean orientation of that cluster with respect to the drill hole in question. The orthogonal spacings for a given cluster were pooled for all six holes and analyzed by GDIST. The same procedure was employed with respect to the pooled data for holes 4, 5, and 6 based on the partitions shown in figure 17. The best fitting distribution is the exponential or the chi squared; the lognormal is usually also an acceptable form.

The statistics for the orthogonal spacings within fracture families exhibit large differences among the families. The median spacing ranges from 0.32 to 1.47 ft for the all-holes-pooled data, and from 0.28 to 1.91 ft for the holes 4+5+6 pooled data. In both poolings, the smallest spacing is exhibited by the family that dips steeply NNW. The next to smallest spacing is that of cluster 5, all holes pooled, which dips steeply W. The flat-lying fracture family, identified as cluster 4 of the holes 4+5+6 pooling, exhibits the largest spacing of any listed family.

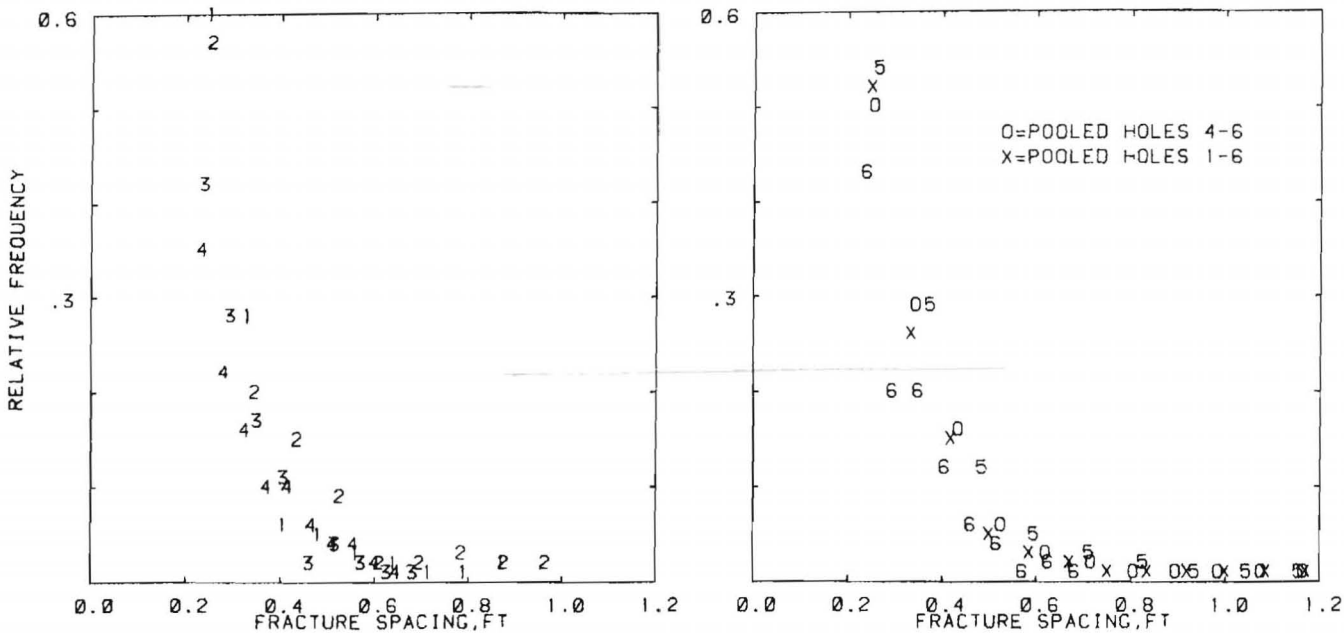

Drill hole	1	2	3	4	5	6	Pooled 4+5+6	Pooled 1 to 6
Spacings observed	207	198	202	266	251	236	753	1,360
Maximum ft	0.90	1.00	0.70	0.66	1.20	0.70	1.20	1.20
Mininum ft	0.20	0.20	0.20	0.20	0.20	0.20	0.20	0.20
Arithmetic mean ft	0.29	0.32	0.29	0.31	0.34	0.31	0.32	0.31
Median ft	0.25	0.28	0.28	0.28	0.31	0.30	0.30	0.28
Mode ft	0.20	0.20	ND	0.20	0.20	0.25	0.20	0.20
Std dev ft	0.12	0.14	0.08	0.10	0.14	0.09	0.11	0.11
Skewness	2.63	2.13	1.46	1.12	2.06	1.17	1.94	2.13
Mean log of spacing	−1.30	−1.22	−1.26	−1.23	−1.15	−1.22	−1.20	−1.23
Std dev of logs	0.31	0.35	0.25	0.29	0.35	0.28	0.31	0.31
Distributions[1]	None	None	E	E	L,E	E	None	None
Best fit	E	E	E	E	E	E	E	E

ND No appropriate value was determinable.
[1] Acceptable fit at the 5-pct significance level (L = lognormal, E = exponential).

FIGURE 19.—Lakeshore Mine oriented core, GDIST analyses of the spacing between successive fractures as measured along drill core. Relative frequency (spacings in each class ÷ total spacings) is plotted at the midpoint of the corresponding class interval; the numeral indicating the drill hole number is centered on the plotted point. Below the histograms are listed the parameters of the distributions.

Summary, Lakeshore Oriented Core

Within the six drill holes, six steeply dipping and one flat-lying family of fractures are identifiable. The family that dips steeply NNW is identified most consistently in the cluster solutions and exhibits the smallest orthogonal spacing. Fracture families dip steeply to all quadrants except the SE. The flat-lying family is identified in only three of the four drilling directions (three of the six holes), probably because (1) its mean orientation borders the 60° zone for all six holes and (2) its frequency of occurrence (1/spacing) is less than those of the more numerous, steeply dipping families.

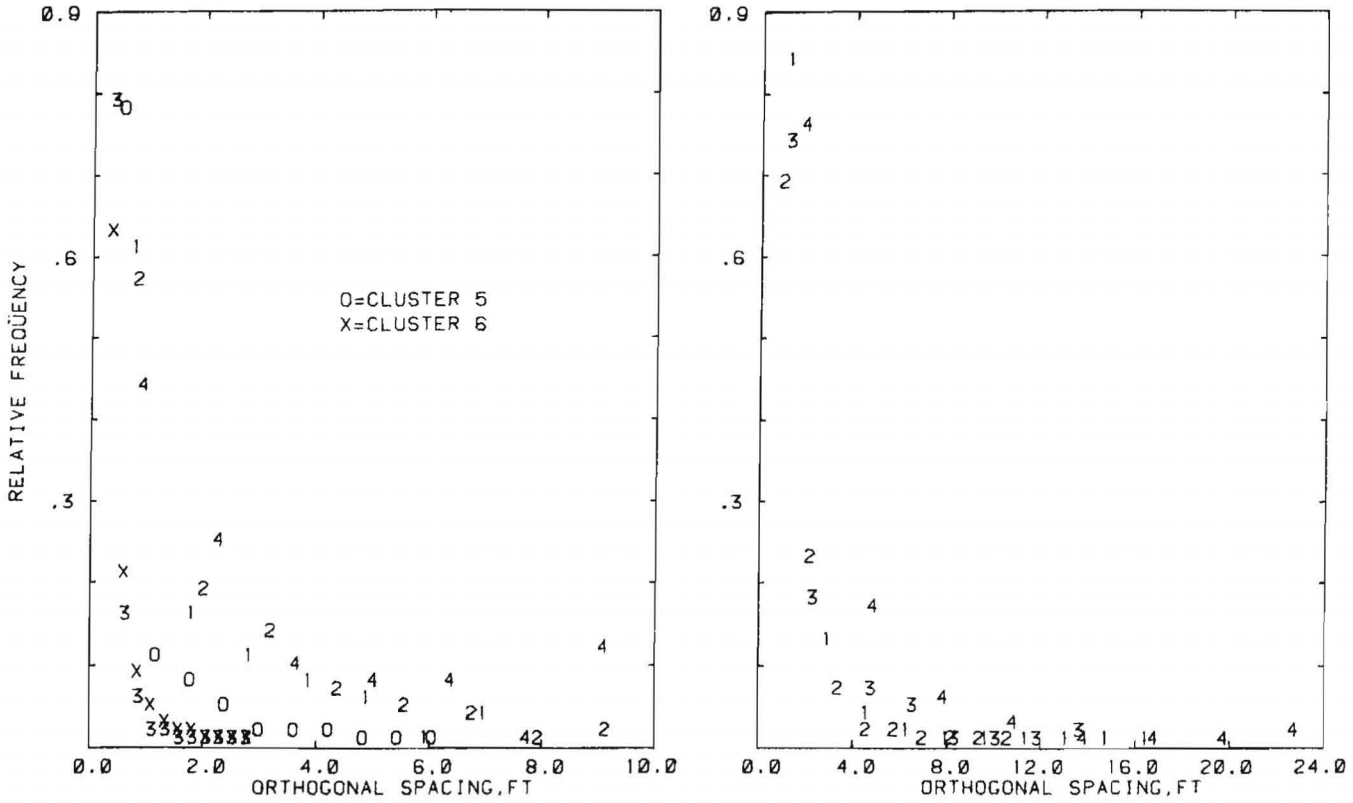

	Pooled holes 1+2+3+4+5+6						Pooled holes 4+5+6			
Cluster	1	2	3	4	5	6	1	2	3	4
Spacings observed	322	219	107	85	303	745	60	72	635	46
Maximum ft	17.05	10.96	14.29	23.98	6.25	2.83	7.38	9.61	2.81	9.67
Minimum ft	0.16	0.15	0.15	0.17	0.16	0.15	0.16	0.15	0.18	0.15
Arithmetic mean ft	1.17	1.20	1.56	2.61	0.69	0.44	1.54	1.85	0.35	2.78
Median ft	0.66	0.78	0.77	1.47	0.39	0.32	0.91	0.94	0.28	1.91
Mode ft	0.16	0.19	0.22	0.17	ND	0.23	0.45	ND	0.18	0.28
Std dev ft	1.62	1.40	1.92	3.30	0.77	0.34	1.63	1.91	0.22	2.84
Skewness	5.01	3.63	3.32	3.66	3.09	2.79	1.62	1.64	4.18	1.13
Mean log of spacing	−0.35	−0.26	−0.12	0.39	−0.74	−1.01	−0.10	0.08	−1.18	0.40
Std dev of logs	0.97	0.93	1.07	1.10	0.78	0.58	1.05	1.09	0.46	1.24
Distributions[1]	L,χ	L,E	L,E,χ	L,E,χ	χ	None	L,E,χ	L,E,χ,Γ	None	L,E
Best fit	L	E	χ	E	χ	E	χ	χ	E	E

ND No appropriate value was determinable.
[1] Acceptable fit at the 5-pct significance level (L = lognormal, E = exponential), χ = chi squared, Γ = gamma).

FIGURE 20.—Lakeshore Mine oriented core, GDIST analyses of orthogonal fracture spacing within fracture families. Left, Pooled drill holes 1 to 6; right, pooled holes 4 to 6. Relative frequency (spacing in each class ÷ total spacings) is plotted at the midpoint of the class interval; the numeral indicating the cluster number is centered on the plotted point. Below the histograms are listed the parameters of the distributions.

LAKESHORE MULTIPLE SCANLINE MAPPING

Fracture Orientation

All the fracture orientations determined by the scanline mapping are presented in PEA diagrams, one for each mapping site, figures 21 to 24, which also show the best FRACTAN partitioning into clusters. As is true of the fracture pattern in the oriented drill cores, the best interpretation appears to be obtained by combining the results from several sites to form larger sampling groups. Sites 2 to 7 and 8 to 15 comprise simple geographic groupings, each group representing a mining panel. FRACTAN partitions, figure 25, were made for the pooled data from these two groups of sites.

The PEA diagrams suggest that either the flat-lying fractures are few in number or there is a minor bias against identifying fractures of slight dip on a vertical exposure. Evidence of a bias with respect to fracture azimuth is not persuasive.

Comparisons of the mean orientations of the fracture families, as derived from the FRACTAN analyses of the data sets for the 15 individual sites and the 2 poolings, reveal approximate correspondences at 5 orientations, listed by column in table 3. On the average, an individual site exhibits three of these five most prominent fracture families. All five of these families dip steeply; the dip direction for four families ranges from S to NW. The E- and S-dipping families are essentially absent from sites 2 to 7; six of the eight sites 8 to 15 exhibit either the SSW- or the WSW-dipping family, but not both; the NW-dipping family is present at all 15 sites. The clusters listed as "not correlated" (table 3) are in all instances small relative to the total number of fractures mapped at any site.

TABLE 3.—Lakeshore scanline mapping: Mean dip and dip azimuth (dipaz) of clusters as determined by FRACTAN analysis

(Fracture families grouped to show correlations; dip given in two opposite directions (e.g., N–S) implies approximately vertical orientation; below each dip, dipaz pair is given the corresponding W3/n)

Mapping site	Dip direction, deg					
	74-116 E	10-20, 172-196 N-S	175-217 SSW	226-268 WSW	137-161, 300-346 NW	Not correlated
1	90, 106 22/24	—	—	74, 226 85/101	80, 161 48/52	37, 38 11/12 63, 270 12/12
2	—	—	54, 188 28/32	88, 256 24/26	88, 137 85/93	53, 58 15/18 81, 218 11/12 47, 267 19/21
3	—	—	—	68, 250 26/30	89, 140 117/170	61, 6 12/13 45, 55 18/20
4	—	—	64, 192 12/13	86, 248 36/48	85, 310 42/46 87, 332 6/6	90, 39 6/6 72, 156 6/6
5	—	—	70, 188 7/8	86, 64 20/25	87, 320 88/107	—
6	—	76, 20 9/10	69, 195 16/17	81, 235 39/47	88, 315 89/117	—
7	—	87, 10 18/20	64, 205 8/8	80, 240 10/10	83, 304 93/133	57, 242 22/24
Pooled 2 to 7	—	—	70, 202 43/45	84, 244 249/339	89, 321 536/702	—
8	69, 74 20/24	—	56, 217 14/15	78, 234 14/14	87, 324 98/126	79, 269 11/12
9	66, 81 22/26	—	70, 198 57/68	—	77, 307 63/74 83, 345 10/10	66, 152 10/11
10	—	80, 196 33/40	—	—	76, 309 114/155	—
11	—	84, 172 25/29	—	—	80, 300 102/128	—
12	58, 94 14/16	—	61, 199 26/28	—	78, 311 100/135	—
13	42, 91 16/18	89, 16 13/14	62, 175 26/29	68, 243 13/14	78, 305 93/114	—
14	39, 104 16/18	85, 185 55/65	—	—	73, 300 112/135	—
15	78, 81 18/23	—	—	71, 242 9/9	86, 326 91/118	—
Pooled 8 to 15	84, 116 48/52	74, 12 46/51 72, 179 260/307	60, 215 61/66	86, 268 281/355	78, 315 518/571 88, 346 26/26	48, 282 22/23 60, 334 16/17

— No appropriate cluster identified.

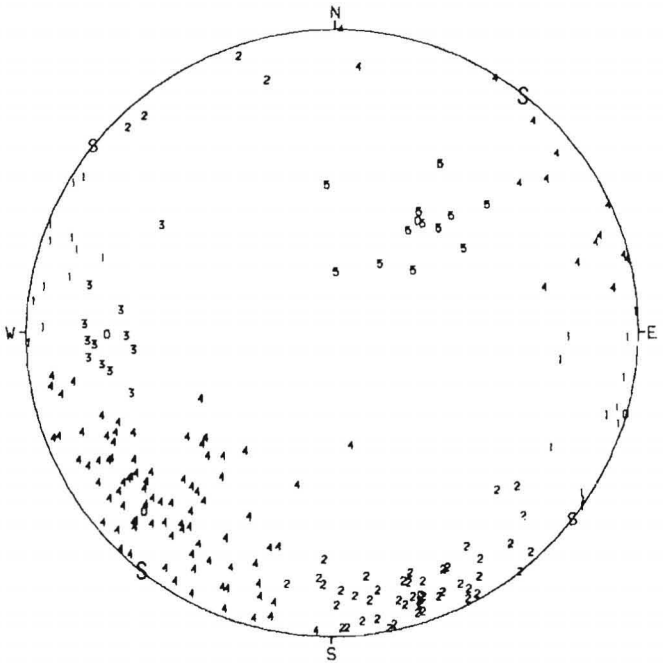

SITE 1

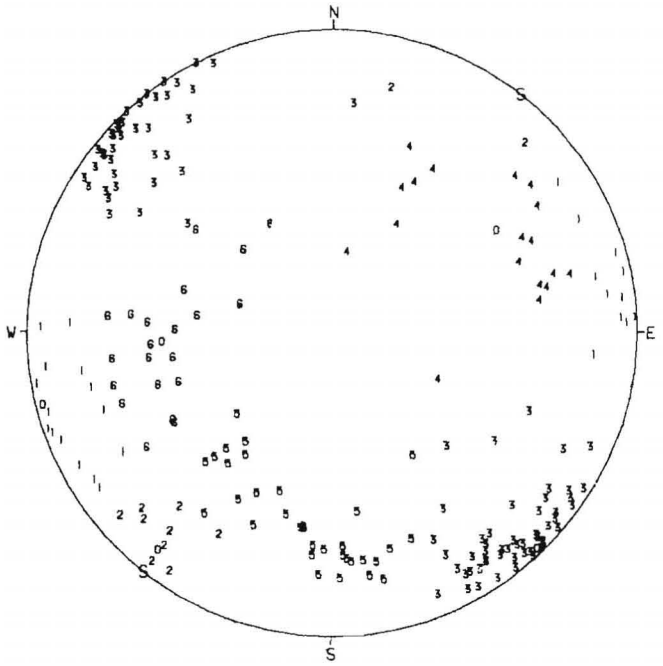

SITE 2

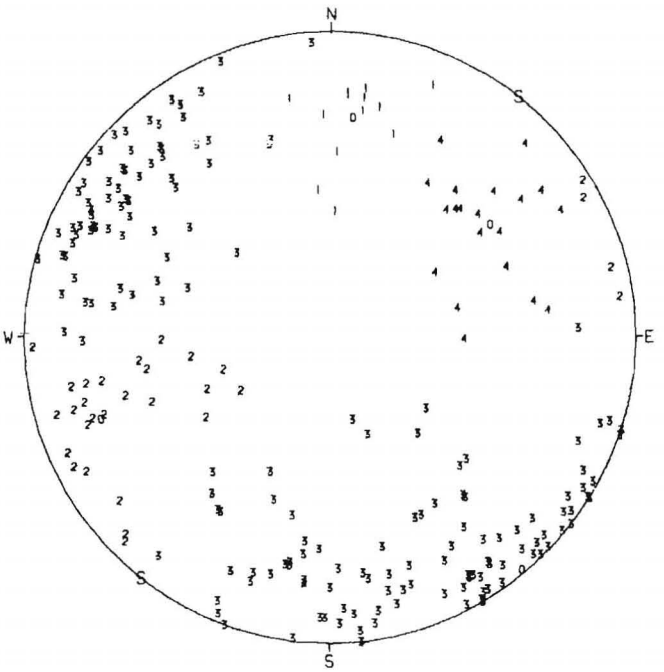

SITE 3

FRACTAN r	Clusters				Eigenvalues		
	No.	Obs	Dip	Az	W1	W2	W3
			SITE 1				
10.00	1	24	90	106	1	1	22
	2	52	80	161	1	3	48
	3	12	63	270	0	0	12
	4	101	74	226	6	10	85
	5	12	37	38	0	1	11
			SITE 2				
11.00	1	26	88	256	1	1	24
	2	12	81	218	0	1	11
	3	93	88	137	3	5	85
	4	18	53	58	1	2	15
	5	32	54	188	1	3	28
	6	21	47	267	0	2	19
			SITE 3				
10.00	1	13	61	6	0	1	12
	2	30	68	250	1	3	26
	3	170	89	140	11	42	117
	4	20	54	55	1	1	18

FIGURE 21.—Lakeshore Mine scanline mapping, sites, 1, 2, and 3, polar equal-area plots, upper hemisphere.

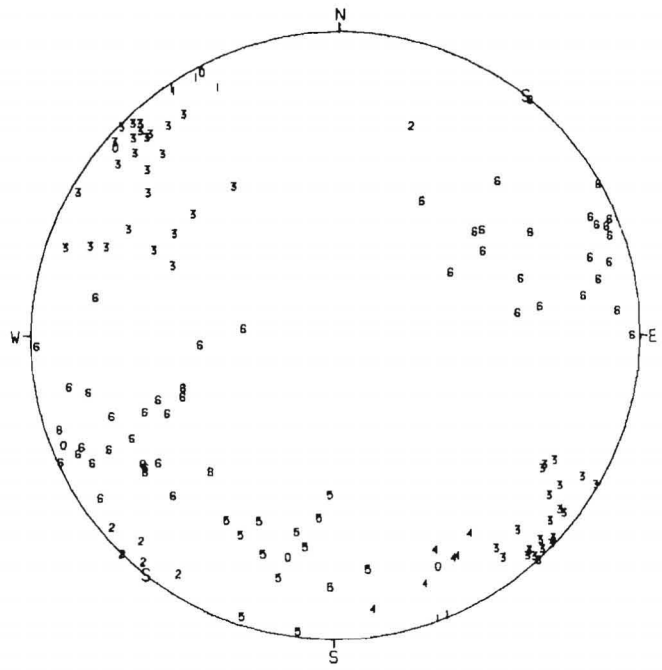

SITE 4

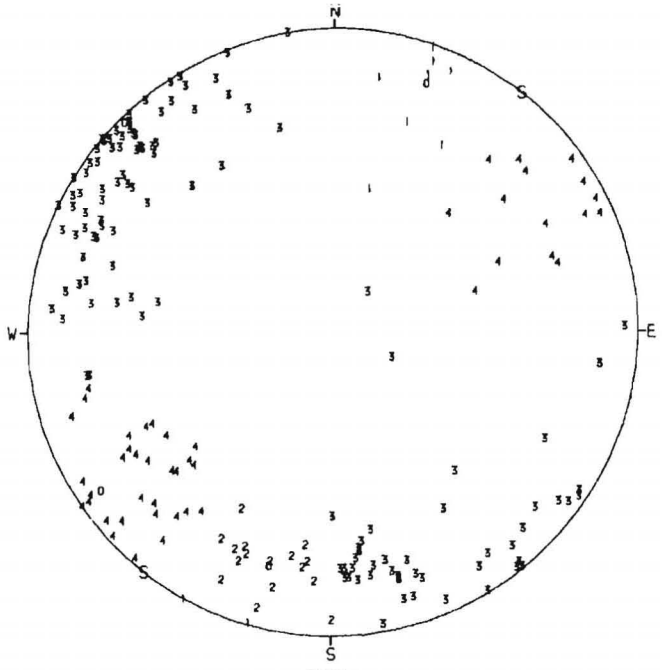

SITE 6

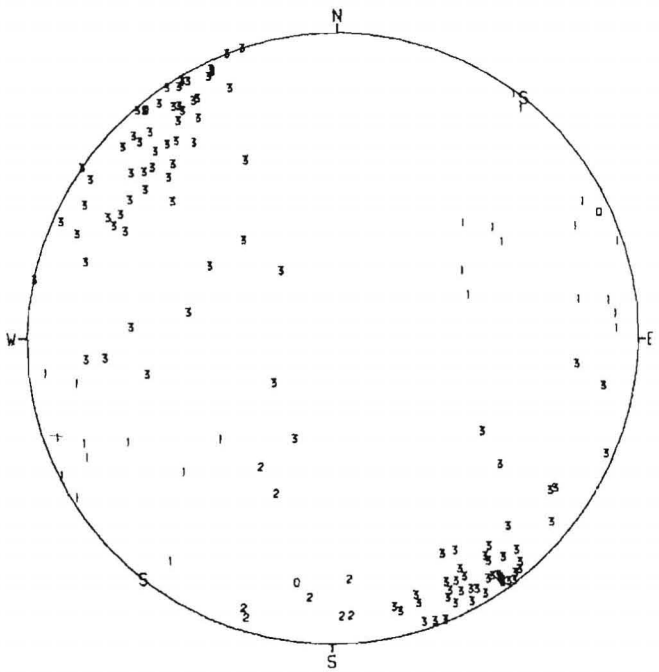

SITE 5

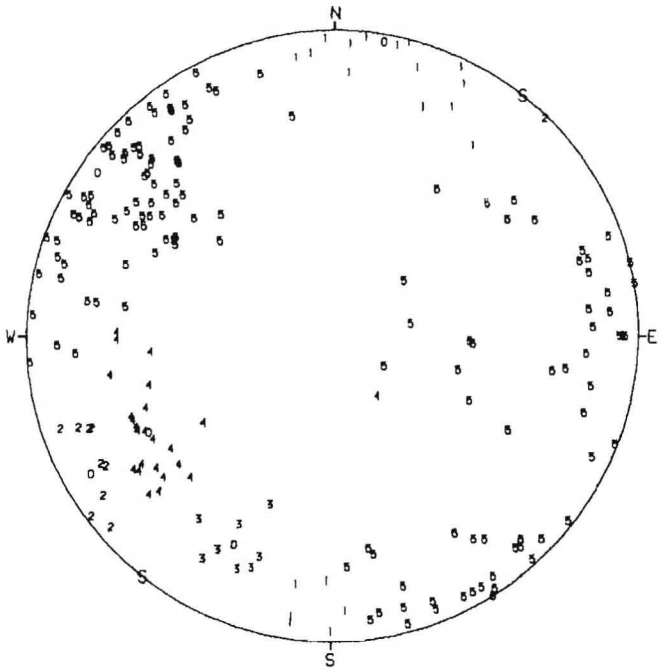

SITE 7

FRACTAN r	Clusters				Eigenvalues		
	No.	Obs	Dip	Az	W1	W2	W3
			SITE 4				
11.00	1	6	87	332	0	0	6
	2	6	90	39	0	0	6
	3	46	85	310	1	3	42
	4	6	72	156	0	0	6
	5	13	64	192	0	1	12
	6	48	86	248	2	10	36
			SITE 5				
11.00	1	25	86	64	1	4	20
	2	8	70	188	0	1	7
	3	107	87	320	6	13	88

FRACTAN r	Clusters				Eigenvalues		
	No.	Obs	Dip	Az	W1	W2	W3
			SITE 6				
11.00	1	10	76	20	0	1	9
	2	17	69	195	0	0	16
	3	117	88	315	6	22	89
	4	47	81	235	1	7	39
			SITE 7				
11.00	1	20	87	10	0	1	18
	2	10	80	240	0	0	10
	3	8	64	205	0	0	8
	4	24	57	242	1	1	22
	5	133	83	304	15	25	93

FIGURE 22.—Lakeshore Mine scanline mapping, sites 4, 5, 6, and 7, polar equal-area plots, upper hemisphere.

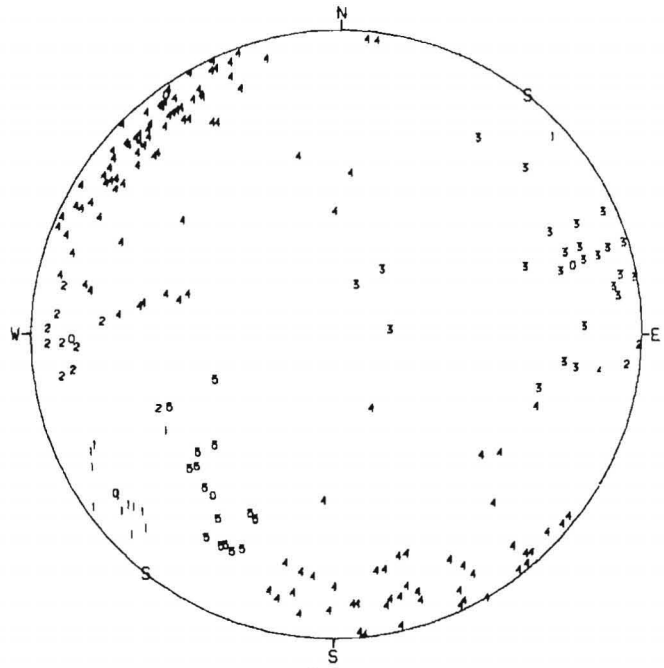

SITE 8

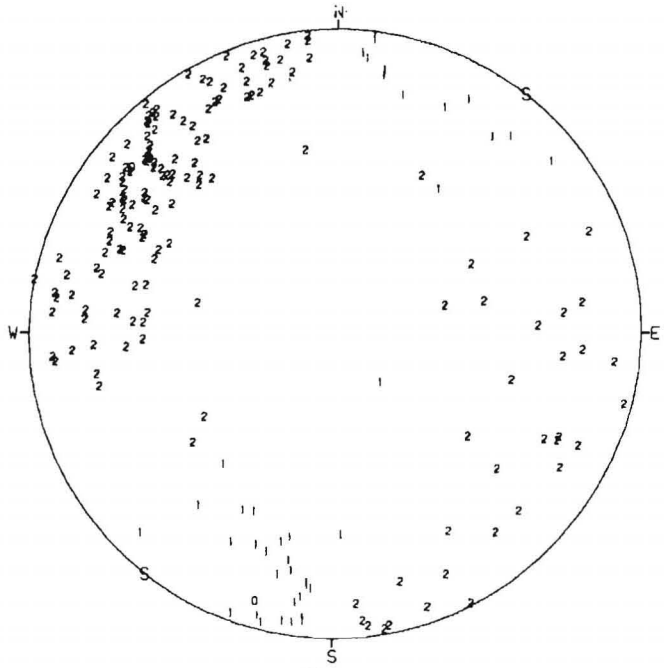

SITE 10

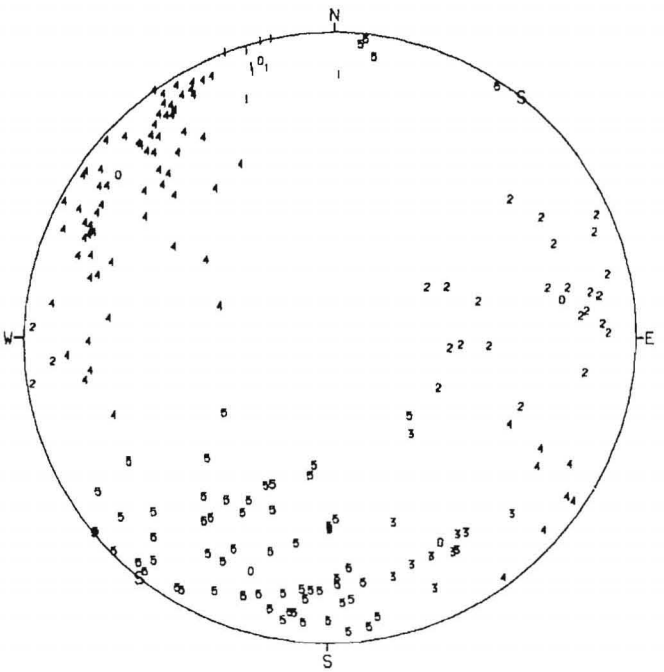

SITE 9

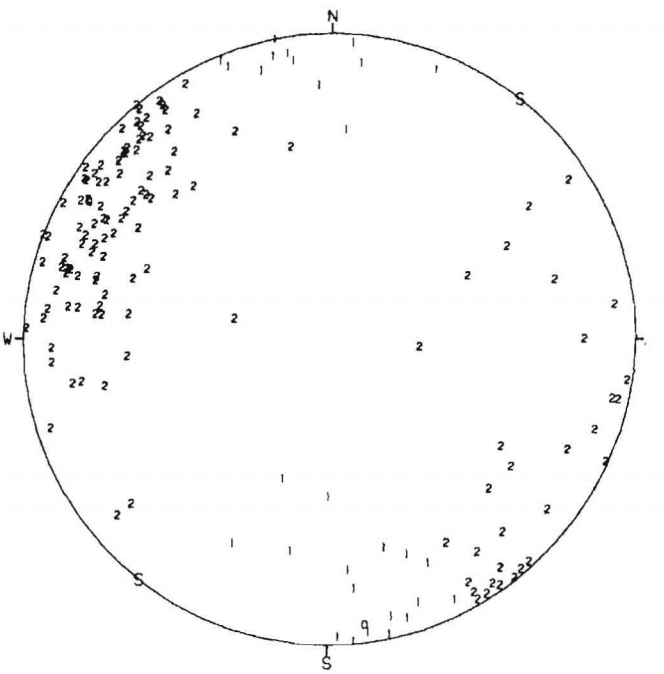

SITE 11

FRACTAN r	Clusters				Eigenvalues		
	No.	Obs	Dip	Az	W1	W2	W3
			SITE 8				
11.00	1	14	78	234	0	0	14
	2	12	79	269	0	1	11
	3	24	69	74	1	3	20
	4	126	87	324	7	20	98
	5	15	56	217	0	1	14
			SITE 9				
10.50	1	10	83	345	0	0	10
	2	26	66	81	1	3	22
	3	11	66	152	0	0	10
	4	74	77	307	4	7	63
	5	68	70	198	5	6	57

FRACTAN r	Clusters				Eigenvalues		
	No.	Obs	Dip	Az	W1	W2	W3
			SITE 10				
11.00	1	40	80	196	2	5	33
	2	155	76	309	15	26	114
			SITE 11				
10.50	1	29	84	172	1	3	25
	2	128	80	300	10	16	102

FIGURE 23.—Lakeshore Mine scanline mapping, sites 8, 9, 10, and 11, polar equal-area plots, upper hemisphere.

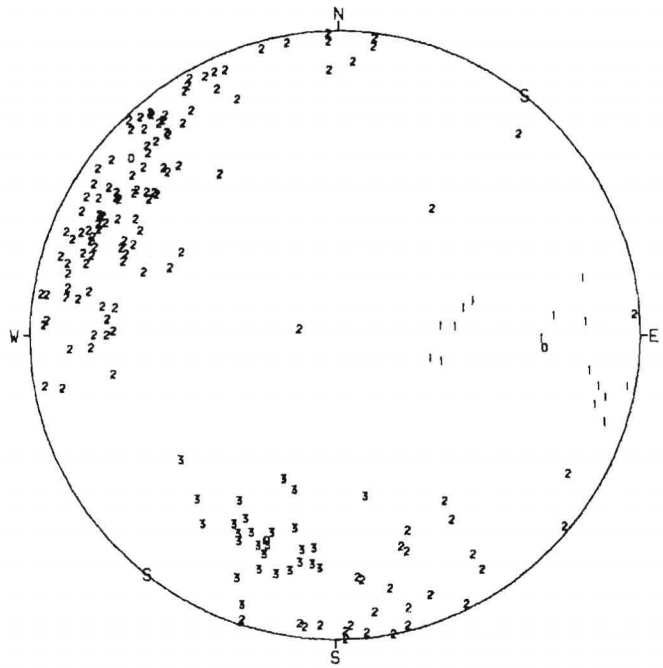

SITE 12

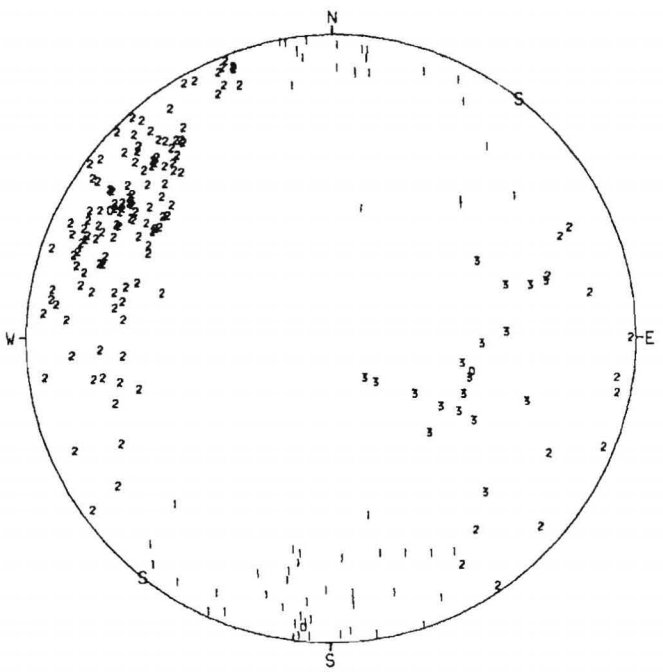

SITE 14

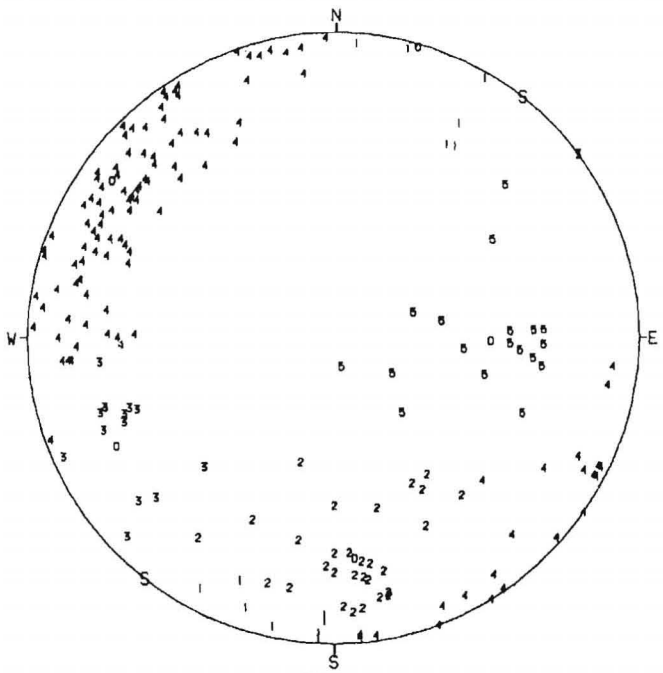

SITE 13

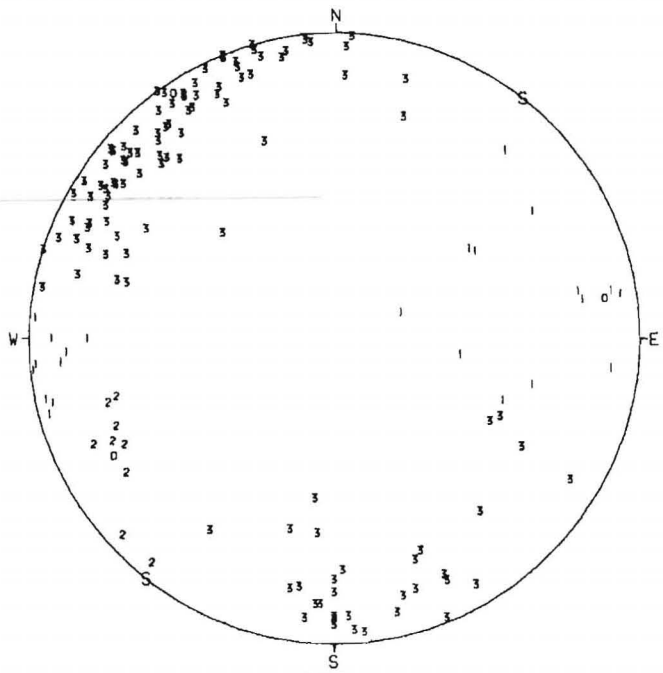

SITE 15

FRACTAN r	Clusters				Eigenvalues		
	No.	Obs	Dip	Az	W1	W2	W3
			SITE 12				
10.50	1	16	58	94	0	2	14
	2	135	78	311	6	29	100
	3	28	61	199	1	1	26
			SITE 13				
10.50	1	14	89	16	0	1	13
	2	29	62	175	1	2	26
	3	14	68	243	0	1	13
	4	114	78	305	4	17	93
	5	18	42	91	1	2	16

FRACTAN r	Clusters				Eigenvalues		
	No.	Obs	Dip	Az	W1	W2	W3
			SITE 14				
10.50	1	65	85	185	4	7	55
	2	135	73	300	6	17	112
	3	18	39	104	1	2	16
			SITE 15				
10.50	1	23	78	81	1	4	18
	2	9	71	242	0	0	9
	3	118	86	326	6	21	91

FIGURE 24.—Lakeshore Mine scanline mapping, sites 12, 13, 14, and 15, polar equal-area plots, upper hemisphere.

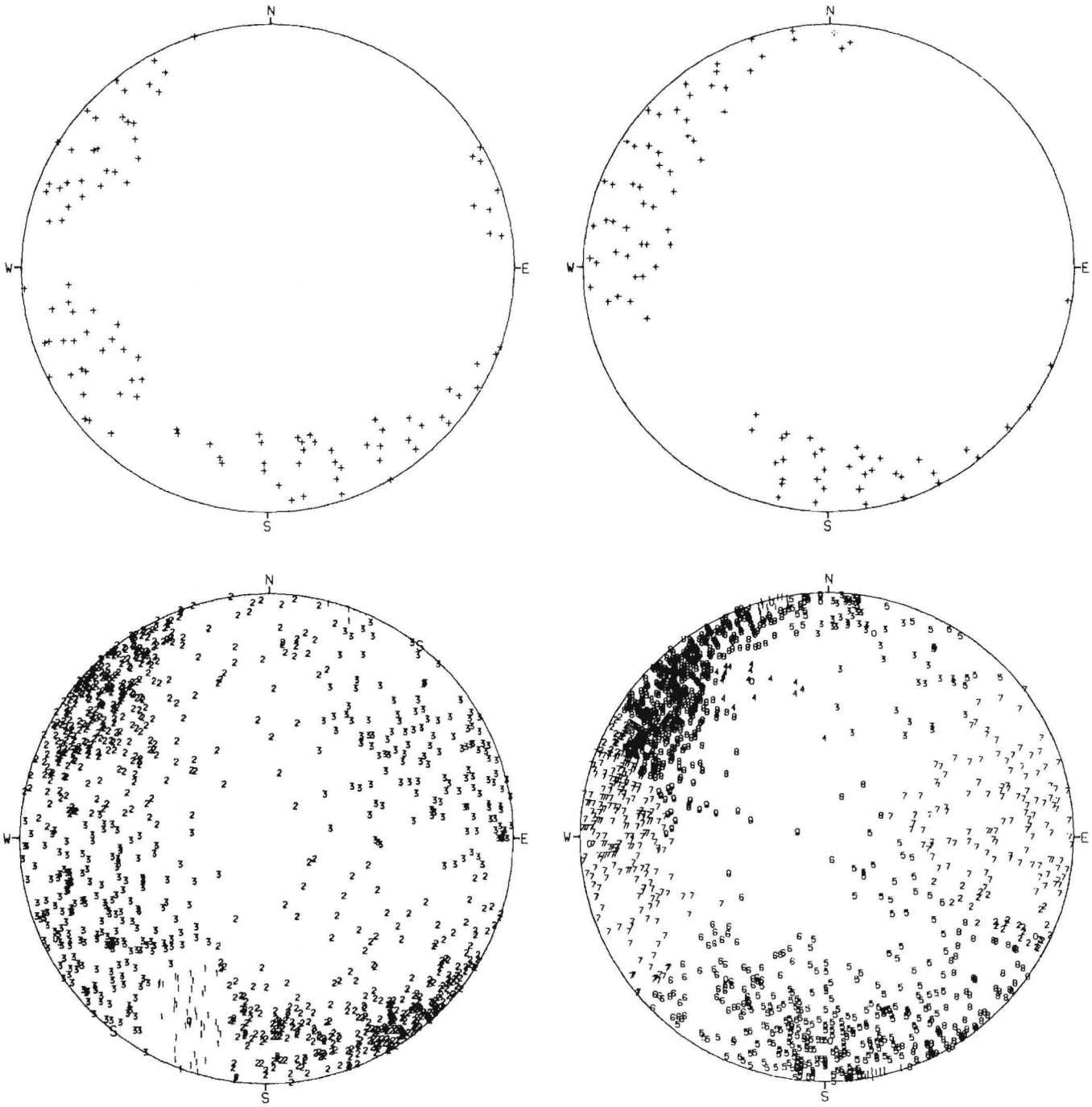

FRACTAN r	Clusters				Eigenvalues		
	No.	Obs	Dip	Az	W1	W2	W3
	SITES 2 TO 7 POOLED						
10.00	1	45	70	202	0	2	43
	2	702	89	321	51	114	536
	3	339	84	244	25	66	249

FRACTAN r	Clusters				Eigenvalues		
	No.	Obs	Dip	Az	W1	W2	W3
	SITES 8 TO 15 POOLED						
8.00	1	26	88	346	0	0	26
	2	52	84	116	0	4	48
	3	51	74	12	1	4	46
	4	17	60	334	0	1	16
	5	307	72	179	14	33	260
	6	66	60	215	1	4	61
	7	355	86	268	23	51	281
	8	571	78	315	18	35	518
	9	23	48	282	0	1	22

FIGURE 25.—Lakeshore Mine scanline mapping, pooled sites 2 to 7 (left) and 8 to 15 (right), polar equal-area plots, upper hemisphere. Top, Dense points by FRACTAN cluster solution; bottom, numerals corresponding to the cluster numbers denote the poles of the joint planes.

Fracture Spacing

The distributions of spacings between successive fractures along the scanlines A, C, and D, without regard for fracture families, shown in figures 26 and 27, were obtained by code GDIST for the individual mapping sites 1 to 15 and for the pooled data sets, sites 2 to 7 and sites 8 to 15. The spacings are most often describable by a lognormal distribution, with medians ranging from 0.5 to 0.8 ft.

The spacings between successive fractures of similar orientation, shown in figure 28, were obtained from the two sets of pooled data as follows: The FRACTAN cluster analyses, figure 25, partition the pooled fractures of sites 2 to 7 into three clusters and the pooled fractures of sites 8 to 15 into nine clusters. The orthogonal spacings between successive fractures of a given cluster were computed by equation 1, using the value of δ corresponding to the mean orientation of that cluster with respect to the scanlines. The orthogonal spacings for a given cluster were pooled for sites 2 to 7 (and 8 to 15) and analyzed by GDIST. The best fitting distributions are the lognormal and the exponential.

The median orthogonal spacing within a family exhibits extremely large variability, ranging from 0.33 to 3.46 ft among the nine largest clusters. For both poolings the family having the smallest median orthogonal spacing, 0.34 and 0.33 ft respectively, is nearly vertical and dips NW; the family that ranks second as to fracture spacing, 1.34 and 1.41 ft respectively, is nearly vertical and dips WSW; and the family that ranks third, with median spacing of 2.43 and 1.56 ft, respectively, dips steeply SSW at sites 2 to 7 and S at sites 8 to 15.

Fracture Trace Length

Trace length is calculated separately for each fracture family identified by the FRACTAN analyses, figure 25, which partition all the measured fractures into three families for pooled mapping sites 2 to 7 and into nine families for pooled sites 8 to 15. In addition, clusters 2 and 4 of site 1 were analyzed separately since site 1 is oriented at right angles to the other sites.

For the four-scanline scheme employed at Lakeshore, since scanline B of figure 11 was used only for measurements on fractures that also crossed scanlines A or C, only the trace lengths in classes 1 to 9 were determined. The results are summarized in table 4. Each listed value of N_i is the total of the fractures of a given family and class interval that were measured at all of the pooled sites 2 to 7 or 8 to 15; for example, at sites 8 to 15, a total of nine fractures of cluster 7 were determined to be of trace length class 4.

For each fracture family, three estimates of mean trace length $\hat{\theta}'$ were calculated, each based on a different combination of the N_i; for the two pooled groups each such estimate is an average over all of sites 2 to 7 or 8 to 15. The scatter among each set of three estimates is on the order of that among the listed averages for the 14 families; hence, the entire group can be characterized as having mean trace lengths of about 1.1 ft, with little difference between families. Consistent with this point of view, one may observe that the most prominent cluster, which dips NW, has the smallest calculated mean trace length (0.9 ft) among sites 2 to 7, whereas it has the largest mean trace length (1.8 ft) among sites 8 to 15. Since the 1.1 ft is the mean of an exponential distribution, some of the fracture traces of any family will be much longer.

Summary, Lakeshore Scanline Mapping

A mapping site typically exhibits three prominent fracture families that can be identified at other sites. The family that dips almost vertically, trending to the NE, was identified at all 15 sites and exhibits by far the smallest orthogonal spacing. The second and third most prominent families respectively are near vertical with NNW trend and steeply dipping with easterly trend; for sites 2 to 7 this generalization is apparent from the FRACTAN results (table 3), but the orthogonal spacing information is required in order to rank the families exhibited at sites 8 to 15. A flat-lying family is not identified. Assuming an exponential distribution of fracture trace lengths, the fracture families exhibit mean trace lengths on the scraping drift walls ranging from 0.7 to 1.8 ft, 1.1 ft being a good overall estimate for the families.

TABLE 4.—Lakeshore scanline mapping: Mean trace length analyses for clusters defined in figures 21 and 25

	Site 1		Pooled sites 2 to 7			Pooled sites 8 to 15								
Cluster	2	4	1	2	3	1	2	3	4	5	6	7	8	9
N_1	4	4	10	202	86	8	11	23	4	84	17	95	165	3
N_2	0	0	0	7	9	0	2	0	0	4	1	3	3	0
N_3	1	1	4	56	21	0	6	1	0	14	2	17	39	1
N_4	0	0	8	15	20	0	0	0	0	10	3	9	14	0
N_5	0	0	0	0	1	0	0	0	0	0	0	0	0	0
N_6	1	0	0	0	0	0	0	0	0	0	0	0	1	0
N_7	0	1	2	42	29	2	3	4	0	14	8	11	26	0
N_8	6	8	13	217	112	11	19	11	6	109	27	130	180	11
N_9	3	5	8	162	60	5	10	11	6	71	7	89	142	7
sin α	0.98	0.47	0.93	1.00	0.99	1.00	0.90	0.96	0.62	0.92	0.87	0.99	0.50	0.44
Eq 9	1.1	1.7	0.9	0.9	1.0	0.9	0.9	1.1	1.1	0.9	1.1	0.8	1.7	1.5
Eq 11	1.2	1.4	1.2	.8	1.0	.7	.9	.7	1.1	.9	1.0	.8	1.6	1.5
Eq 12	1.1	1.9	2.1	1.1	1.5	.7	1.3	.8	1.1	1.2	1.8	1.1	2.2	1.9
AV	1.1	1.7	1.4	.9	1.2	.7	1.0	.9	1.1	1.0	1.3	.9	1.8	1.6

NOTE.—Top: The number of fractures observed in trace length classes 1 to 9 defined in figure 11. Bottom: The values of mean trace length $\hat{\theta}'$ (ft) calculated from the appropriate equation in table 1 (s = 1.33 ft).

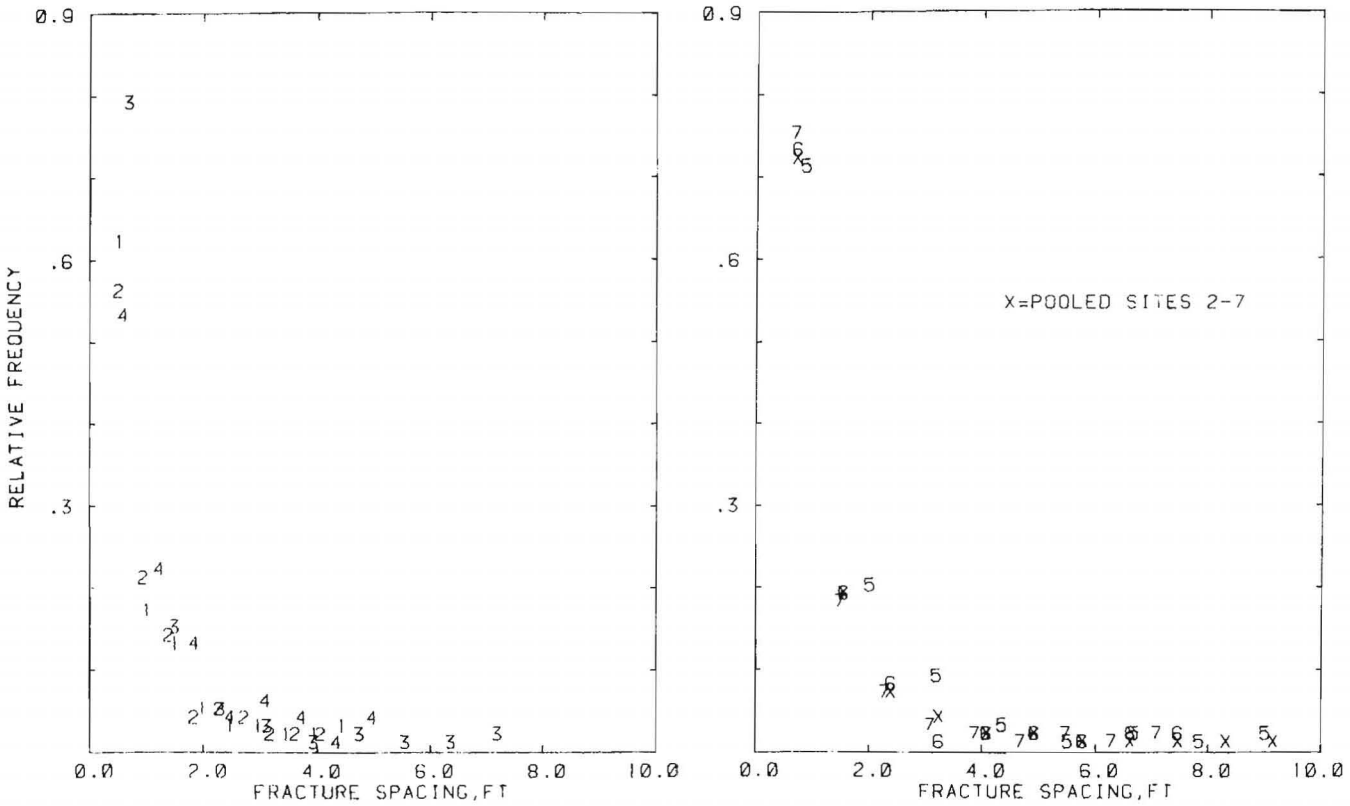

Scanline mapping site		1	2	3	4	5	6	7	Pooled 2-7
Spacings observed		173	171	189	117	120	156	163	916
Maximum	ft	4.60	4.20	7.50	5.20	9.50	7.80	7.40	9.50
Minimum	ft	0.20	0.20	0.20	0.20	0.20	0.20	0.20	0.20
Arithmetic mean	ft	0.85	0.84	0.75	1.19	1.22	0.92	0.89	0.94
Median	ft	0.50	0.60	0.50	0.70	0.80	0.60	0.60	0.60
Mode	ft	0.20	0.20	0.20	0.30	0.30	0.30	0.20	0.20
Std dev	ft	0.85	0.74	0.89	1.09	1.29	1.03	0.91	0.99
Skewness		2.23	1.96	3.85	1.72	3.17	3.65	3.53	3.23
Mean log of spacing		−0.54	−0.49	−0.67	−0.18	−0.19	−0.47	−0.46	−0.44
Std dev of logs		0.69	0.78	0.81	0.85	0.87	0.83	0.81	0.84
Distributions[1]		L,χ,Γ	L,E	L,χ	L,E,χ	L,E,χ	L,χ	L,E,χ	L
Best fit		Γ	L	χ	L	E	χ	L	L

[1] Acceptable fit at the 5-pct significance level (L = lognormal, E = exponential, χ = chi squared, Γ = gamma).

FIGURE 26.—Lakeshore Mine scanline mapping, individual sites 1 to 7 and pooled sites 2 to 7. GDIST analyses of the spacing between successive fractures as measured along scanlines A, C, and D. Relative frequency (spacings in each class ÷ total spacings) is plotted at the midpoint of the corresponding class interval; the numeral corresponding to the site number is centered on the plotted point. Below the histograms are listed the parameters of the distributions.

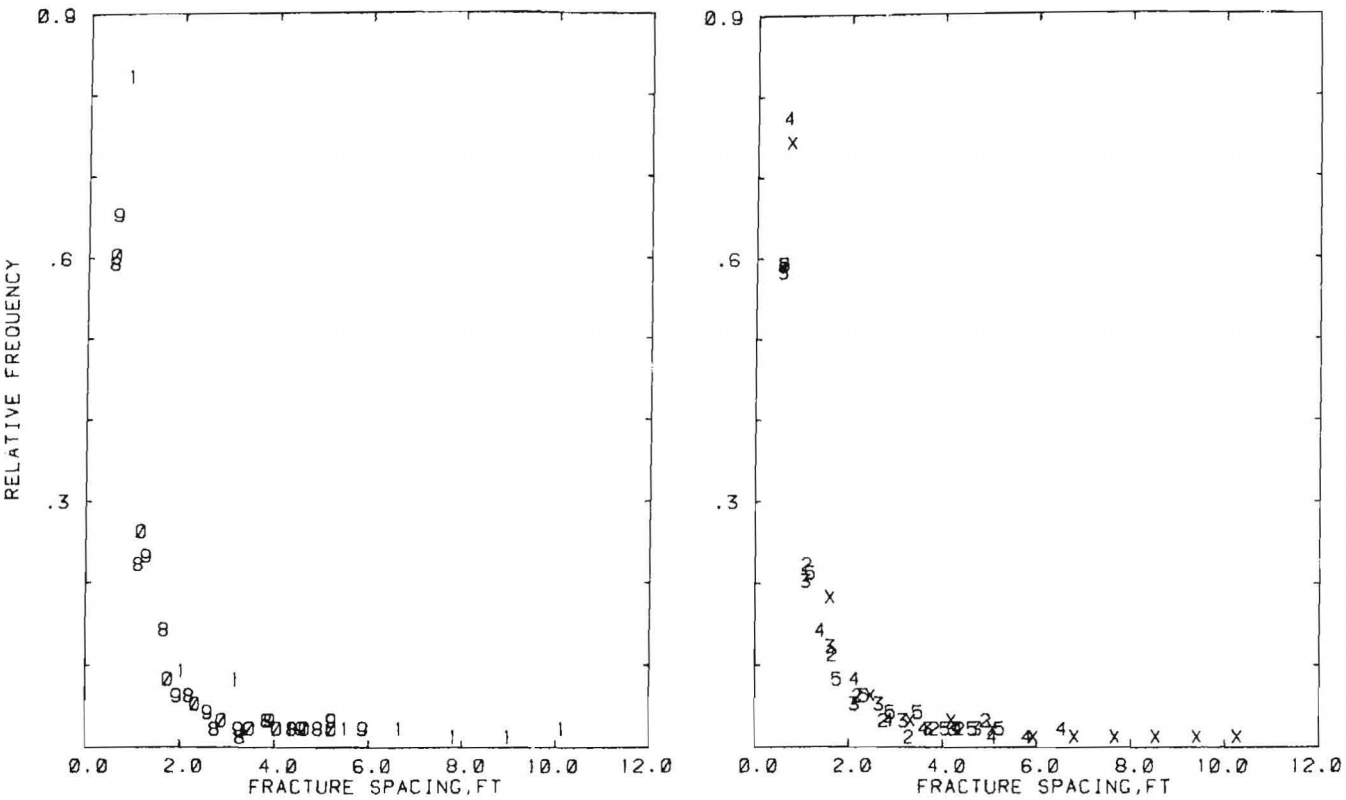

Scanline mapping site	8	9	10	11	12	13	14	15	Pooled 8-15
Spacings observed	168	154	163	135	158	158	183	143	1,262
Maximum, ft	5.10	6.10	5.40	10.60	5.10	4.90	6.80	5.40	10.60
Minimum, ft	0.20	0.20	0.20	0.20	0.20	0.20	0.20	0.20	0.20
Arithmetic mean, ft	0.86	0.94	0.88	1.05	0.92	0.92	0.80	0.99	0.91
Median, ft	0.60	0.60	0.50	0.60	0.60	0.60	0.50	0.70	0.60
Mode, ft	0.20	0.20	0.20	0.20	0.30	0.30	0.30	0.20	0.20
Std dev, ft	0.82	1.08	0.92	1.41	0.94	0.87	0.84	0.99	0.99
Skewness	2.32	2.75	2.68	3.72	2.50	2.08	3.31	1.93	3.07
Mean log of spacing	−0.51	−0.49	−0.51	−0.42	−0.45	−0.42	−0.57	−0.40	−0.48
Std dev of logs	0.84	0.87	0.84	0.91	0.83	0.81	0.78	0.87	0.84
Distributions[1]	L	L	L,E	χ	L	L,E,χ,Γ	L,χ	L,χ,Γ	None
Best fit	L	L	L	χ	L	Γ	χ	Γ	L

[1] Acceptable fit at the 5-pct significance level (L = lognormal, E = exponential, χ = chi squared, Γ = gamma).

FIGURE 27.—Lakeshore Mine scanline mapping, individual sites 8 to 15 and pooled sites 8 to 15. GDIST analyses of the spacing between successive fractures as measured along scanlines A, C, and D. Relative frequency (spacings in each class ÷ total spacings) is plotted at the midpoint of the corresponding class interval; the numeral corresponding to the second digit of the site number (X = pooled sites) is centered on the plotted point. Below the histograms are listed the parameters of the distributions.

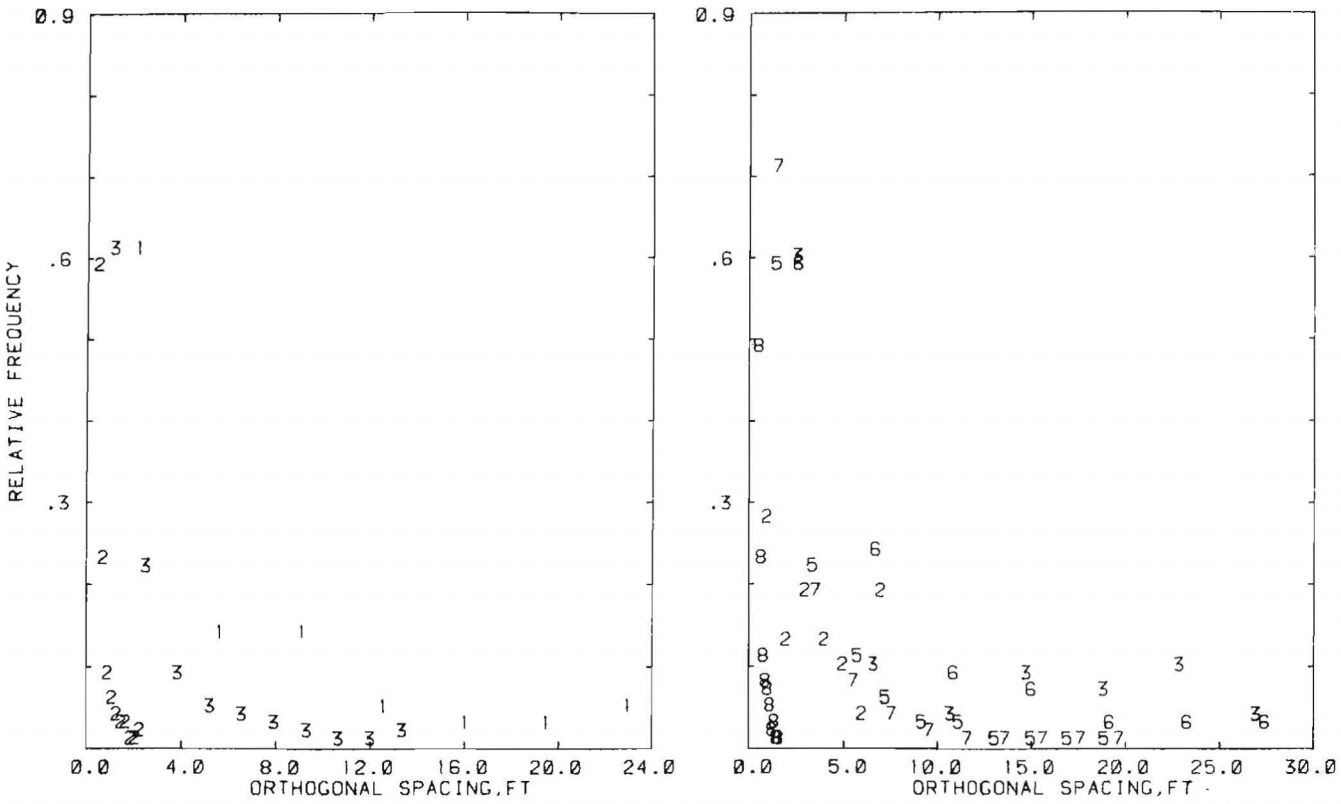

	Pooled sites 2 to 7			Pooled sites 8 to 15					
Cluster	1	2	3	2	3	5	6	7	8
Spacings observed	45	359	354	33	32	298	53	322	252
Maximum ft	24.45	2.14	13.81	7.24	28.67	19.54	29.19	20.38	1.36
Minimum ft	0.27	0.20	0.27	0.21	0.26	0.22	0.26	0.26	0.21
Arithmetic mean ft	5.09	0.45	2.05	3.14	7.40	2.55	5.43	2.08	0.41
Median ft	2.43	0.34	1.34	2.79	2.77	1.56	3.46	1.41	0.33
Mode ft	0.27	0.22	0.36	ND	1.21	0.52	ND	ND	0.24
Std dev ft	5.90	0.30	2.20	2.27	8.49	2.73	5.73	2.21	0.22
Skewness	1.71	2.21	2.46	0.46	1.13	2.25	2.06	3.34	1.64
Mean log of spacing	0.95	−0.97	0.28	0.75	1.22	0.42	1.19	0.33	−1.00
Std dev of logs	1.26	0.53	0.92	1.04	1.38	1.05	1.07	0.90	0.45
Distributions[1]	L,E	None	L	NLEχU	L	L,E,χ	L,E	L,E,χ	None
Best fit	L	E	L	E	L	E	L	L	E

ND No appropriate value was determinable.
[1] Acceptable fit at the 5-pct significance level (N = normal, L = lognormal, E = exponential, χ = chi squared, U = uniform).

FIGURE 28.—Lakeshore Mine scanline mapping, GDIST analyses of orthogonal fracture spacing within fracture families. Left, Pooled sites 2 to 7; right, pooled sites 8 to 15. Relative frequency (spacings in each class ÷ total spacings) is plotted at the midpoint of the corresponding class interval; the numeral indicating the cluster number is centered on the plotted point. Clusters with fewer than 10 observations are omitted. Below the histograms are listed the parameters of the distributions.

LAKESHORE FRACTURES—SUMMARY

The orientation and spacing characteristics of the most prominent fracture families are collected in table 5 to facilitate comparison of the results obtained from oriented core with those obtained by scanline mapping. Analyses of the oriented core indicate seven major fracture families, two of which are not identified in the scanline mapping data; on the average four of these seven are found in any single drill hole. Scanline mapping indicates five major fracture families, one of which is not identified by the oriented-core analysis; on the average three of these five are found at any single mapping site.

As shown in figure 13, the scanline mapping sites 2 to 7 extended over a distance of about 300 ft, mapping sites 8 to 15 extended over the adjoining 200 ft to the NE, and the oriented-core drill holes penetrated the next 200-ft zone. Some changes of jointing characteristics would not be surprising over a distance of 700 ft, and table 5 indeed suggests the existence of such a trend. The three most prominent fracture families, however, which are the three clusters identified for pooled sites 2 to 7, appear in all three of the sampled zones. The two most numerous families, which are both approximately vertical and trend to the NE and NW, appear with surprisingly consistent mean orthogonal spacings of 0.3 and 1.4 ft, respectively, in all three zones.

Orthogonal spacing values are influenced by the partitioning of the fractures into families. As more and more fractures are removed to form additional families, the numbers of fractures in the other families are decreased, which tends to increase the calculated spacing. This effect will be greater for a small family than for a large one, and hence one can expect less consistent spacing results for the families that have the largest spacings. The spacing from fracture to fracture, irrespetive of fracture family, which is not subject to the influence of partitioning, is only half as great in the oriented cores as that mapped on exposures.

TABLE 5.—Lakeshore Mine: Fracture families indicated by the two methods

ORIENTED CORE, POOLED DRILL HOLES 1 to 6[1]							
Dip, dip azimuth	72, 30	48, 70	—	39, 201	60, 229	71, 267	80, 338.
W3/n	337/387	236/280	—	131/150	98/104	376/452	892/1318.
Dip	Steep	Moderate	—	Moderate	Vertical	Steep	Vertical.
Dip direction	NE	ENE	—	SSW	SW	W	NNW.
Cluster	1	2	—	3	4	5	6.
Orthogonal spacing	0.66 ft	0.78 ft	—	0.77 ft	1.47 ft	0.39 ft	0.32 ft.
SCANLINE MAPPING, POOLED SITES 8 to 15[2]							
Dip, dip azimuth	—	84, 116	72, 179	60, 215	86, 268	—	78, 315.
W3/n	—	48/52	260/307	61/66	281/355	—	518/571.
Dip	—	Steep	Steep	Steep	Vertical	—	Vertical.
Dip direction	—	E	S	SSW	WSW	—	NW.
Cluster	—	2	5	6	7	—	8.
Orthogonal spacing	—	2.79 ft	1.56 ft	3.46 ft	1.41 ft	—	0.33 ft.
SCANLINE MAPPING, POOLED SITES 2 to 7[2]							
Dip, dip azimuth	—	—	—	70, 202	84, 244	—	89, 321.
W3/n	—	—	—	43/45	249/339	—	536/702.
Dip	—	—	—	Steep	Vertical	—	Vertical.
Dip direction	—	—	—	SSW	WSW	—	NW.
Cluster	—	—	—	1	3	—	2.
Orthogonal spacing	—	—	—	2.43 ft	1.34 ft	—	0.34 ft.

—No appropriate cluster identified.
[1]Fracture spacing, irrespective of fracture orientation, median = 0.28 ft.
[2]Fracture spacing, irrespective of fracture orientation, median = 0.60 ft.

SAN MANUEL MINE DATA

The San Manuel Mine is a porphyry-type copper deposit located about 45 miles northeast of Tucson, AZ. Principal host rocks for the copper mineralization are Precambrian quartz monzonite (the Oracle Granite batholith) and the later intruded dikes and irregular masses of porphyry, which include quartz monzonite porphyry, monzonite porphyry, and dacite porphyry. The trough-shaped ore body pitches southwesterly, its two limbs trending NE-SW. The ore body is cut off above by the San Manuel Fault, which dips 26° SW and can be traced for several miles. The San Manuel Fault is offset by a N25°W system of steep easterly dipping faults, which cut transversely across the ore body, and these in turn are offset by the still younger Vent Raise Fault (strike about N60°E, dip 65° to 90°SE), which transects the ore body longitudinally. The south limb of the ore body averages about 1,000 ft wide, and the north limb is up to 400 ft wide (*32*).

When the present data acquisition began, mining had been going on for about 20 years; ore extraction from the 1415 and 1715 (feet below surface) production levels having been completed, mining was currently being done from the 2015 and 2315 levels. Figure 29 shows all prior ("Mined Out") and current ("Active Cave") ore extraction areas on the 2315 level in the fourth quarter of 1977. The usual practice is to undercut the ore by drifting and crosscutting on the level 15 ft above the grizzly (production) level and then blasting out the remaining pillars. The fragmented ore drops by gravity from the caving stope through draw raises to the grizzly drifts.

Two sites were chosen for drilling, one in the south limb (panel 41) and one in the north limb (panel 2). Diamond drilling to produce oriented core, holes 1, 2, and 3 in panel 41 and holes 4, 5, and 6 in panel 2, figure 30, was conducted by a drill crew for about 6 weeks beginning September 29, 1977. At that time only grizzly drifts 4, 11,

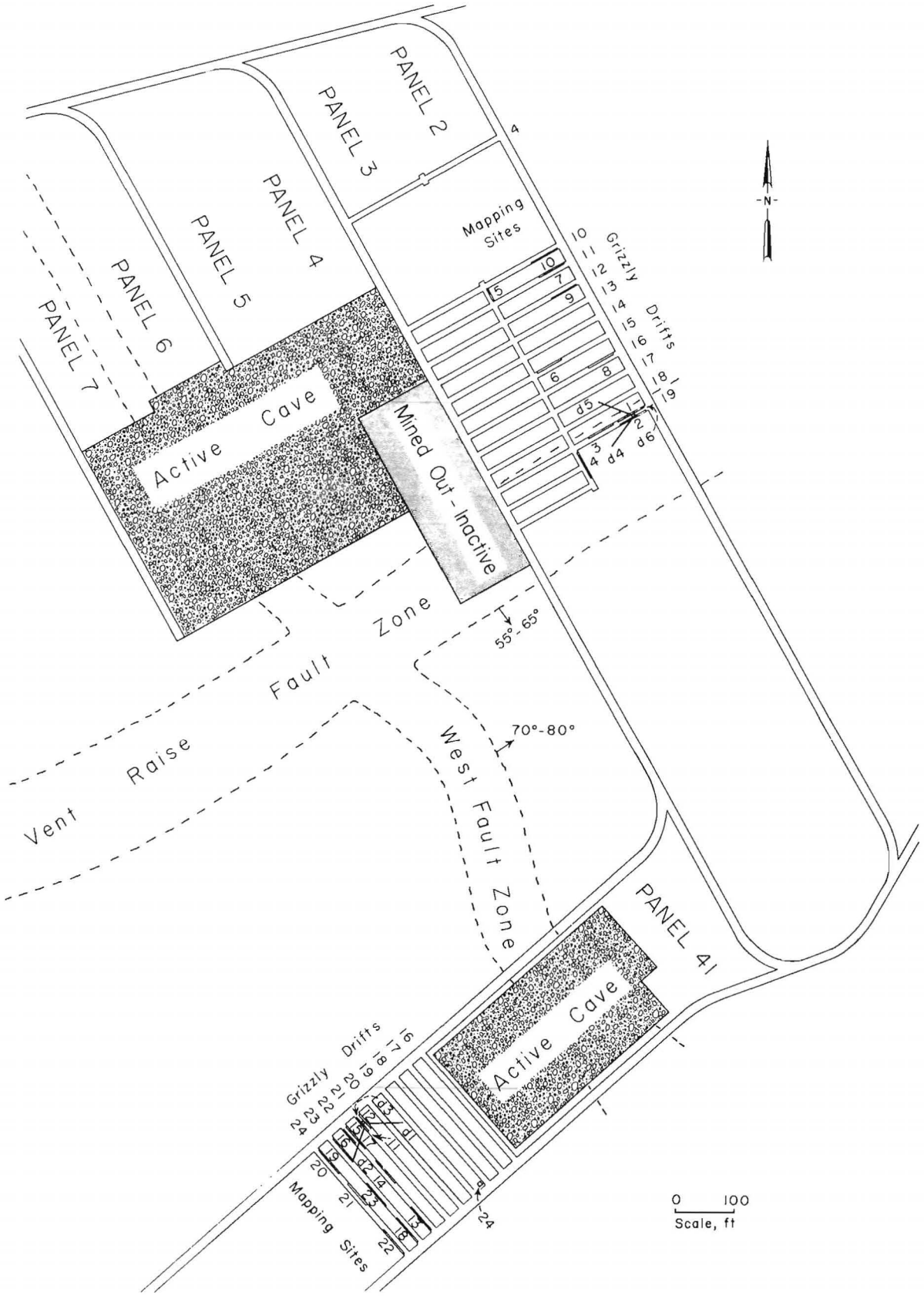

FIGURE 29.—San Manuel Mine: Plan view of 2315 level showing in panel 2, scanline mapping sites 1 to 10 and diamond drill holes d4 to d6 for oriented core, and in panel 41, scanline mapping sites 11 to 24 and diamond drill holes d1 to d3 for oriented core.

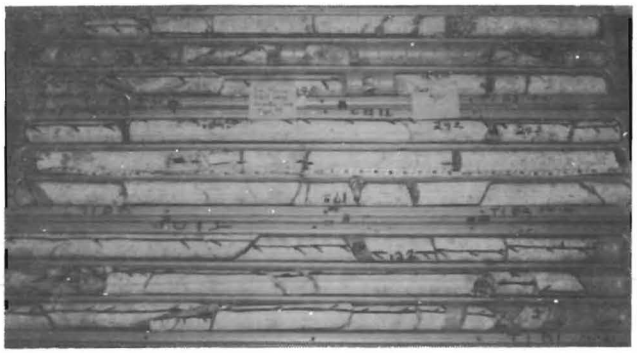

HOLE 1, 0 TO 37 FT

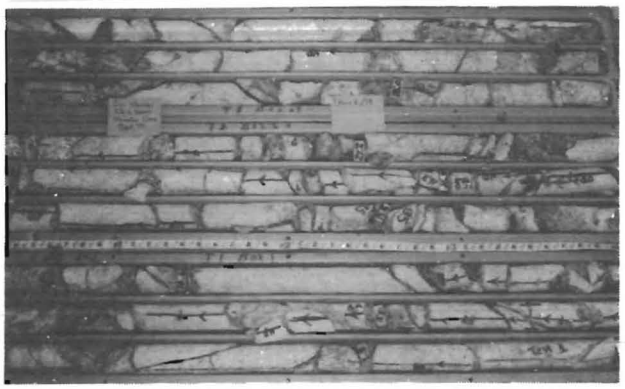

HOLE 4, 0 TO 38 FT

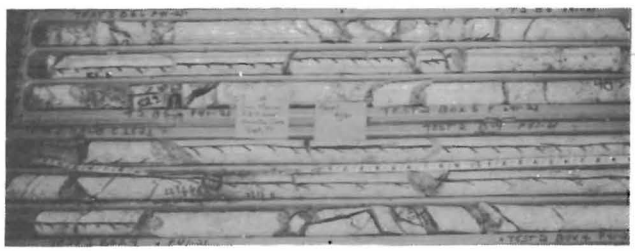

HOLE 2, 38 TO 60 FT

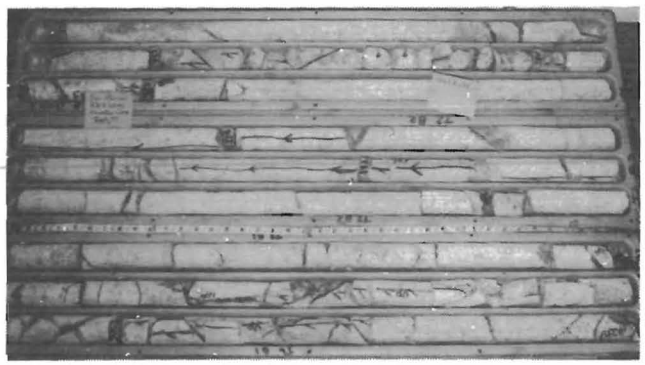

HOLE 5, 0 TO 38 FT

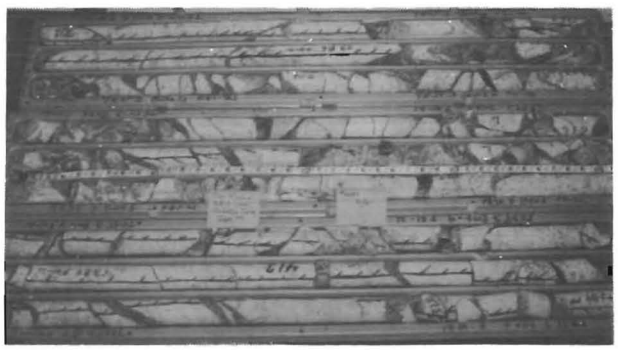

HOLE 3, 36 TO 71 FT

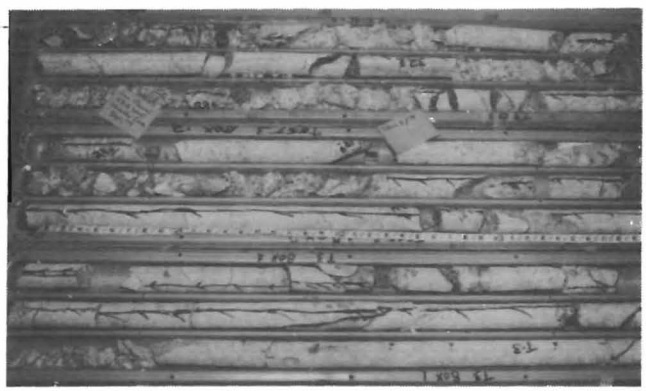

HOLE 6, 0 TO 38 FT

HOLE 3, 71 TO 104 FT

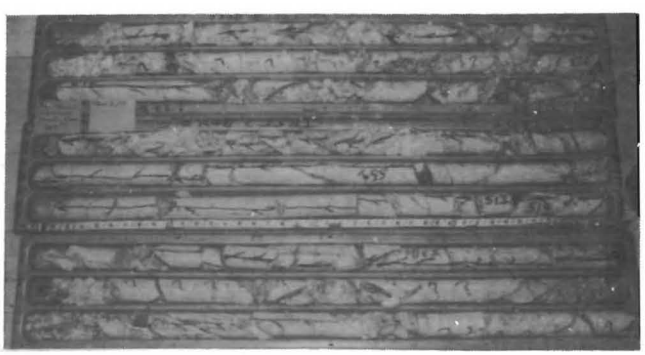

HOLE 6, 38 TO 77 FT

FIGURE 30.—San Manuel Mine oriented diamond drill cores.

and 19 existed in panel 2; in panel 41, the grizzly drifts up to 20 and the north end of grizzly drift 21 had been driven. At each of the two sites two 3-in-diam holes were drilled 60 ft, inclined 20° above the horizontal, and one vertical hole was drilled 110 ft upward.

The split 5-ft-long double-tube core barrel and the impression method of core orienting were employed. Core recovery was approximately 95 pct, but the core orientation was frequently lost when a section of rubble was recovered.

Fracture mapping along multiple scanlines was performed intermittently from September 1977 to April 1978, at sites 1 to 10 in panel 2 and at sites 11 to 24 in panel 41, as the grizzly drifts were driven. Most of the sites necessarily were in grizzly drifts, the longer connecting drifts having been concrete-lined much earlier. Sites 4 and 5 were in "panel 2/3 access drift" at right angles to the grizzly drifts. At site 24, which was on the two southerly walls of a raise, 20-ft-long, vertical scanlines were employed instead of the usual 50-ft-long horizontal section. Some of the horizontal sites were only 20 to 30 ft long (5, 11, 12, 15, 16, and 17), owing to the limited surfaces of the exposures.

SAN MANUEL ORIENTED CORE

Fracture Orientation

The selected FRACTAN cluster solutions, according to the stated criteria, are shown in figures 31 to 34. In addition to the cluster analyses for the six individual drill holes, FRACTAN partitions were made for the pooled data from holes 1, 2, and 3 and for the pooled data from holes 4, 5, and 6. PEA plots of dense points, given only for the pooled sets of data, are helpful in identifying significant clusters that may be poorly represented in the data because their poles deviate by more than 60° from the drill hole axis.

For each of the individual drill holes, the fracture-plane normals are concentrated within 60° of the drill hole axis. Because of this directional bias, the fracture pattern appears to be somewhat different for each hole. The best interpretation appears to be that provided by combining the fractures from all the drill holes at each site, thus compensating for the underrepresentation of fractures for which $\delta > 60°$. Arranging the fracture families, as in table 6, to exhibit coinciding orientations among drill holes, one finds four orientations that appear in two of the three drill holes at both sites; at least two of these four orientations appear in every drill hole. One of these four families is flat dipping; the other three dip steeply SSE, SW, and W, respectively.

A fifth family, dipping moderately to steeply eastward, is listed only for individual drill hole 1, although this family is identified in both pooled sets of data (and in several of the nonselected cluster solutions) and is represented by dense points in both pooled sets. A sixth family, dipping moderately to the SE, is indicated by only three drill holes. On the average, each drill hole exhibits three of these six families, the orientations of which depend on the drill hole orientation. The clusters listed as "not correlated" may represent localized fracturing, may be chance effects in the data, or may be due to misoriented core. Figures 33B and 34B show the angular zones of coverage achieved by the three-drill-hole configurations employed, which tend to explain the failure to detect a particular fracture family in a particular drill core. One suspects that a four-hole arrangement would have provided more definitive data, but the mutual confirmation provided by the two sites indicates that an economical solution was achieved.

Fracture Spacing

The spacings from fracture to fracture along the drill cores, without regard for fracture orientation, are shown in figure 35. The spacings, best described by exponential

TABLE 6.—San Manuel oriented core: Mean dip and dip azimuth (dipaz) of clusters as determined by FRACTAN analysis

(Fracture families grouped to show correlations; below each dip, dipaz pair is given the corresponding W3/n)

Drill hole	Dip direction, deg						
	0-360 Flat	67-90 E	124-157 SE	149-180 SSE	205-250 SW	254-300 W	Not correlated
1	—	68, 81 75/98	—	79, 151 15/18	—	52, 268 18/21	30, 57 9/10
2	15, 240 13/15	—	—	75, 169 56/79	72, 218 42/48	76, 254 26/31	—
3	8, 339 168/229	—	45, 124 31/34	—	67, 221 44/51	—	73, 312 21/25
1+2+3	9, 240 177/233	71, 90 70/76	41, 130 35/37	78, 149 46/51	75, 205 70/80	75, 254 26/27	76, 41 41/44 47, 260 26/27 41, 57 40/42 55, 309 39/42
4	20, 285 16/17	—	—	60,180 77/100	83, 232 88/110	84, 278 26/30	—
5	—	—	77, 136 16/19	—	71, 250 17/19	69, 294 110/138	86, 353 12/14
6	20, 223 46/55	—	44, 135 9/9	70, 169 21/24	—	—	37, 40 53/70
4+5+6	9, 50 52/59 24, 235 20/20 25, 302 24/25	54, 67 55/64	51, 157 28/30	84, 171 55/63	73, 240 112/129 49, 218 14/14	74, 300 135/158	51, 192 40/43

— No appropriate cluster identified.

distributions, are quite small in all six holes, the median spacing ranging from 0.30 to 0.43 ft. The median spacing at the panel 41 site (holes 1 to 3 is slightly greater than that at the panel 2 site, 0.35 versus 0.30 ft.

The orthogonal spacings between successive fractures of similar orientation are shown in figure 36 for holes 1, 2, and 3 and in figure 37 for holes 4, 5, and 6. These results were obtained from the pooled data at each of the two sites as follows: The FRACTAN cluster analysis, figure 33 or 34, partitioned the fractures from three pooled holes into 10 clusters. For each drill hole the orthogonal fracture spacings within a given cluster were computed by equation 1, using the appropriate angle δ corresponding to the mean orientation of that cluster with respect to the specified drill hole. The orthogonal spacings for a given cluster were pooled for the three drill holes at the site and analyzed by GDIST. The best fitting distribution of orthogonal spacings is usually the lognormal (11 of 20 clusters), followed by the chi squared (5 clusters) and the exponential (4 clusters).

The statistics for the orthogonal spacings within fracture families exhibit large differences among the families. The median spacing ranges from 0.49 to 2.83 ft for the panel 41 site (holes 1, 2, 3) and from 0.44 to 3.38 ft for the panel 2 site (discounting cluster 5 for which there are only 12 observed spacing values). The smallest median spacing for holes 1, 2, and 3 corresponds to the flat-lying fracture family, whereas the most numerous fracture family for holes 4, 5, and 6 dips steeply WNW. On the other hand, holes 1, 2, and 3 contain four families having median spacings of 1 ft or less, whereas holes 4, 5, and 6 contain five such families, one steeply dipping family in each quadrant plus one flat-lying family.

Summary, San Manuel Oriented Core

Analyses of the six drill cores indicate the presence of the same six fracture families at both sites. The fracture families that are identified consistently by the orientation analyses are essentially the same as those that have the smallest orthogonal spacings—the four families that have the smallest spacings at the panel 41 site are members of column groupings 1, 2, 4, and 5 of table 6; the five families that have the smallest spacings at the panel 2 site are members of column groupings 1, 2, 4, 5, and 6 of table 6. These five most prominent fracture families comprise one steeply dipping family in each of the four quadrants plus one flat-lying family.

SAN MANUEL MULTIPLE SCANLINE MAPPING

Fracture Orientation

All the fracture orientations determined by the scanline mapping are presented in PEA diagrams, one for each mapping site, figures 38 to 44, which also show the best FRACTAN partitioning into clusters. Mapping sites 1 to 10 and 11 to 24 comprise two simple geographic groupings, each representing a mining panel. FRACTAN partitions, figure 45, were made for the pooled data from these two groups of sites.

PEA plots for the individual sites in most instances exhibit angular zones containing few or no fracture plane poles, which might suggest the existence of a sampling bias. These are apparently local effects, however, because the plots of the pooled data exhibit an overall stippling of poles.

Comparisons of the mean orientations of the fracture families, derived from the FRACTAN partitions of the data sets for the 24 individual mapping sites and the 2 poolings, reveal approximate correspondences at 6 orientations, listed by column in table 7. On the average, an individual site exhibits four of these six most prominent fracture families. All six families dip moderately to steeply, distributed fairly evenly over the 360° of azimuth.

TABLE 7.—San Manuel scanline mapping: Mean dip and dip azimuth (dipaz) of clusters as determined by FRACTAN analysis

(Fracture families grouped to exhibit correlations; dip given in two opposite directions (e.g., SE-NW) implies approximately vertical orientation; below each dip, dipaz pair is given the corresponding W3/n)

Mapping site	Dip direction, deg						
	321-14 N	21-70 NE	84-100 E	118-156, 308-318 SE-NW	184-200 S	216-268 SW	Not correlated
1	40, 325 14/16 77, 13 14/15	65, 70 7/7	82, 100 8/9	67, 136 14/15 72, 156 7/7	—	89, 238 7/7 65, 244 11/11	—
2	31, 337 16/18 47, 14 6/6 74, 14 6/6	55, 66 5/5	87, 86 6/6	83, 126 12/13	66, 185 7/7	79, 228 19/20 65, 255 10/10	27, 223 9/10
3	74, 10 4/4	34, 40 7/7 78, 67 6/6	—	—	—	72, 224 22/24 52, 238 2/2 77, 268 14/16	18, 271 6/6
4	38, 321 13/14 71, 334 7/7 22, 7 11/12	56, 21 11/12	73, 97 10/11	86, 133 39/43	72, 195 12/13	—	—
5	88, 338 46/78	—	—	—	74, 184 10/10	—	—
6	35, 340 24/26	69, 34 26/29	—	—	—	72, 251 31/36	53, 298 28/34

TABLE 7.—San Manuel scanline mapping: Mean dip and dip azimuth (dipaz) of clusters as determined by FRACTAN analysis—Con.

Mapping site	Dip direction, deg						
	321-14 N	21-70 NE	84-100 E	118-156, 308-318 SE-NW	184-200 S	216-268 SW	Not correlated
7	21, 351 10/12	76, 33 17/18	—	70, 308 9/10	—	78, 253 35/42	25, 299 7/7
8	26, 354 15/16	79, 34 6/6	—	61, 318 8/10	—	71, 230 33/42	27, 293 7/7
9	—	20, 55 11/13	47, 114 5/5	74, 126 12/13	68, 194 19/20	70, 236 44/48	48, 151 6/6
10	—	36, 58 5/5	70, 84 6/6	71, 118 7/7	19, 200 12/14	54, 218 2/2 74, 224 32/36	43, 127 6/6
Pooled 1 to 10	57, 356 82/93	42, 31 96/116	—	78, 132 180/241	—	67, 237 334/479	—

Mapping site	Dip direction						
	323-10 N	37-97 ENE	50-90 229-241 ENE-WSW	106-161 282-342 SE-NW	120-185 SSE	220-272 WSW	Not correlated
11	56, 356 5/6	—	90, 59 3/3	88, 134 16/17	33, 145 5/5 52, 170 3/3	28, 256 2/2	25, 284 3/3
12	48, 348 5/6	—	—	82, 315 20/23	35, 120 21/22	—	16, 315 5/5
13	58, 351 8/8	—	71, 241 12/13	74, 130 17/19 89, 161 9/10 77, 310 9/9	—	28, 234 22/29	72, 279 10/10
14	—	57, 37 26/32	—	85, 108 53/62 75, 152 23/29	—	35, 272 54/60	—
15	54, 349 23/27	49, 69 4/4	70, 50 6/6	—	49, 145 26/29	15, 220 4/4	48, 313 10/11
16	37, 4 6/7	—	83, 90 8/8	89, 336 5/5	48, 136 15/18	—	59, 211 10/12 59, 294 4/4
17	79, 0 7/7	58, 63 8/8 41, 91 6/6	84, 73 3/3	74, 138 4/4 85, 326 2/2	57, 127 2/2	41, 248 6/6	—
18	56, 10 12/15	—	—	80, 137 70/93	—	65, 246 21/24	32, 211 11/12
19	55, 10 7/7	28, 79 22/23	80, 62 13/14	83, 322 24/27	34, 122 6/6 30, 173 9/10	—	—
20	47, 323 7/7 65, 356 7/8	39, 55 8/9	—	72, 140 9/10 75, 317 15/16	29, 150 10/10	35, 239 7/8 58, 271 5/5	43, 108 6/6
21	—	63, 81 9/10	—	81, 119 5/5 76, 156 14/16 79, 283 7/8 69, 331 23/26	48, 185 13/14	—	38, 108 12/13
22	55, 336 7/7 35, 339 3/3	—	—	84, 122 6/6 78, 138 5/5 88, 342 31/33	38, 155 12/12	63, 255 10/12 36, 271 5/5	24, 199 8/8
23	46, 346 12/14	—	85, 229 20/23	84, 114 14/15 86, 329 15/16	52, 182 25/28	28, 252 11/12	—
24	—	63, 85 4/4 36, 97 6/6	85, 50 3/3 71, 248 10/10	86, 282 5/5 84, 319 7/7	37, 150 6/6 50, 177 7/7	38, 271 9/10	—
Pooled 11 to 24	40, 344 87/95	39, 69 96/109	—	87, 316 404/580	41, 154 196/225	41, 251 169/199	—

— No appropriate cluster identified.

Fracture Spacing

The distributions of spacings between successive fractures along the scanlines, without regard for fracture orientation, shown in figures 46, 47, and 48, were obtained by code GDIST for the individual mapping sites 1 to 24 and for the pooled data sets, sites 1 to 10 and sites 11 to 24. The spacings, ordinarily describable by a lognormal or an exponential distribution, are very little different between the two mining panels, the medians ranging from 0.7 to 1.3 ft in panel 2, and from 0.7 to 1.1 ft in panel 41.

The spacings between successive fractures of the same family, shown in figure 49, were obtained from the two sets of pooled data as follows: The FRACTAN cluster analyses, figure 45, partition the pooled fractures of sites 1 to 10 into four clusters and the pooled fractures of sites 11 to 24 into five clusters. The orthogonal spacings between successive fractures of a given cluster were computed by equation 1, using the value of δ corresponding to the mean orientation of that cluster with respect to the scanlines. The orthogonal spacings for a given cluster were pooled for sites 1 to 10 (and 11 to 24) and analyzed by GDIST. The best fitting distributions are the chi squared and the lognormal.

The median orthogonal spacing within a family exhibits only moderate variability, ranging from 0.93 to 2.09 ft at sites 1 to 10 and from1.05 to 1.76 ft at sites 11 to 24.

Fracture Trace Length

Trace length was calculated separately for each fracture family identified by the FRACTAN analyses (fig 45), which partition all the measured fractures into four families for pooled mapping sites 1 to 10 and into five families for pooled sites 11 to 24.

The results are set out in tables 8 and 9, respectively, depending on whether the sites were mapped by a four- or five-scanline scheme. After sites 1 to 4 were mapped, the four-scanline scheme with 1.33-ft scanline spacing was changed to a five-scanline scheme with 1-ft spacings. For panel 2, the N_i for sites 1 to 3 were pooled to increase the

TABLE 8.—San Manuel scanline mapping: Mean trace length analyses for sites mapped by a four-scanline scheme, clusters as defined in figure 45

	Sites 1+2+3				Site 4			Site 24W		
Cluster	1	2	3	4	2	3	4	1	4	5
N_1	0	1	4	7	0	1	1	0	0	0
N_2	1	0	4	1	0	1	0	0	0	0
N_3	8	2	10	9	2	8	1	5	1	1
N_4	2	0	1	4	0	4	2	1	1	0
N_5	1	3	6	28	0	8	3	0	4	4
N_6	0	0	0	3	1	2	0	1	1	1
N_7	4	3	1	13	1	1	3	0	0	1
N_8	6	6	17	55	12	27	11	1	0	1
N_9	1	1	5	8	1	1	2	0	0	0
N_{10}	8	8	8	14	1	6	2	1	0	0
sin α	0.57	0.62	0.84	0.92	0.41	0.97	0.10	0.59	0.96	0.80
s ft	1.33	1.33	1.33	1.33	1.33	1.33	1.33	1.00	1.00	1.00
Eq 9	2.8	4.0	1.9	2.8	2.3	2.0	17.3	2.6	15.2	6.9
Eq 10	2.0	1.8	2.2	3.9	2.7	4.4	31.9	3.4	12.0	6.3
Eq 11	2.2	2.7	1.7	5.3	4.9	3.1	31.9	1.7	2.0	13.1
Eq 12	4.3	9.0	2.8	7.7	3.8	4.9	42.1	2.8	8.4	16.9
Av	2.8	4.4	2.2	4.9	3.4	3.6	30.8	2.6	9.4	10.8

NOTE.—Top: The number of fractures observed in trace length classes 1 to 10 defined in figure 11. Bottom: The values of mean trace length $\hat{\theta}'$ (ft) calculated from the appropriate equation in table 1.

TABLE 9.—San Manuel scanline mapping: Mean trace length analyses for sites mapped by a five-scanline scheme, clusters as defined in figure 45

	Site 5				Sites 6 to 10				Sites 11 to 23					Site 24S		
Cluster	1	2	3	4	1	2	3	4	1	2	3	4	5	3	4	5
N_1	3	1	1	0	3	10	5	21	33	10	12	16	21	0	0	0
N_2	0	0	0	2	0	3	5	12	17	3	8	8	6	1	0	0
N_3	0	1	1	1	0	1	6	14	17	1	6	14	6	0	0	3
N_4	0	1	2	0	1	0	1	9	10	1	5	2	4	0	2	0
N_5	0	2	2	0	0	1	2	14	40	5	4	10	8	0	2	2
N_6	1	2	4	0	0	4	3	14	29	5	4	7	9	0	0	1
N_7	0	0	1	0	0	0	0	10	17	3	3	9	7	0	0	1
N_8	2	0	1	1	1	0	3	10	23	1	6	5	1	0	2	0
N_9	0	0	12	4	1	7	6	46	102	13	7	19	12	2	4	0
N_{10}	3	1	6	3	7	8	13	37	68	11	13	34	27	0	0	2
N_{11}	2	1	5	1	2	3	6	28	43	14	7	22	13	3	1	1
N_{12}	1	1	1	2	5	5	12	31	42	8	11	19	18	1	1	0
N_{13}	5	1	1	3	5	4	5	15	50	9	7	17	13	0	0	4
N_{14}	1	2	0	0	7	5	13	18	32	8	8	18	17	1	0	0
N_{15}	1	1	1	0	2	8	7	15	37	7	5	22	29	2	0	0
sin α	0.82	0.41	0.97	0.10	0.57	0.62	0.84	0.92	1.00	0.60	0.28	0.63	0.34	0.80	0.97	0.78
Eq 13	2.1	4.3	4.6	43.1	2.4	5.0	2.7	3.8	4.1	5.1	9.2	3.8	6.3	5.2	8.4	1.6
Eq 14	1.6	3.3	4.2	52.6	2.9	3.5	2.2	3.4	3.5	4.2	8.6	3.4	5.3	2.1	4.6	2.4
Eq 15	3.1	4.2	6.1	39.9	3.1	3.3	2.5	2.9	3.1	3.9	6.4	3.1	4.9	5.6	4.1	1.9
Eq 16	1.0	3.7	4.3	31.1	2.3	2.5	1.9	2.9	3.4	4.6	6.0	3.6	5.5	6.9	4.6	2.6
Eq 17	1.8	2.9	8.3	37.3	1.9	3.9	2.2	3.8	3.4	4.2	8.8	3.6	5.4	5.0	6.7	1.4
Eq 18	1.6	4.3	12.0	41.1	2.4	6.3	2.7	4.5	4.5	6.1	9.4	4.8	7.7	10.6	7.4	2.7
Av	1.9	3.8	6.6	40.9	2.5	4.1	2.4	3.5	3.6	4.7	8.1	3.7	5.9	5.9	6.0	2.1

NOTE.—Top: The number of fractures observed in trace length classes 1 to 15 defined in figure 12. Bottom: The values of mean trace length $\hat{\theta}'$ (ft) calculated from the appropriate equation in table 1 (s = 1 ft).

sample size, but site 4 was analyzed separately because its orientation is different. Similarly, the N_i for sites 6 to 10 were pooled to increase the sample size, but site 5 was analyzed separately because its orientation is different.

For panel 41, the N_i for sites 11 to 23 were pooled, but site 24 was analyzed separately because there the scanlines were vertical rather than horizontal. Site 24S, the south wall of the raise, was mapped by the five-scanline system, but the west wall, site 24W, offered only enough space for a four-scanline system.

For each fracture family mapped by a four-scanline scheme, four estimates of mean trace length $\hat{\theta}'$ were calculated (six estimates for five-scanline mapping), each based on a different set of the N_i; for the pooled groups of sites, 1 to 3, 6 to 10, and 11 to 23, each such estimate is an average $\hat{\theta}'$ over all the respective pooled sites. The multiple estimates are finally averaged to facilitate comparisons.

Omission from tables 8 and 9 of selected clusters for individual sites implies the lack of sufficient data to make meaningful calculations. Even so, the extreme average values, 30.8, 1.9, 40.9 and 2.1 ft, are obtained from individual sites having lengths of 50, 20, and 30 ft, which means that for this intensity of fracturing at least a 100-ft length of multiple-scanline mapping is required to achieve stable trace length averages. The very large values, exceeding 30 ft, correspond to $\sin \alpha = 0.1$, which suggests that this method does not produce reliable trace length estimates for fractures that intersect the scanlines at very small angles.

Eliminating the single-site estimates, one can arrive at overall average $\hat{\theta}'$ values of 2.5, 4.1, 2.4, and 3.5 ft respectively for clusters 1, 2, 3, and 4 at sites 6 to 10 in panel 2, which are significantly smaller than the 3.6- to 8.1-ft average values for clusters 1 to 5 at sites 11 to 23 in panel 41.

Summary, San Manuel Scanline Mapping

A mapping site typically exhibits four prominent fracture families that can be identified at other sites. These families occur at six different orientations, moderately to steeply dipping to all quadrants. Selecting the most prominent families is difficult because all are so well represented and they do not differ greatly as to spacing. The three most prominent, based chiefly on their consistent appearance (at the most mapping sites), are the vertical, NE-trending family, the family dipping moderately northward, and the family dipping moderately to steeply southwesterly. Median orthogonal fracture spacing within these three families ranges from 0.93 to 1.76 ft, with little difference between panel 2 and panel 41. Assuming an exponential distribution of fracture trace lengths, these three families exhibit mean trace lengths on the grizzly drift walls ranging from 2.4 to 3.5 ft in panel 2 (clusters 1, 3, and 4) and from 3.6 to 5.9 ft in panel 41 (clusters 1, 2, and 5).

SAN MANUEL FRACTURES—SUMMARY

The orientation and spacing characteristics of the most prominent fracture families are collected in table 10 to facilitate comparison of the results obtained from oriented core with those obtained by scanline mapping. The principal fracture orientations reported by Wilson (*36-37*) from measurements on the 1415 level and by Kendorski and Mahtab (*22*) from measurements on the 2015 level are among the families listed in table 10.

Analyses of the oriented core indicates six major fracture families, one of which, flat dipping, is not identified in the scanline mapping data. Similarly, scanline mapping indicates six major families, one of which, north dipping, is not identified by oriented-core analysis. On the average, a single drill hole exhibits three of the six major families, and a single mapping site exhibits four of the six.

Orthogonal spacing between fractures of a given family, which is influenced by the partitioning of the fractures into families, differs relatively little between the two methods, the median ranging from 0.49 to 3.38 ft for drill core and from 0.93 to 2.09 ft for scanline mapping. However, the spacing between successive fractures irrespective of fracture orientation is less than half as great in the oriented cores as on the exposures.

TABLE 10.—San Manuel Mine: Fracture families indicated by the two methods

PANEL 2: ORIENTED CORE, POOLED DRILL HOLES 4, 5, AND 6[1]								
Dip, dip azimuth	9, 50	—	—	54, 67	51, 157	84, 171	73, 240	74, 300.
W3/n	52/59	—	—	55/64	28/30	55/63	112/129	14/135.
Dip	Flat	—	—	Moderate	Moderate	Vertical	Steep	Steep.
Dip azimuth	—	—	—	E	SSE	SE	SW	W.
Cluster	10	—	—	2	4	1	7	3.
Orthogonal spacing	0.99 ft	—	—	0.88 ft	0.52 ft	1.40 ft	0.69 ft	0.44 ft.
PANEL 2: SCANLINE MAPPING, POOLED SITES 1 to 10[2]								
Dip, dip azimuth	—	57, 356	42, 31	—	78, 132	—	67, 237	—
W3/n	—	82/93	96/116	—	180/241	—	334/479	—
Dip	—	Moderate	Moderate	Steep	Steep	Steep	Steep	—
Dip azimuth	—	N	NE	E	SE-NW	S	SW	—
Cluster	—	1	2	—	3	—	4	—
Orthogonal spacing	—	1.56 ft	2.09 ft	—	0.93 ft	—	1.20 ft	—
PANEL 41: ORIENTED CORE, POOLED DRILL HOLES 1, 2, AND 3[3]								
Dip, dip azimuth	9, 240	—	—	71, 90	78, 149	41, 130	75, 205	75, 254.
W3/n	177/233	—	—	70/76	46/51	35/37	70/80	26/27.
Dip	Flat	—	—	Steep	Steep	Moderate	Steep	Steep.
Dip azimuth	—	—	—	E	SSE	SE	SW	W.
Cluster	10	—	—	4	3	8	5	2.
Orthogonal spacing	0.49 ft	—	—	1.00 ft	0.90 ft	2.83 ft	0.84 ft	1.57 ft.
PANEL 41: SCANLINE MAPPING, POOLED SITES 11 to 24[4]								
Dip, dip azimuth	—	40, 344	—	39, 69	87, 316	41, 154	—	41, 251.
W3/n	—	87/95	—	96/109	404/580	196/225	—	169/199.
Dip	—	Moderate	—	Moderate	Vertical	Moderate	Vertical	Moderate.
Dip azimuth	—	N	—	ENE	SE-NW	SSE	ENE-WSW	WSW.
Cluster	—	2	—	3	1	4	—	5.
Orthogonal spacing	—	1.76 ft	—	1.05 ft	1.30 ft	1.57 ft	—	1.13 ft.

— No appropriate cluster identified.
[1]Fracture spacing, irrespective of fracture orientation, median = 0.30 ft.
[2]Fracture spacing, irrespective of fracture orientation, median = 0.90 ft.
[3]Fracture spacing, irrespective of fracture orientation, median = 0.35 ft.
[4]Fracture spacing, irrespective of fracture orientation, median = 0.80 ft.

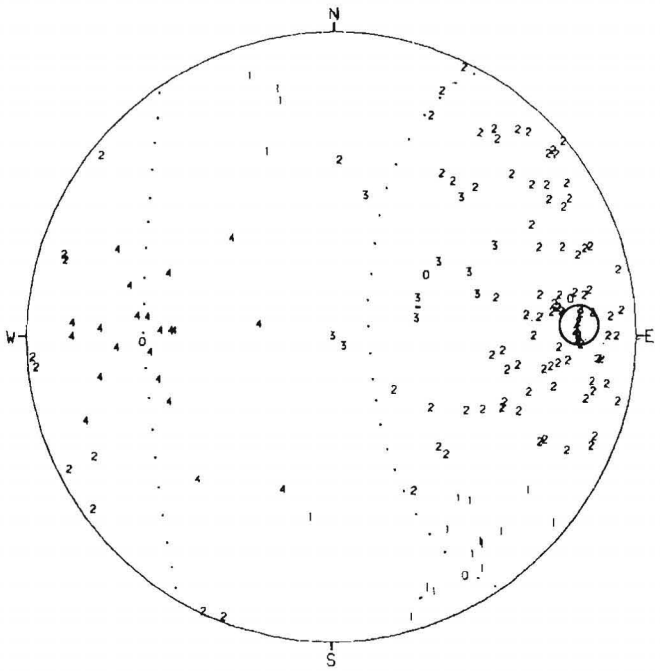

HOLE 1

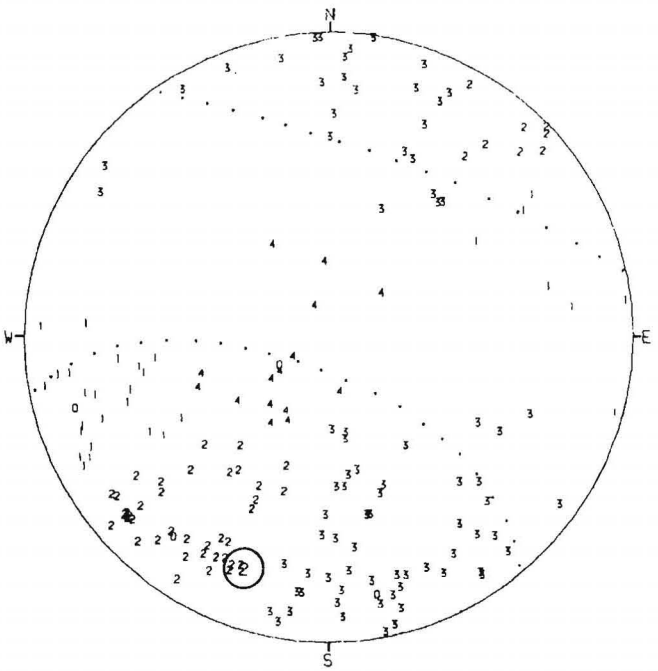

HOLE 2

FRACTAN r	Clusters					Eigenvalues		
	No.	Obs	Est	Dip	Az	W1	W2	W3
HOLE 1 (INCL +20, AZ 88)								
10.50	1	18	37	79	151	1	2	15
	2	98	99	68	81	6	16	75
	3	10	14	30	57	0	1	9
	4	21	40	52	268	1	2	18
HOLE 2 (INCL +20, AZ 200)								
12.50	1	31	50	76	254	1	4	26
	2	48	50	72	218	1	5	42
	3	79	91	75	169	6	17	56
	4	15	30	15	240	1	1	13
HOLE 3 (INCL +90)								
9.00	1	25	85	73	312	1	3	21
	2	51	131	67	221	3	4	44
	3	34	48	45	124	1	2	31
	4	229	231	8	339	1	40	168

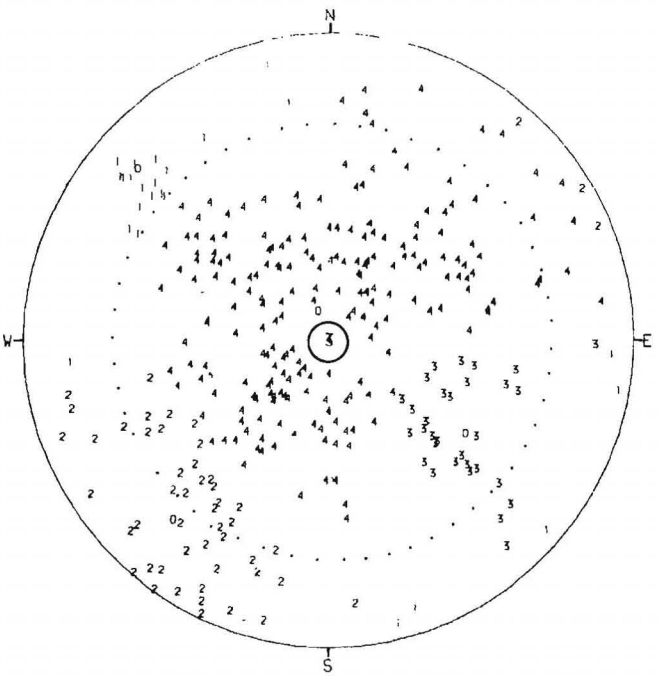

HOLE 3

FIGURE 31.—San Manuel Mine oriented core, holes 1, 2, and 3, polar equal-area plots, upper hemisphere.

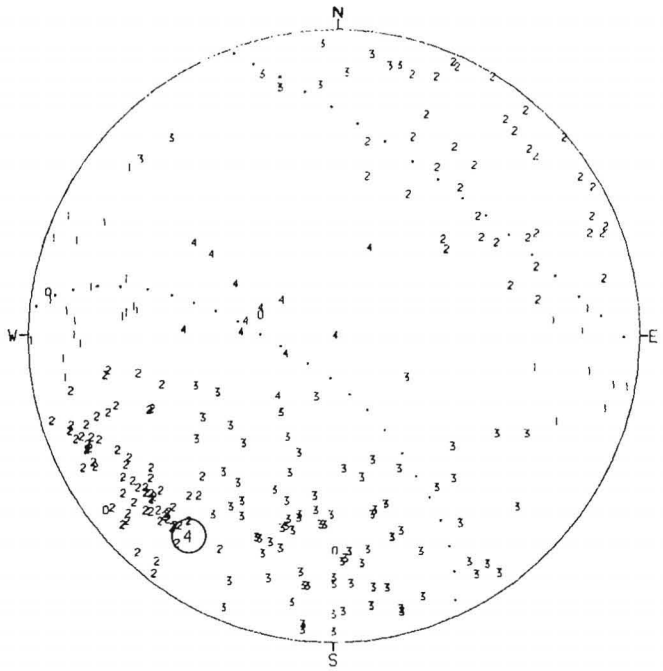

HOLE 4

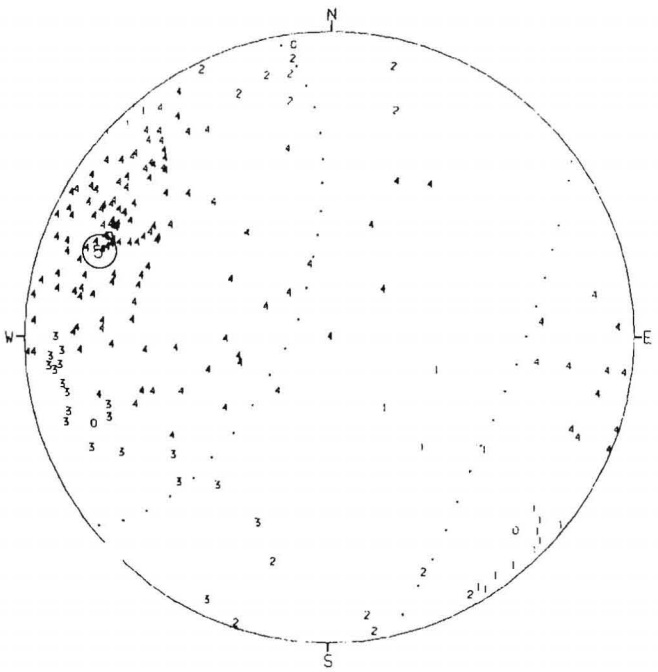

HOLE 5

FRACTAN r	Clusters					Eigenvalues		
	No.	Obs	Est	Dip	Az	W1	W2	W3
HOLE 4 (INCL +20, AZ 216)								
9.65	1	30	62	84	278	1	3	26
	2	110	117	83	232	6	15	88
	3	100	121	60	180	8	14	77
	4	17	40	20	285	1	1	16
HOLE 5 (INCL +20, AZ 290)								
9.60	1	19	25	77	136	0	2	16
	2	14	31	86	353	1	1	12
	3	19	24	71	250	0	2	17
	4	138	138	69	294	12	17	110
HOLE 6 (INCL +90)								
13.00	1	24	70	70	169	1	2	21
	2	9	13	44	135	0	0	9
	3	70	88	37	40	5	12	53
	4	55	59	20	223	4	5	46

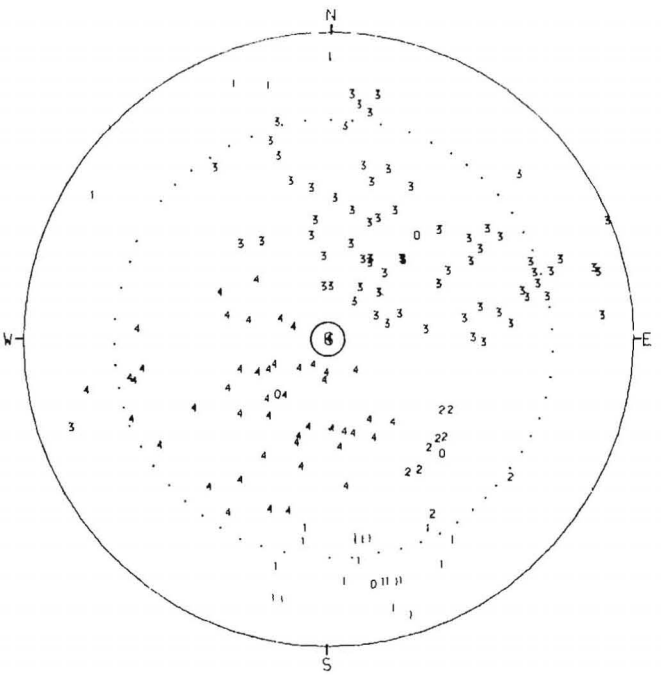

HOLE 6

FIGURE 32.—San Manuel Mine oriented core, holes 4, 5, and 6, polar equal-area plots, upper hemisphere.

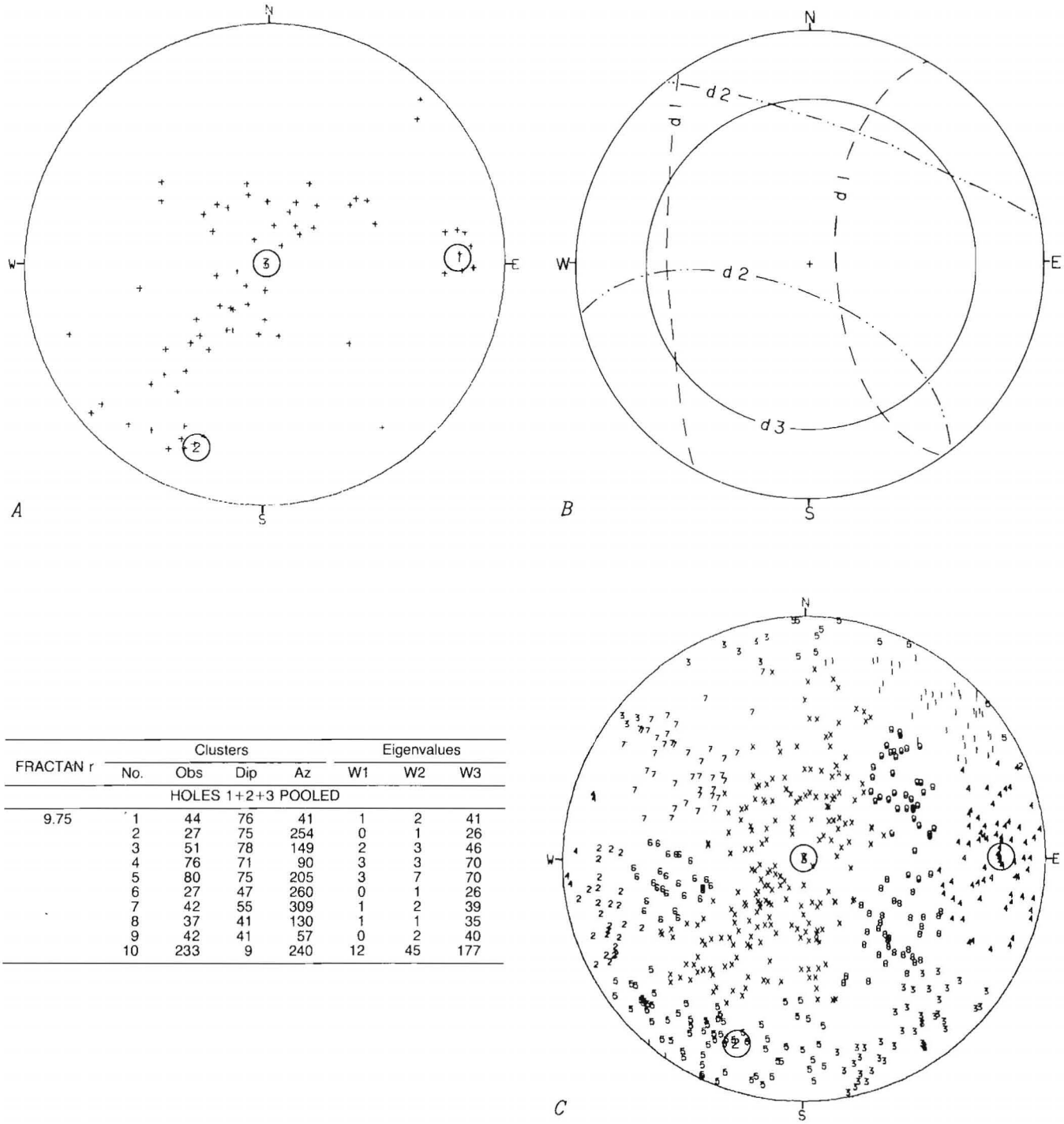

FRACTAN r	Clusters				Eigenvalues		
	No.	Obs	Dip	Az	W1	W2	W3
HOLES 1+2+3 POOLED							
9.75	1	44	76	41	1	2	41
	2	27	75	254	0	1	26
	3	51	78	149	2	3	46
	4	76	71	90	3	3	70
	5	80	75	205	3	7	70
	6	27	47	260	0	1	26
	7	42	55	309	1	2	39
	8	37	41	130	1	1	35
	9	42	41	57	0	2	40
	10	233	9	240	12	45	177

FIGURE 33.—San Manuel Mine oriented core, pooled holes 1 + 2 + 3, polar equal-area plots, upper hemisphere. *A*, Dense points determined by FRACTAN cluster solution; *B*, 60° cones about the three drill hole axes; *C*, numerals corresponding to the cluster numbers denote the poles of the joint planes (X = 10).

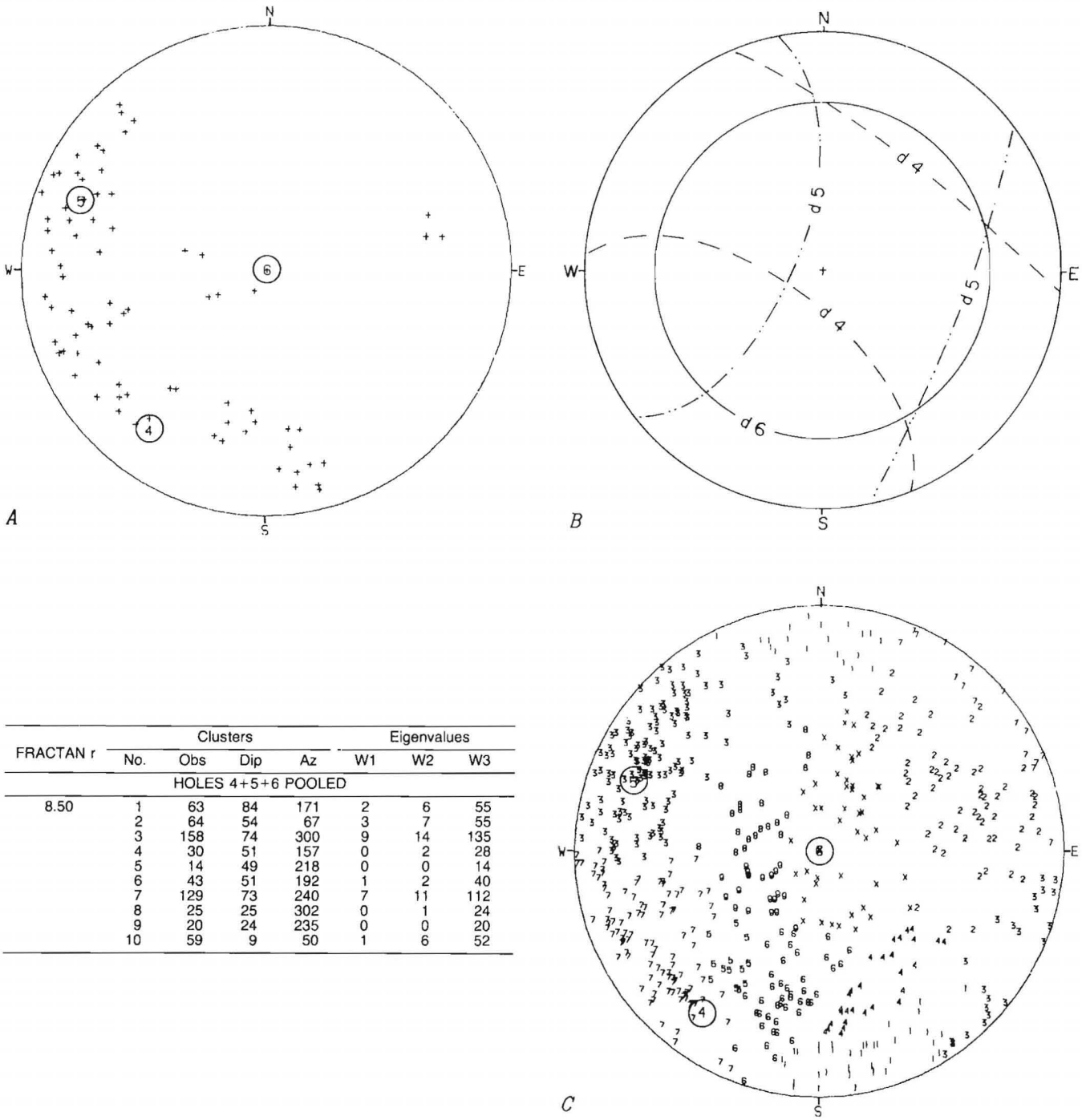

FRACTAN r	Clusters				Eigenvalues		
	No.	Obs	Dip	Az	W1	W2	W3
HOLES 4+5+6 POOLED							
8.50	1	63	84	171	2	6	55
	2	64	54	67	3	7	55
	3	158	74	300	9	14	135
	4	30	51	157	0	2	28
	5	14	49	218	0	0	14
	6	43	51	192	1	2	40
	7	129	73	240	7	11	112
	8	25	25	302	0	1	24
	9	20	24	235	0	0	20
	10	59	9	50	1	6	52

FIGURE 34.—San Manuel Mine oriented core, pooled holes 4 + 5 + 6, polar equal-area plots, upper hemisphere. *A*, Dense points determined by FRACTAN cluster solution; *B*, 60° cones about the three drill hole axes; *C*, numerals corresponding to the cluster numbers denote the poles of the joint planes (X = 10).

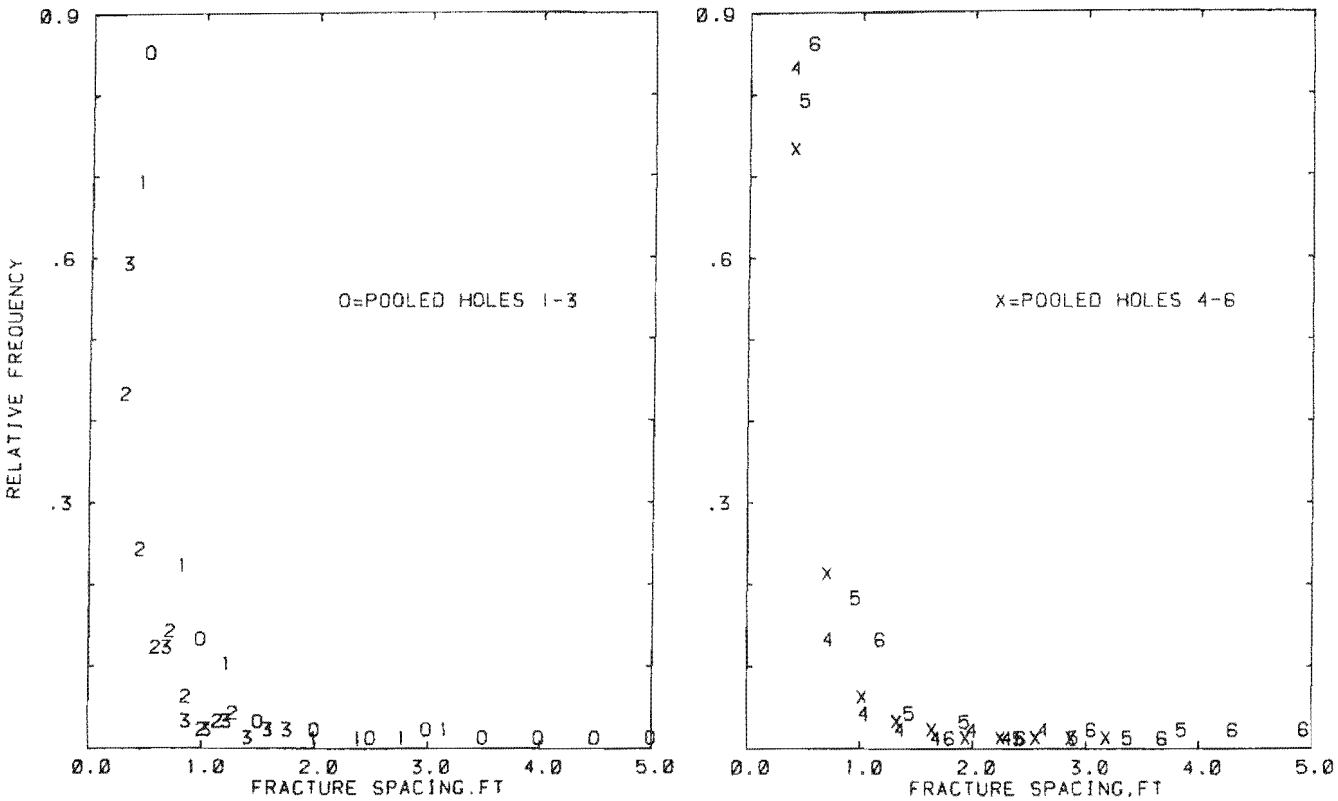

Drill hole		1	2	3	Pooled 1+2+3	Pooled 4+5+6	4	5	6
Spacings observed		94	100	184	378	313	118	103	92
Maximum	ft	3.30	1.30	1.80	3.30	5.20	2.75	4.05	5.20
Minimum	ft	0.20	0.20	0.20	0.20	0.20	0.20	0.20	0.20
Arithmetic mean	ft	0.54	0.45	0.40	0.45	0.49	0.40	0.50	0.59
Median	ft	0.43	0.35	0.35	0.35	0.30	0.30	0.30	0.36
Mode	ft	0.25	0.25	0.20	0.20	0.20	0.25	0.20	0.20
Std dev	ft	0.41	0.26	0.24	0.30	0.54	0.33	0.49	0.74
Skewness		3.59	1.28	2.42	3.34	5.25	4.42	4.25	4.57
Mean log of spacing		−0.79	−0.94	−1.05	−0.96	−0.97	−1.09	−0.95	−0.85
Std dev of logs		0.57	0.52	0.50	0.53	0.62	0.51	0.65	0.69
Distributions[1]		L,E	L,E	L,E	L,E	None	L,E	L,E	E,χ
Best fit		E	E	E	E	χ	E	E	E

[1]Acceptable fit at the 5-pct significant level (L = lognormal, E = exponential, χ = chi squared).

FIGURE 35.—San Manuel Mine oriented core, GDIST analyses of the spacing between successive fractures as measured along drill core. Relative frequency (spacings in each class ÷ total spacings) is plotted at the midpoint of the corresponding class interval; the numeral indicating the drill hole number is centered on the plotted point. Below the histograms are listed the parameters of the distributions.

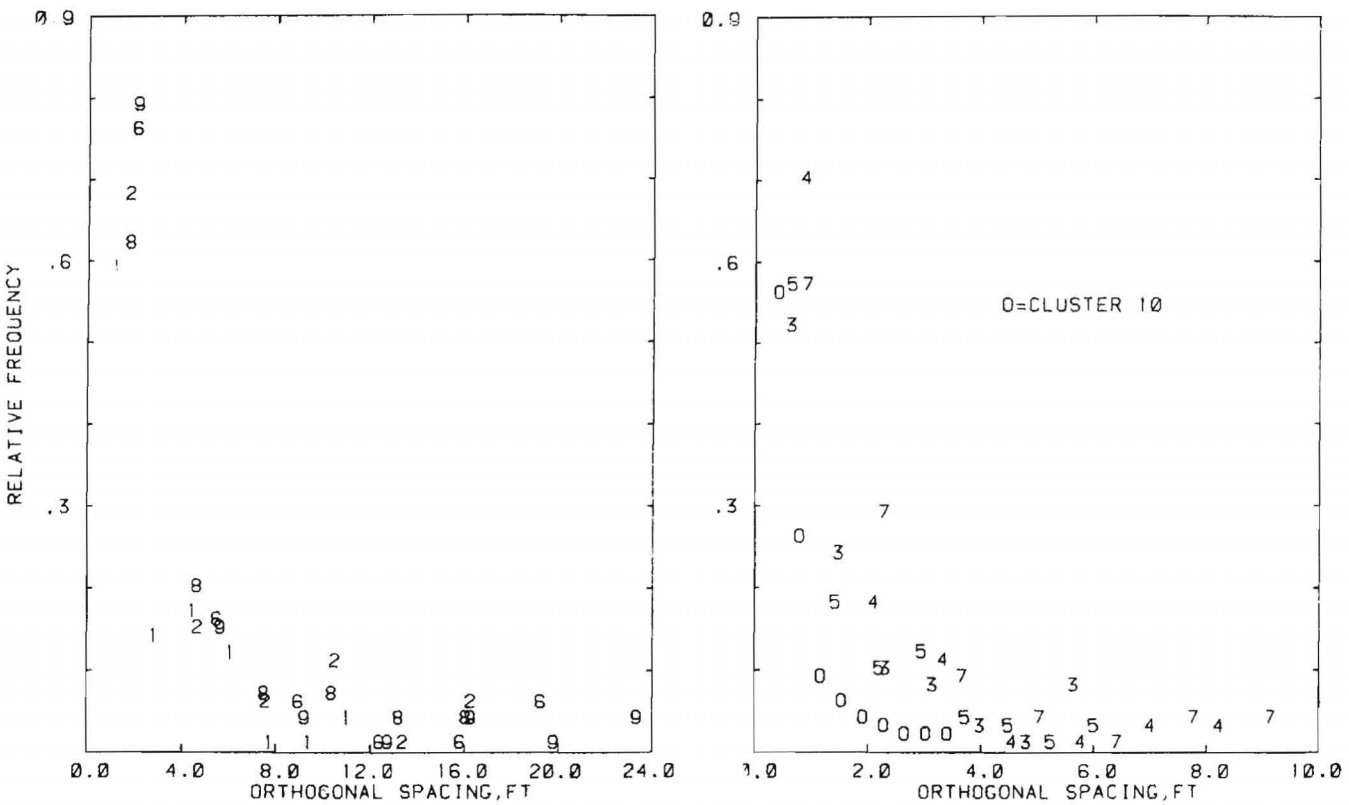

	Pooled holes 1+2+3									
Cluster	1	2	3	4	5	6	7	8	9	10
Spacings observed	38	21	43	59	64	20	36	31	36	173
Maximum ft	11.60	17.49	5.97	8.74	6.30	20.73	9.74	17.23	24.86	3.51
Minimum ft	0.19	0.15	0.15	0.20	0.20	0.17	0.17	0.19	0.15	0.15
Arithmetic mean ft	2.40	3.53	1.49	1.43	1.31	3.21	1.93	4.08	3.28	0.68
Median ft	1.35	1.57	0.90	1.00	0.84	1.58	1.35	2.83	1.90	0.49
Mode ft	0.28	0.15	0.31	0.40	ND	1.43	ND	2.91	ND	0.20
Std dev ft	2.38	4.62	1.48	1.48	1.17	4.59	2.01	3.99	4.79	0.58
Skewness	1.81	1.89	1.74	2.82	1.76	2.97	2.42	1.76	3.10	2.14
Mean log of spacing	0.43	0.56	–0.03	–0.02	–0.08	0.52	0.23	1.00	0.47	–0.65
Std dev of logs	1.00	1.27	0.95	0.86	0.86	1.19	0.97	0.17	1.24	0.70
Distributions[1]	N,L,E,χ	L,E,χ	L,E,χ	L,E,χ	L,E,χ	L,E,χ	L,E,χ,Γ	L,E	L,E,χ	L,E
Best fit	E	L	L	E	χ	L	L	L	L	E

ND = No appropriate value was determinable.
[1]Acceptable fit at the 5-pct significance level (N = normal, L = lognormal, E = exponential, χ = chi squared, Γ = gamma).

FIGURE 36.—San Manuel Mine oriented core, GDIST analyses of orthogonal fracture spacing within fracture families, pooled drill holes 1 + 2 + 3. Relative frequency (spacings in each class ÷ total spacings) is plotted at the midpoint of the corresponding class interval; the numeral indicating the cluster number is centered on the plotted point. Below the histograms are listed the parameters of the distributions.

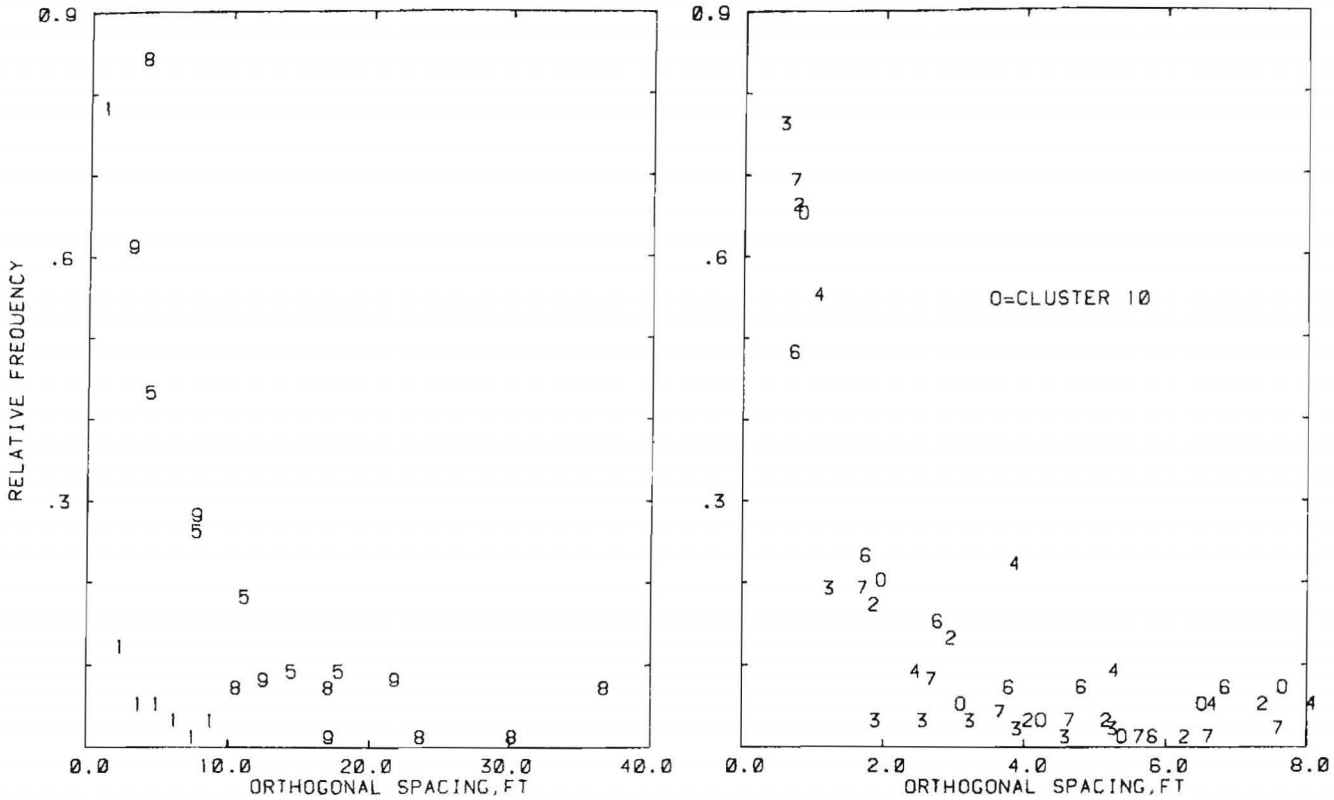

		Pooled holes 4+5+6									
Cluster		1	2	3	4	5	6	7	8	9	10
Spacings observed		47	51	108	24	12	36	94	18	15	47
Maximum	ft	9.10	7.85	5.51	8.68	19.11	7.28	8.01	39.62	23.79	8.15
Minimum	ft	0.15	0.15	0.17	0.31	2.43	0.16	0.17	0.38	0.46	0.20
Arithmetic mean	ft	1.30	1.47	0.71	2.32	7.82	1.84	1.11	5.35	5.62	1.71
Median	ft	0.52	0.88	0.44	1.40	7.03	1.46	0.69	1.23	3.38	0.99
Mode	ft	0.31	0.21	0.20	ND	ND	ND	0.23	ND	ND	0.35
Std dev	ft	1.79	1.64	0.80	2.22	5.07	1.80	1.20	9.73	6.25	2.11
Skewness		2.52	2.23	3.45	1.25	0.94	1.66	2.69	2.77	1.74	1.99
Mean log of spacing		–0.35	–0.11	–0.68	0.37	1.86	0.14	–0.34	0.68	1.16	–0.02
Std dev of logs		1.05	1.01	0.75	1.03	0.66	1.04	0.93	1.37	1.15	1.04
Distributions[1]		N,L,E,χ	L,E,χ	χ	N,L,E,χ	N,L,E,χ	N,L,E,χ,Γ	L,E,χ	L,E,χ	N,L,E,χ	L,E,χ,Γ
Best fit		L	L	χ	χ	L	χ	χ	L	E	L

ND = No appropriate value was determinable.
[1]Acceptable fit at the 5-pct significance level (N = normal, L = lognormal, E = exponential, χ = chi squared, Γ = gamma).

FIGURE 37.—San Manuel Mine oriented core, GDIST analyses of orthogonal fracture spacing within fracture families, pooled drill holes 4 + 5 + 6. Relative frequency (spacings in each class ÷ total spacings) is plotted at the midpoint of the corresponding class interval; the numeral indicating the cluster number is centered on the plotted point. Below the histograms are listed the parameters of the distributions.

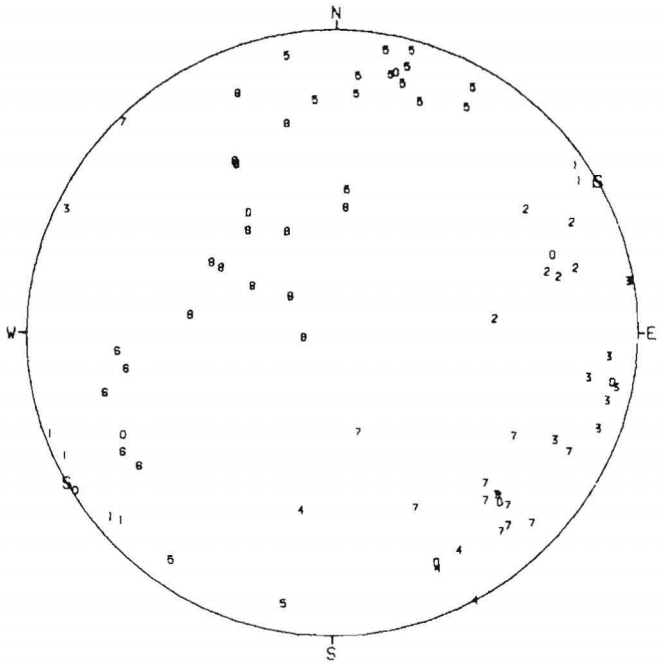

SITE 1

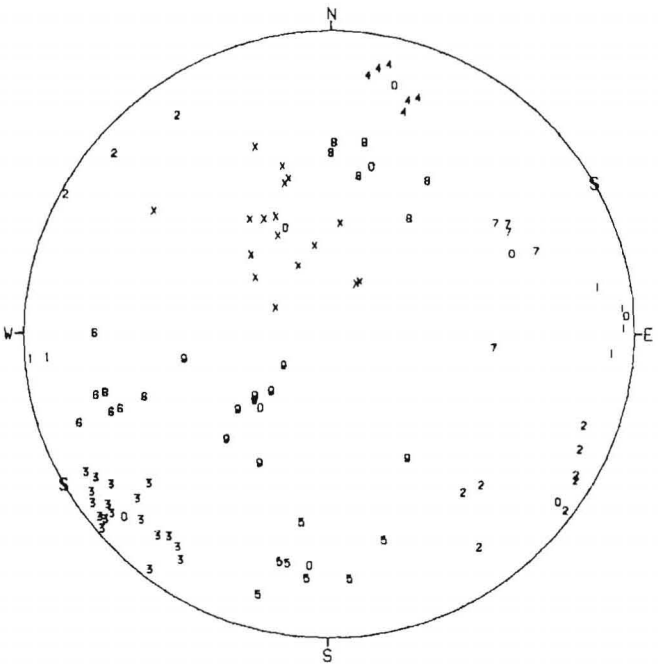

SITE 2

FRACTAN r	Clusters				Eigenvalues		
	No.	Obs	Dip	Az	W1	W2	W3
			SITE 1				
10.50	1	7	89	238	0	0	7
	2	7	65	70	0	0	7
	3	9	82	100	0	1	8
	4	7	72	156	0	0	7
	5	15	77	13	0	1	14
	6	11	65	244	0	0	11
	7	15	67	136	0	1	14
	8	16	40	325	0	2	14
			SITE 2				
11.00	1	6	87	86	0	0	6
	2	13	83	126	0	1	12
	3	20	79	228	0	0	19
	4	6	74	14	0	0	6
	5	7	66	185	0	0	7
	6	10	65	255	0	0	10
	7	5	55	66	0	0	5
	8	6	47	14	0	0	6
	9	10	27	223	0	1	9
	10	18	31	337	1	1	16
			SITE 3				
10.50	1	6	78	67	0	0	6
	2	4	74	10	0	0	4
	3	16	77	268	1	1	14
	4	24	72	224	1	1	22
	5	2	52	238	0	0	2
	6	7	34	40	0	0	7
	7	6	18	271	0	0	6

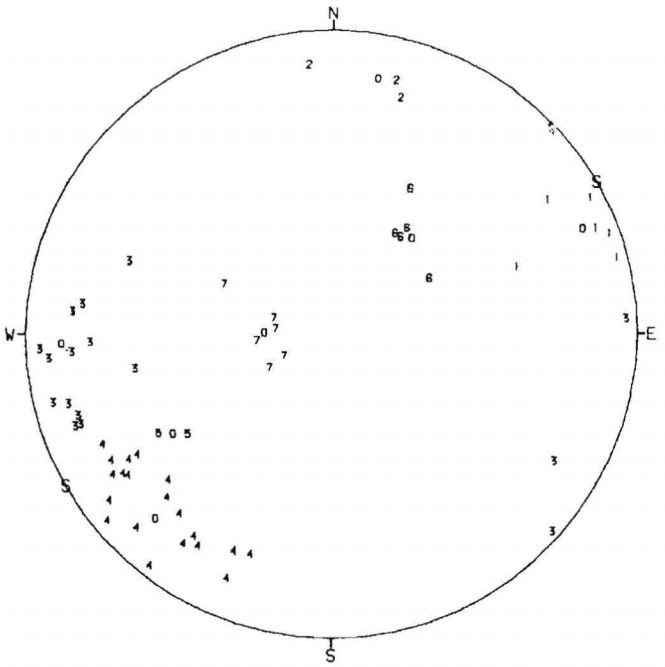

SITE 3

FIGURE 38.—San Manuel Mine scanline mapping, sites, 1, 2, and 3, polar equal-area plots, upper hemisphere.

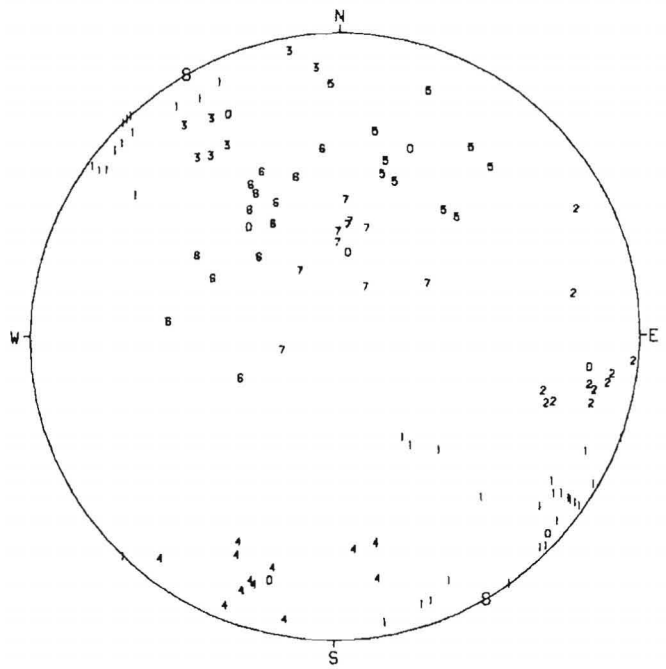

SITE 4

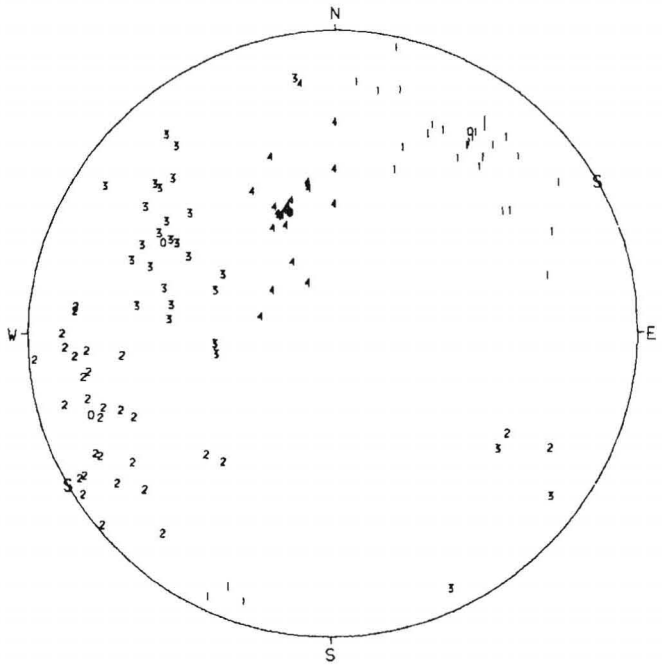

SITE 6

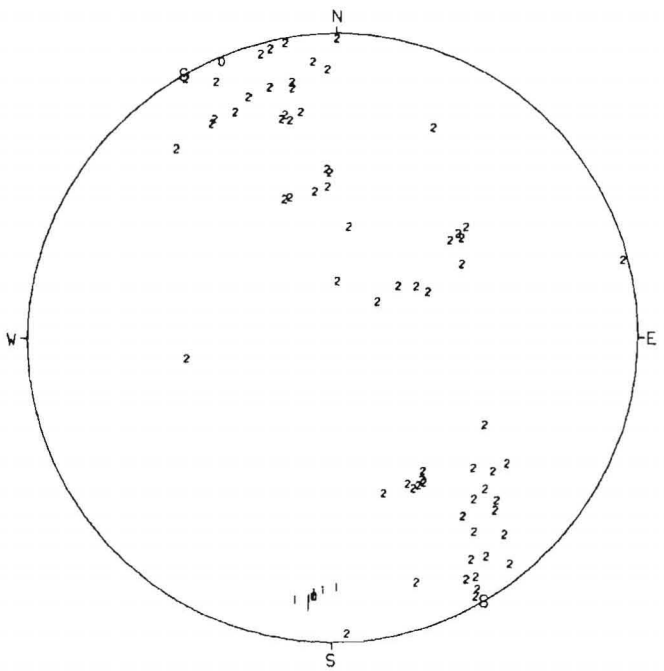

SITE 5

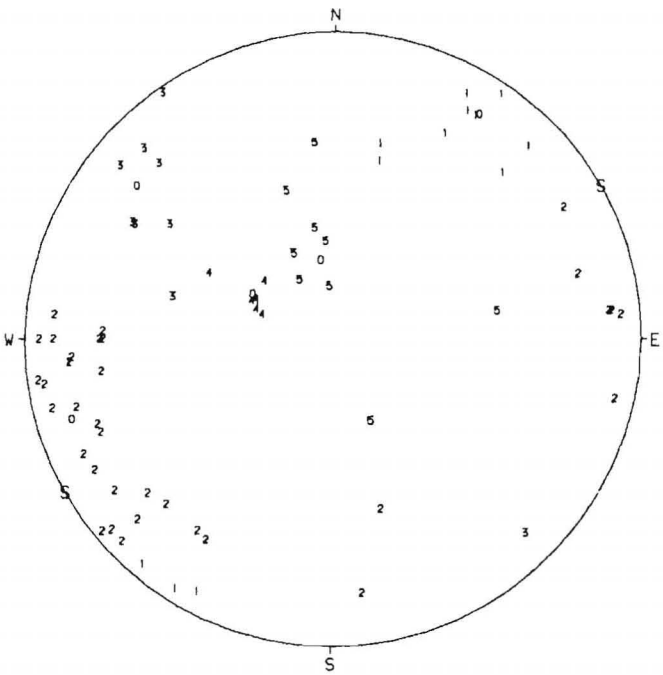

SITE 7

FRACTAN r	Clusters				Eigenvalues		
	No.	Obs	Dip	Az	W1	W2	W3
			SITE 4				
11.00	1	43	86	133	2	3	39
	2	11	73	97	0	1	10
	3	7	71	334	0	0	7
	4	13	72	195	0	1	12
	5	12	56	21	0	1	11
	6	14	38	321	0	1	13
	7	12	22	7	0	1	11
			SITE 5				
11.00	1	10	74	184	0	0	10
	2	78	88	338	4	28	46

FRACTAN r	Clusters				Eigenvalues		
	No.	Obs	Dip	Az	W1	W2	W3
			SITE 6				
11.00	1	29	69	34	1	2	26
	2	36	72	251	1	4	31
	3	34	53	298	1	5	28
	4	26	35	340	0	2	24
			SITE 7				
11.00	1	18	76	33	0	1	17
	2	42	78	253	2	5	35
	3	10	70	308	0	1	9
	4	7	25	299	0	0	7
	5	12	21	351	1	1	10

FIGURE 39.—San Manuel Mine scanline mapping, sites 4, 5, 6, and 7, polar equal-area plots, upper hemisphere.

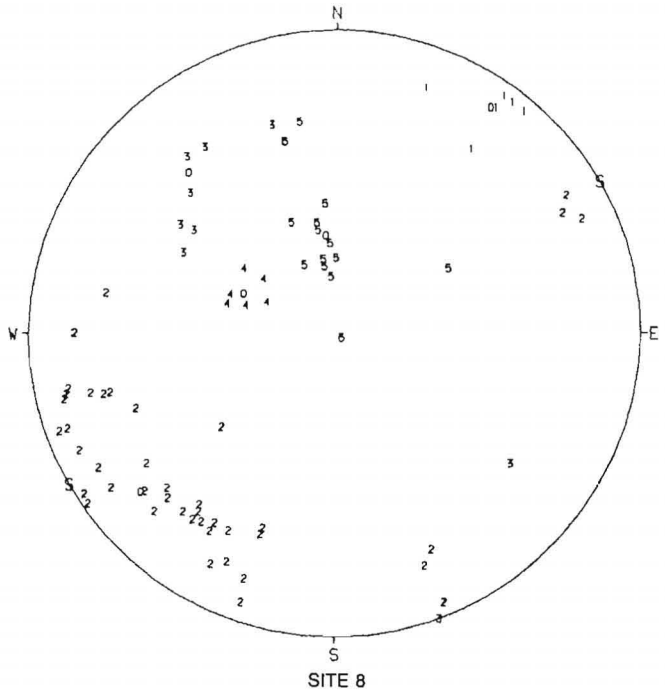

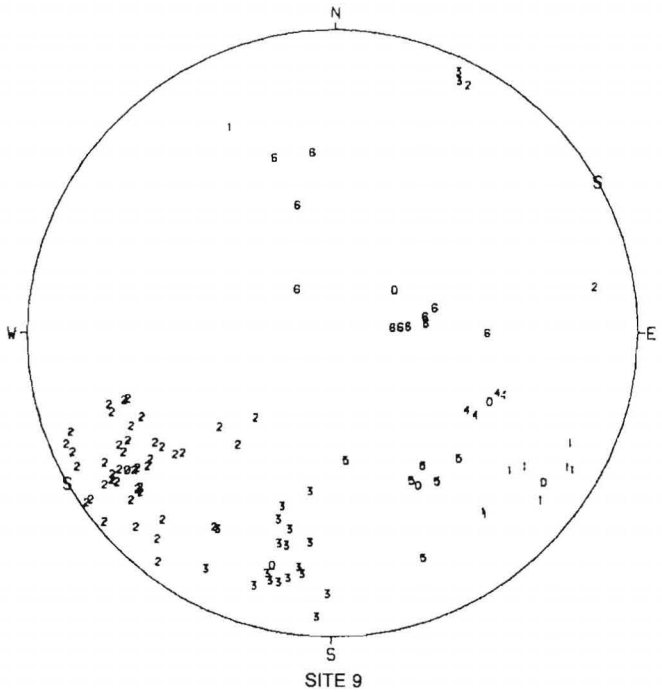

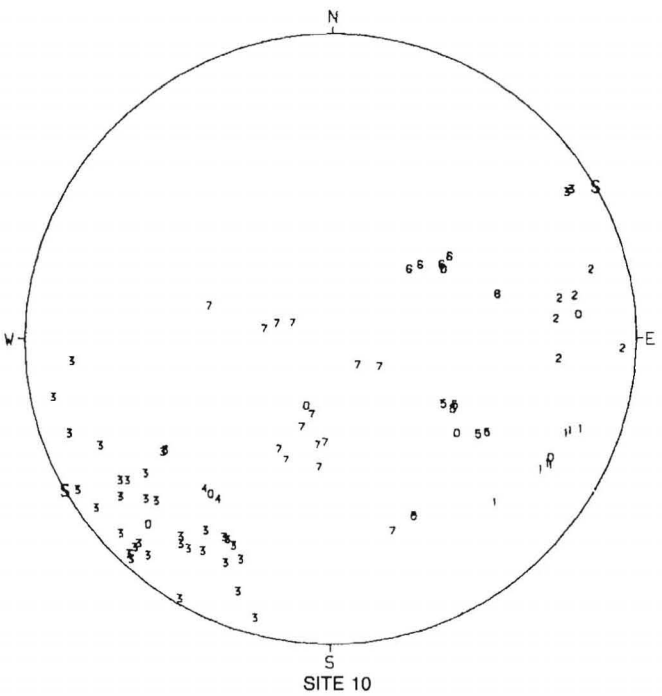

FRACTAN r	Clusters				Eigenvalues		
	No.	Obs	Dip	Az	W1	W2	W3
			SITE 8				
11.00	1	6	79	34	0	0	6
	2	42	71	230	2	7	33
	3	10	61	318	0	1	8
	4	7	27	293	0	0	7
	5	16	26	354	0	1	15
			SITE 9				
10.50	1	13	74	126	0	1	12
	2	48	70	236	1	3	44
	3	20	68	194	0	1	19
	4	5	47	114	0	0	5
	5	6	48	151	0	0	6
	6	13	20	55	0	2	11
			SITE 10				
11.00	1	7	71	118	0	0	7
	2	6	70	84	0	0	6
	3	36	74	224	1	3	32
	4	2	54	218	0	0	2
	5	6	43	127	0	0	6
	6	5	36	58	0	0	5
	7	14	19	200	0	1	12

FIGURE 40.—San Manuel Mine scanline mapping, sites 8, 9, and 10, polar equal-area plots, upper hemisphere.

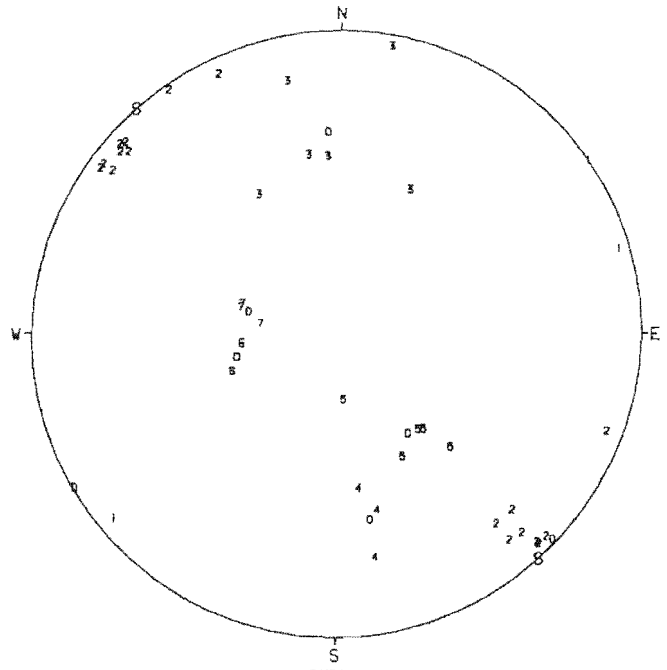

SITE 11

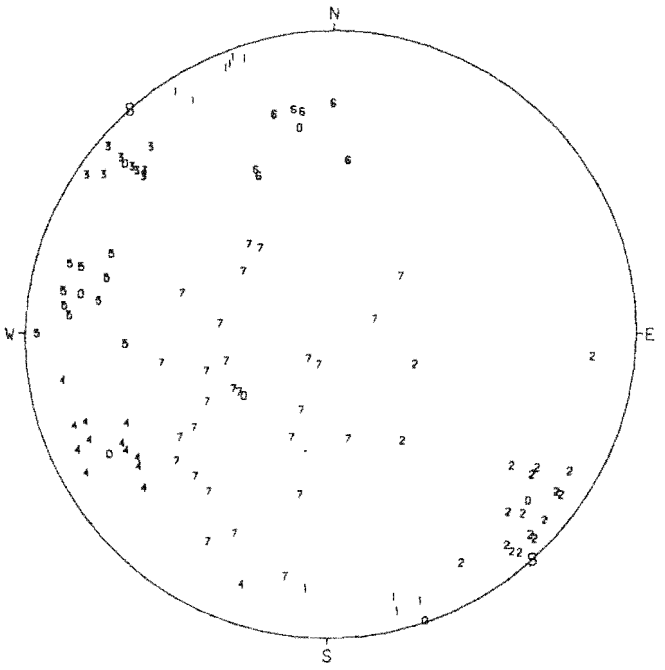

SITE 13

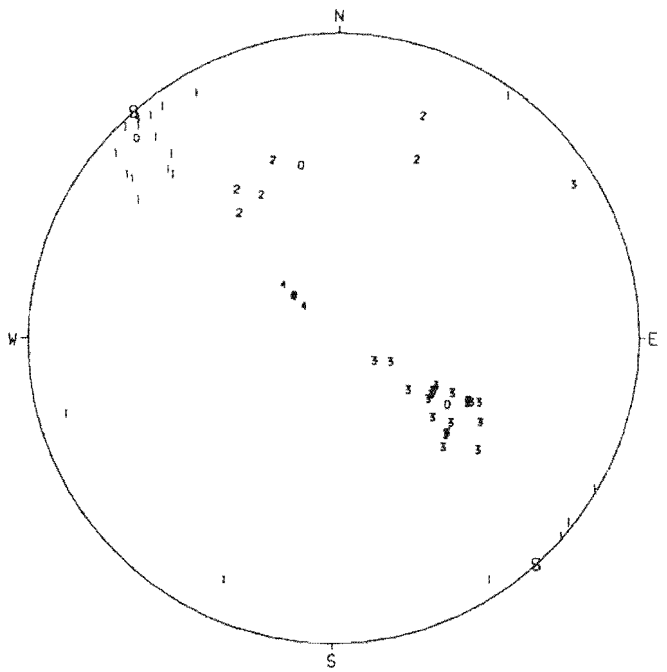

SITE 12

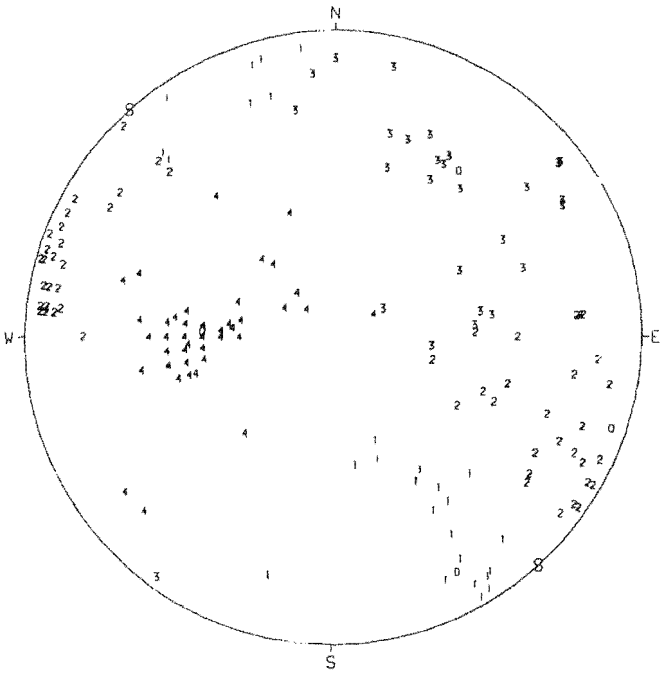

SITE 14

FRACTAN r	Clusters				Eigenvalues		
	No.	Obs	Dip	Az	W1	W2	W3
			SITE 11				
10.50	1	3	9	59	0	0	3
	2	17	88	134	0	1	16
	3	6	56	356	0	1	5
	4	3	52	170	0	0	3
	5	5	33	145	0	0	5
	6	2	28	256	0	0	2
	7	3	25	284	0	0	3
			SITE 12				
11.00	1	23	82	315	1	3	20
	2	6	48	348	0	1	5
	3	22	35	120	1	1	21
	4	5	16	315	0	0	5

FRACTAN r	Clusters				Eigenvalues		
	No.	Obs	Dip	Az	W1	W2	W3
			SITE 13				
11.00	1	10	89	161	0	1	9
	2	19	74	130	1	1	17
	3	9	77	310	0	0	9
	4	13	71	241	0	1	12
	5	10	72	279	0	0	10
	6	8	58	351	0	0	8
	7	29	28	234	2	5	22
			SITE 14				
11.00	1	29	75	152	1	5	23
	2	62	85	108	3	7	53
	3	32	57	37	2	4	26
	4	60	35	272	2	4	54

FIGURE 41.—San Manuel Mine scanline mapping, sites 11, 12, 13, and 14, polar equal-area plots, upper hemisphere.

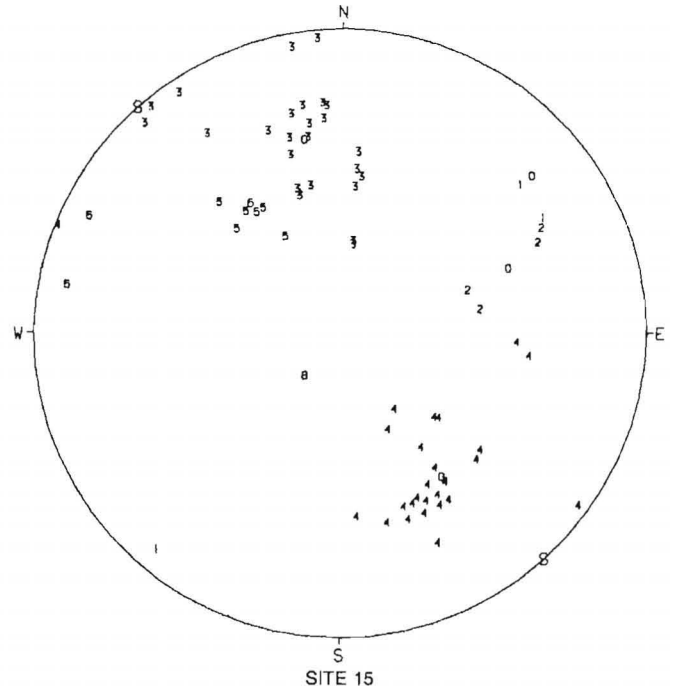

SITE 15

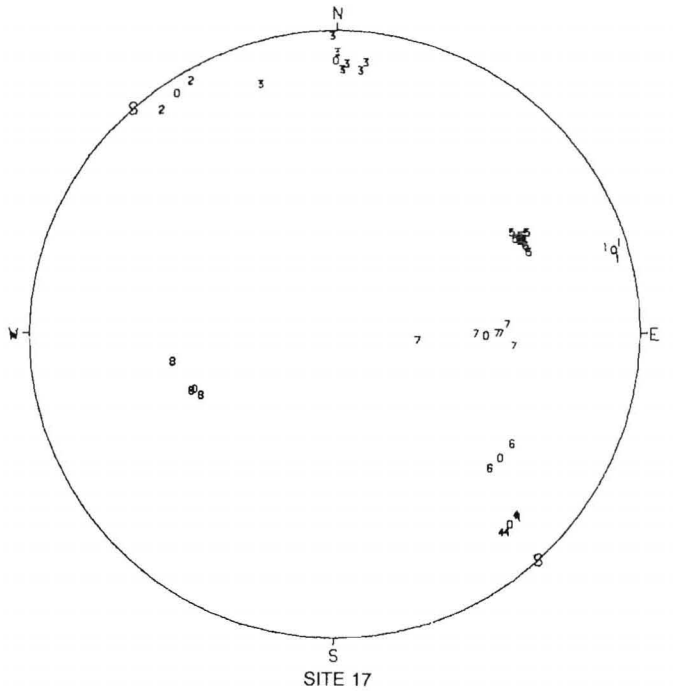

SITE 17

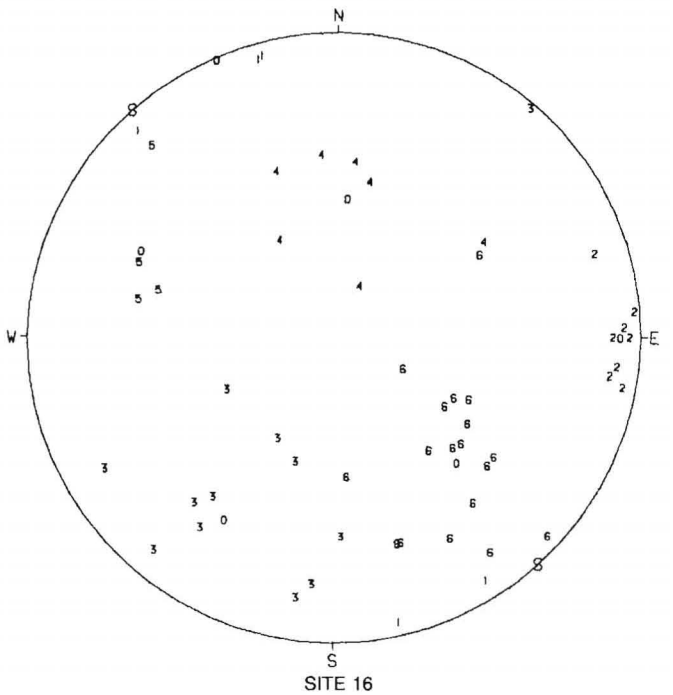

SITE 16

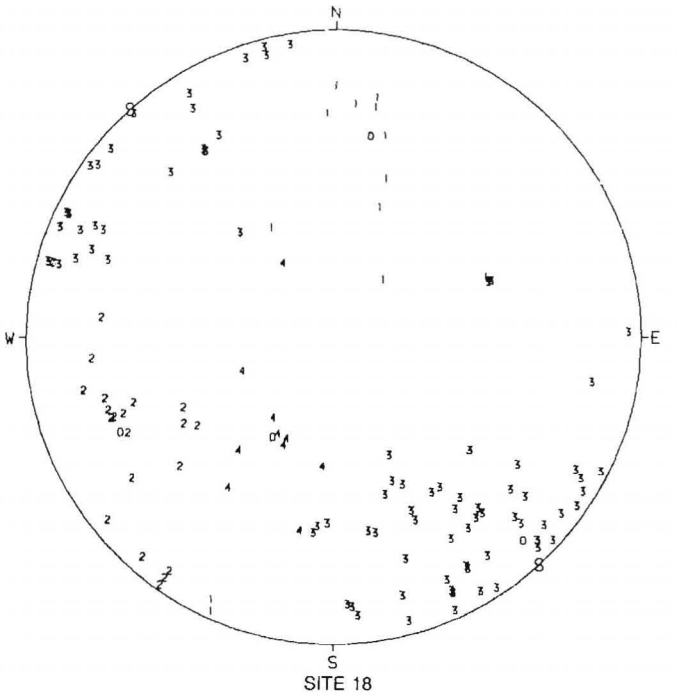

SITE 18

FRACTAN r	Clusters				Eigenvalues		
	No.	Obs	Dip	Az	W1	W2	W3
			SITE 15				
11.00	1	6	70	50	0	0	6
	2	4	49	69	0	0	4
	3	27	54	349	1	3	23
	4	29	49	145	1	2	26
	5	11	48	313	0	1	10
	6	4	15	220	0	0	4
			SITE 16				
10.50	1	5	89	336	0	0	5
	2	8	83	90	0	0	8
	3	12	59	211	1	1	10
	4	7	37	4	0	1	6
	5	4	59	294	0	0	4
	6	18	48	136	1	2	15

FRACTAN r	Clusters				Eigenvalues		
	No.	Obs	Dip	Az	W1	W2	W3
			SITE 17				
10.50	1	3	84	73	0	0	3
	2	2	85	326	0	0	2
	3	7	79	0	0	0	7
	4	4	74	138	0	0	4
	5	8	58	63	0	0	8
	6	2	57	127	0	0	2
	7	6	41	91	0	0	6
	8	6	41	248	0	0	6
			SITE 18				
11.00	1	15	56	10	1	2	12
	2	24	65	246	1	2	21
	3	93	80	137	8	14	70
	4	12	32	211	0	1	11

FIGURE 42.—San Manuel Mine scanline mapping, sites 15, 16, 17, and 18, polar equal-area plots, upper hemisphere

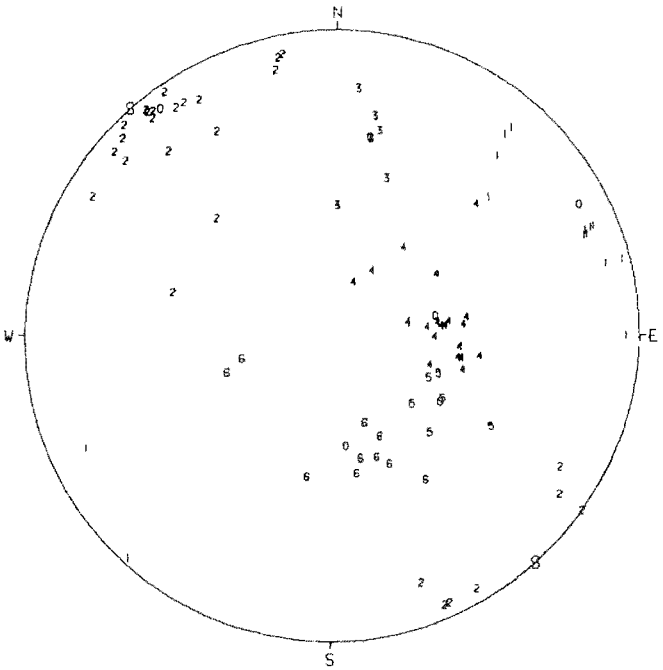

SITE 19

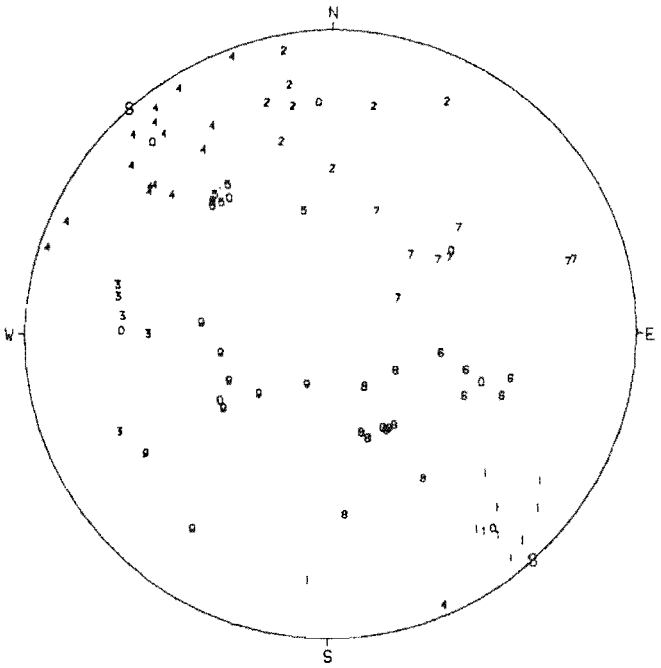

SITE 20

FRACTAN r	Clusters				Eigenvalues		
	No.	Obs	Dip	Az	W1	W2	W3
			SITE 19				
10.50	1	14	80	62	0	1	13
	2	27	83	322	1	2	24
	3	7	55	10	0	0	7
	4	23	28	79	0	1	22
	5	6	34	122	0	0	6
	6	10	30	173	0	1	9
			SITE 20				
11.00	1	10	72	140	0	1	9
	2	8	65	356	0	0	7
	3	5	58	271	0	0	5
	4	16	75	317	0	1	15
	5	7	47	323	0	0	7
	6	6	43	108	0	0	6
	7	9	39	55	0	1	8
	8	10	29	150	0	0	10
	9	8	35	239	0	1	7
			SITE 21				
10.50	1	5	81	119	0	0	5
	2	8	79	283	0	1	7
	3	16	76	156	0	2	14
	4	10	63	81	0	1	9
	5	26	69	331	1	2	23
	6	14	48	185	0	1	13
	7	13	38	108	0	1	12

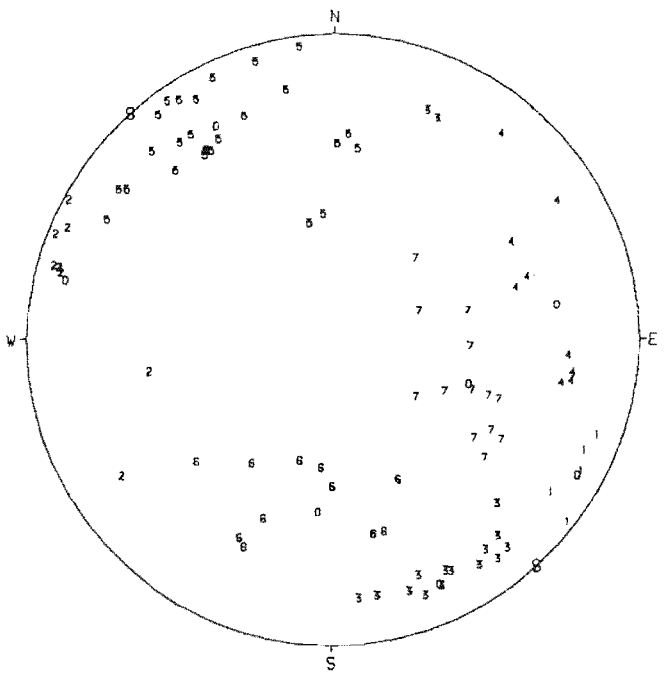

SITE 21

FIGURE 43.—San Manuel Mine scanline mapping, sites 19, 20, and 21, polar equal-area plots, upper hemisphere.

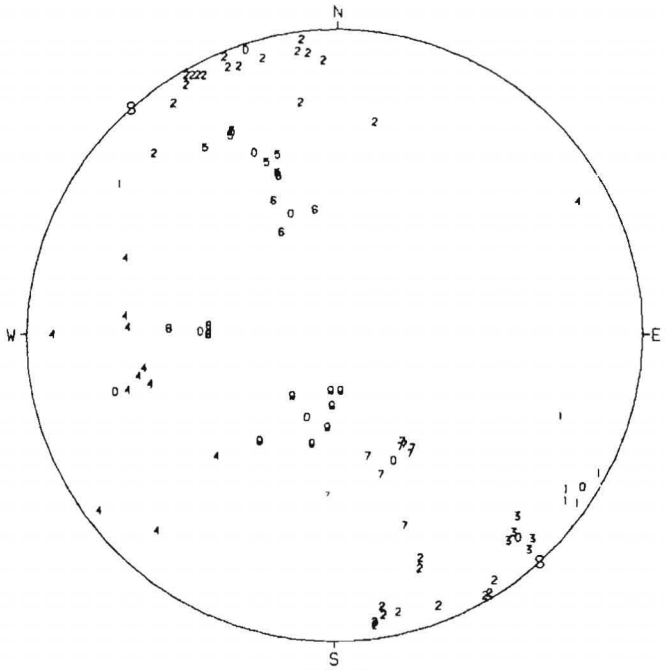

SITE 22

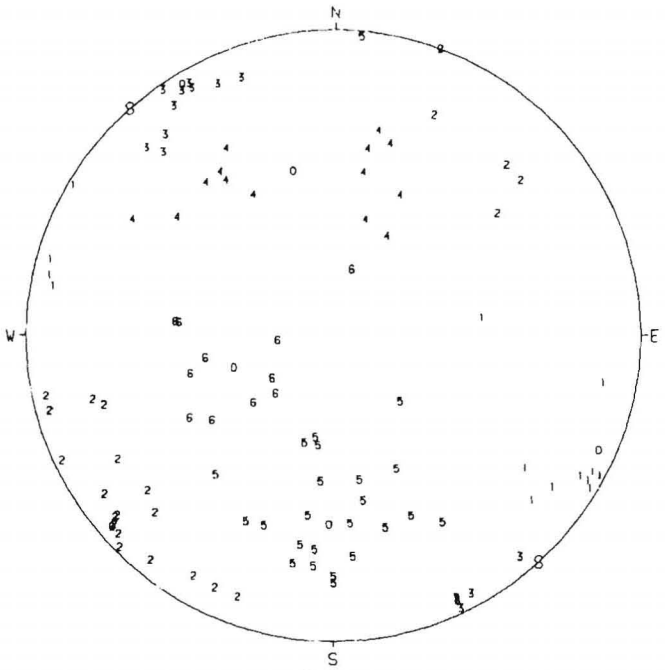

SITE 23

FRACTAN r	Clusters				Eigenvalues		
	No.	Obs	Dip	Az	W1	W2	W3
			SITE 22				
10.50	1	6	84	122	0	0	6
	2	33	88	342	1	2	31
	3	5	78	138	0	0	5
	4	12	63	255	1	1	10
	5	7	55	336	0	0	7
	6	3	35	339	0	0	3
	7	12	38	155	0	0	12
	8	5	36	271	0	0	5
	9	8	24	199	0	0	8
			SITE 23				
11.00	1	15	84	114	1	1	14
	2	23	85	229	1	2	20
	3	16	86	329	0	1	15
	4	14	46	346	0	2	12
	5	28	52	182	1	2	25
	6	12	28	252	0	1	11
			SITE 24				
10.00	1	3	85	50	0	0	3
	2	5	86	282	0	0	5
	3	7	84	319	0	0	7
	4	10	71	248	0	0	10
	5	4	63	85	0	0	4
	6	7	50	177	0	0	7
	7	10	38	271	0	1	9
	8	6	36	97	0	0	6
	9	6	37	150	0	0	6

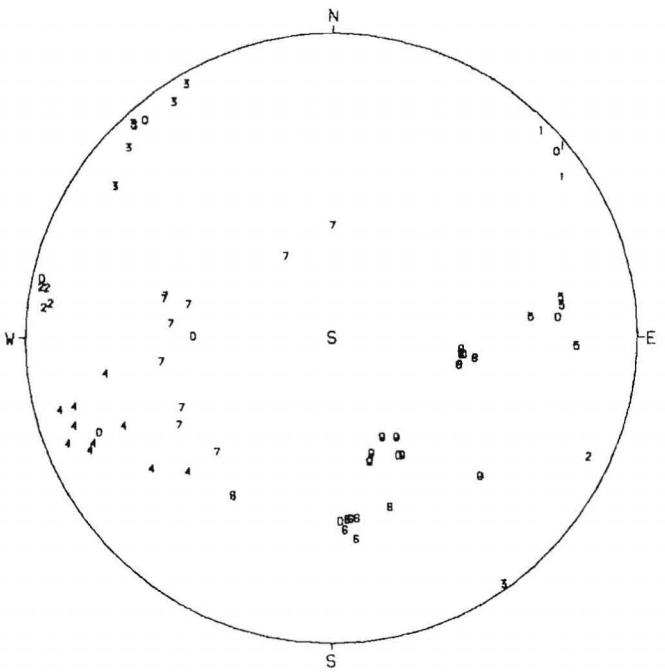

SITE 24

FIGURE 44.—San Manuel Mine scanline mapping, sites 22, 23, and 24, polar equal-area plots, upper hemisphere.

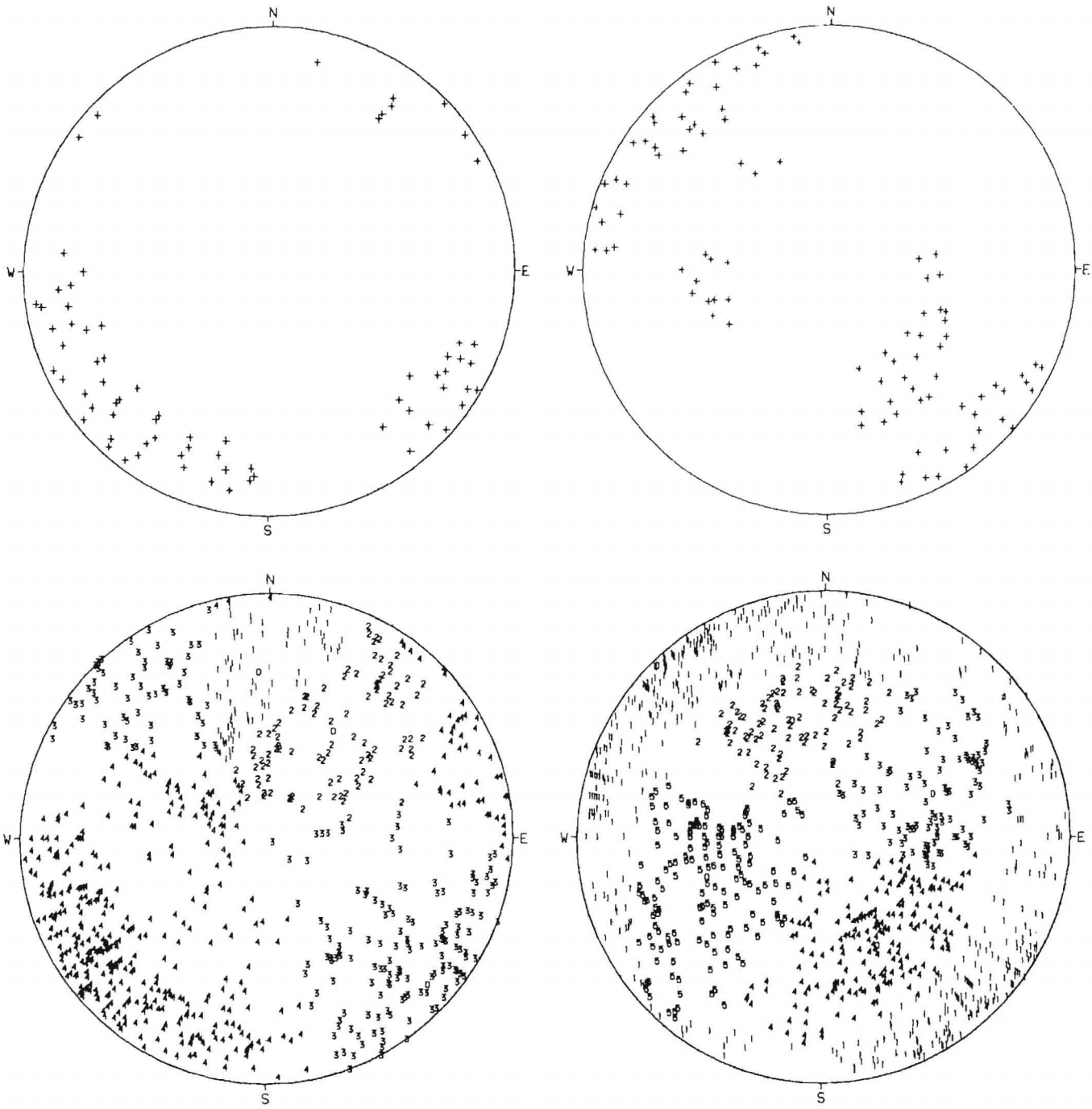

FRACTAN r	Clusters				Eigenvalues		
	No.	Obs	Dip	Az	W1	W2	W3
POOLED SITES 1 TO 10							
10.50	1	93	57	356	2	9	82
	2	116	42	31	4	16	96
	3	241	78	132	15	46	180
	4	479	67	237	63	82	334

FRACTAN r	Clusters				Eigenvalues		
	No.	Obs	Dip	Az	W1	W2	W3
POOLED SITES 11 TO 24							
9.00	1	580	87	316	32	143	404
	2	95	40	344	3	6	87
	3	109	39	69	4	9	96
	4	225	41	154	9	21	196
	5	199	41	251	10	20	169

FIGURE 45.—San Manuel Mine scanline mapping, pooled sites 1 to 10 (left) and 11 to 24 (right), polar equal-area plots, upper hemisphere. Top, Dense points determined by FRACTAN cluster solution; bottom, numerals corresponding to the cluster numbers denote the poles of the joint planes.

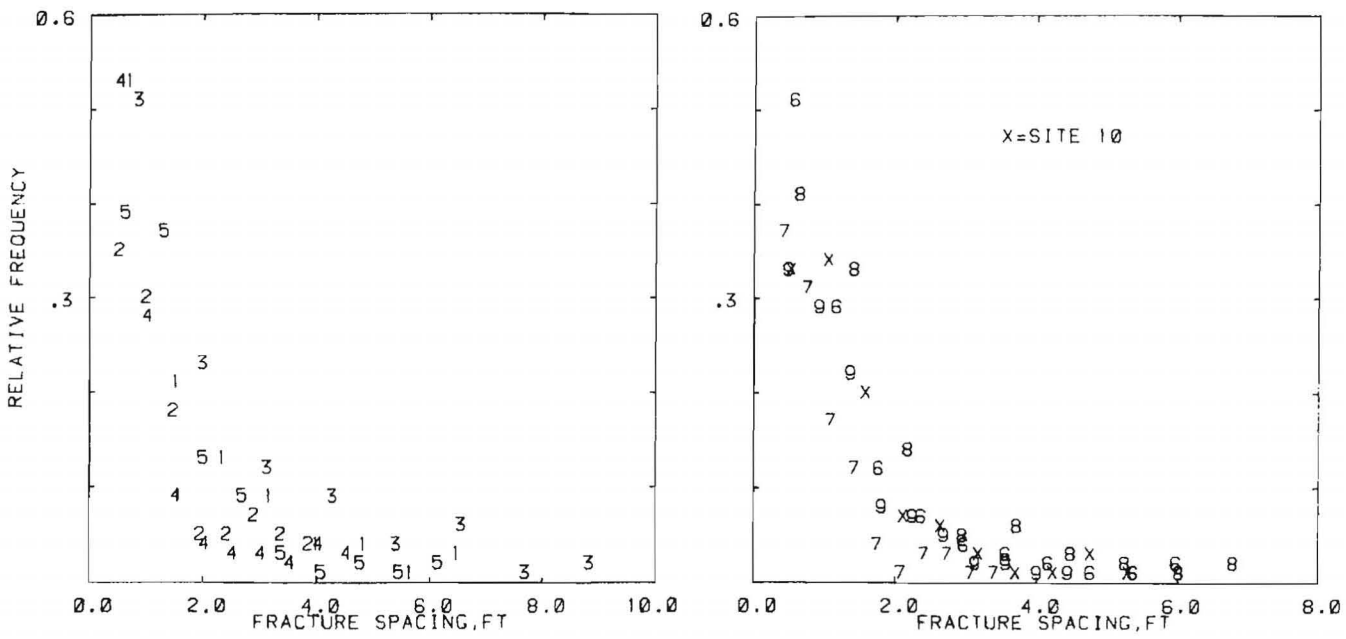

Scanline mapping site		1	2	3	4	5	6	7	8	9	10
Spacings observed		74	119	93	129	260	266	233	202	284	253
Maximum	ft	9.30	4.00	6.80	4.70	3.50	6.20	6.40	7.10	4.60	5.50
Minimum	ft	0.20	0.20	0.20	0.20	0.20	0.20	0.20	0.20	0.20	0.20
Arithmetic mean	ft	1.99	1.21	1.52	1.03	0.79	1.12	1.28	1.48	1.05	1.18
Median	ft	1.30	1.00	1.00	0.70	0.70	0.90	1.00	1.10	0.90	1.00
Mode	ft	0.40	0.60	1.00	0.40	0.70	0.50	ND	0.70	ND	1.00
Std dev	ft	1.95	0.92	1.34	0.99	0.53	0.89	1.03	1.17	0.73	0.87
Skewness		1.57	1.22	1.67	2.05	1.87	2.23	2.38	1.82	1.42	2.07
Mean log of spacing		0.22	–0.10	0.07	–0.32	–0.42	–0.15	–0.01	0.12	–0.19	–0.08
Std dev of logs		1.02	0.79	0.86	0.81	0.63	0.73	0.72	0.76	0.72	0.73
Distributions[1]		L,E,χ,Γ	L,E,	L,E,χ	None	None	L,E	L	L,E	None	None
Best fit		χ	E	χ	L	L	L	L	L	L	L

ND No appropriate value was determinable.
[1]Acceptable fit at the 5-pct significance level (L = lognormal, E = exponential, χ = chi squared, Γ = gamma).

FIGURE 46.—San Manuel Mine scanline mapping, sites 1 to 10. GDIST analyses of the spacing between successive fractures as measured along scanlines. Relative frequency (spacings in each class ÷ total spacings) is plotted at the midpoint of the corresponding class interval; the numeral corresponding to the site number (X = 10) is centered on the plotted point. Below the histograms are listed the parameters of the distributions.

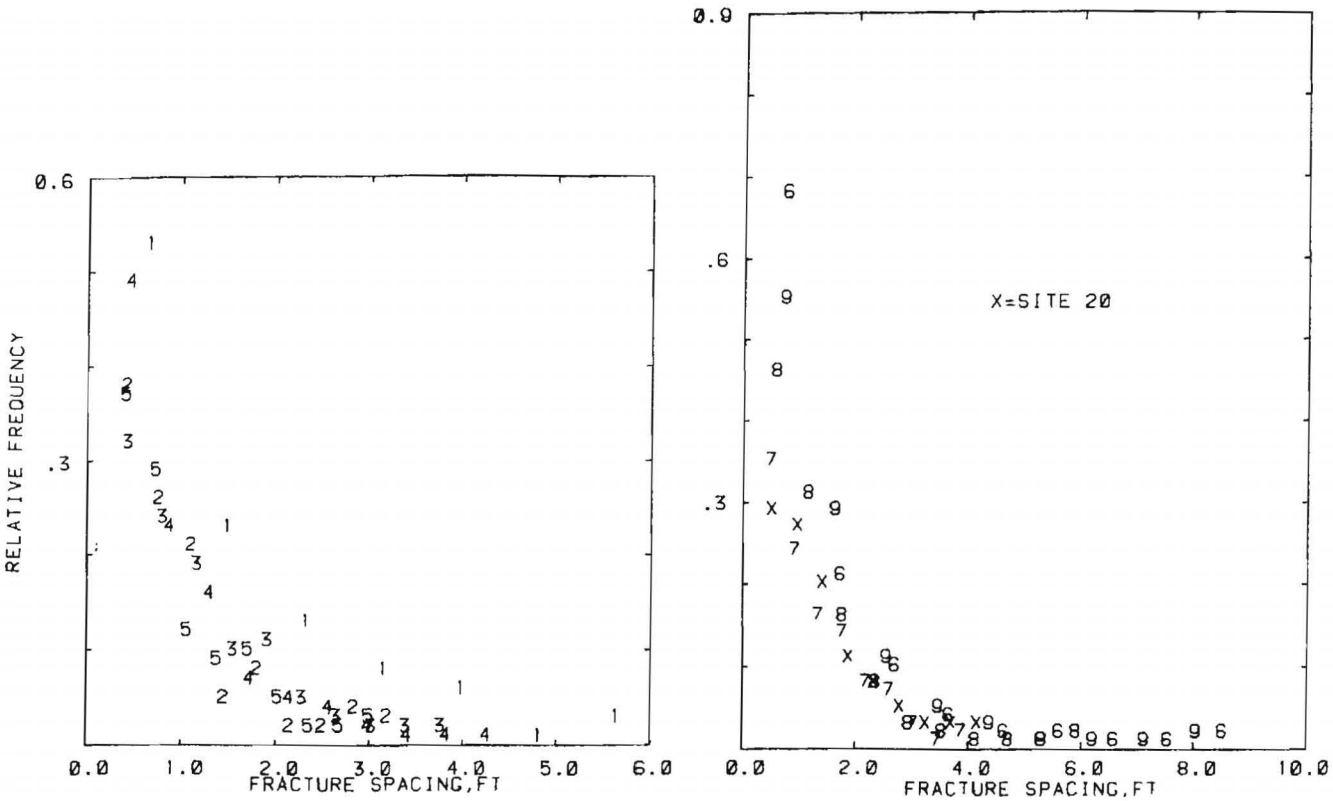

Scanline mapping site		11	12	13	14	15	16	17	18	19	20
Spacings observed		58	155	280	349	221	160	131	292	212	237
Maximum	ft	6.00	3.30	3.90	4.40	3.10	8.90	4.00	6.10	8.40	4.30
Minimum	ft	0.20	0.20	0.20	0.20	0.20	0.20	0.20	0.20	0.20	0.20
Arithmetic mean	ft	1.39	0.87	1.06	0.86	0.88	1.12	1.10	1.03	1.37	1.26
Median	ft	1.00	0.70	0.90	0.70	0.70	0.80	0.90	0.80	1.00	1.10
Mode	ft	ND	0.40	0.50	0.30	0.70	0.20	0.40	0.70	0.70	0.30
Std dev	ft	1.13	0.67	0.72	0.66	0.62	1.08	0.74	0.79	1.24	0.90
Skewness		1.78	1.74	1.19	1.71	1.43	3.21	1.09	2.43	2.67	1.24
Mean log of spacing		0.05	–0.38	–0.19	–0.41	–0.36	–0.22	–0.34	–0.21	–0.01	–0.03
Std dev of logs		0.78	0.70	0.73	0.73	0.69	0.82	0.78	0.71	0.82	0.76
Distributions[1]		L,E,χ	None	L,E	L,E,	L,E,	L,E,χ	L,E	L,E	L,E	L,E
Best fit		E	E	E	E	E	E	E	L	E	L

ND No appropriate value was determinable.
[1]Acceptable fit at the 5-pct significance level (L = lognormal, E = exponential, χ = chi squared).

FIGURE 47.—San Manuel Mine scanline mapping, sites 11 to 20. GDIST analyses of the spacings between successive fractures as measured along scanlines. Relative frequency (spacings in each class ÷ total spacings) is plotted at the midpoint of the corresponding class interval; the numeral corresponding to the second digit of the site number is centered on the plotted point. Below the histograms are listed the parameters of the distributions.

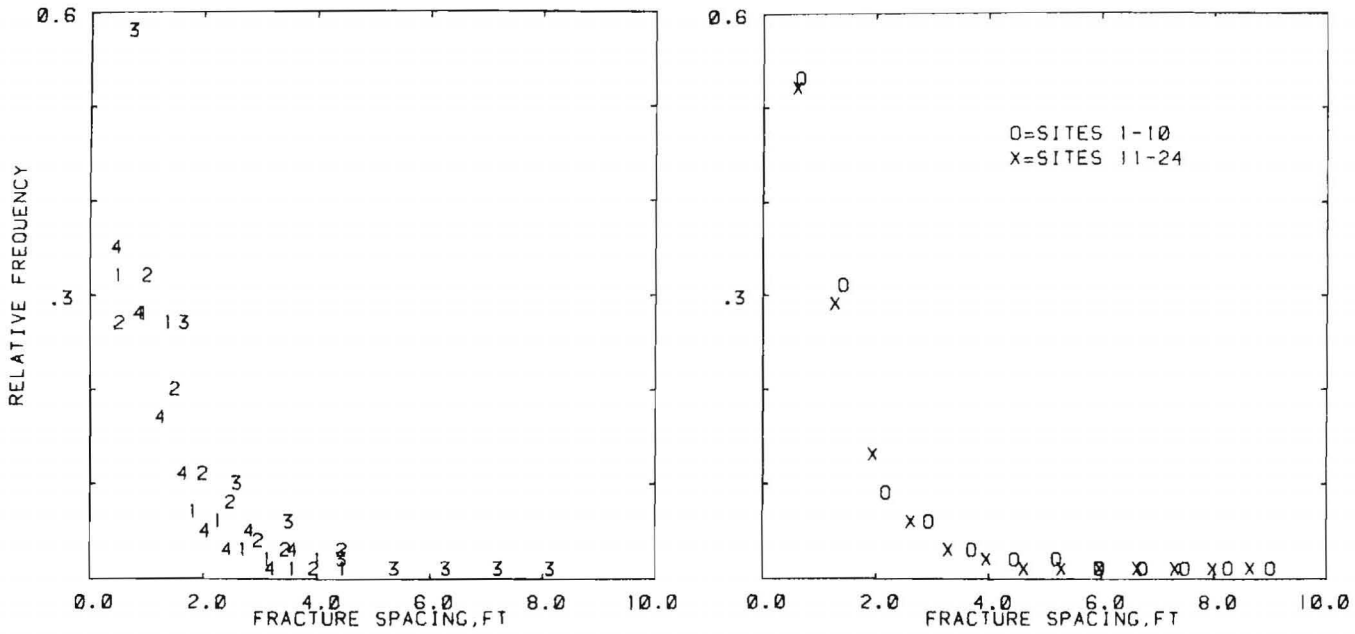

Scanline mapping site	21	22	23	24	Pooled 1-10	Pooled 11-24
Spacings observed	289	243	239	157	1,913	3,023
Maximum ft	4.60	4.60	8.50	3.70	9.30	8.90
Minimum ft	0.20	0.20	0.20	0.20	0.20	0.20
Arithmetic mean ft	1.05	1.22	1.25	0.95	1.18	1.08
Median ft	0.90	1.00	1.00	0.70	0.90	0.80
Mode ft	0.70	0.70	0.20	0.20	0.70	0.70
Std dev ft	0.73	0.85	1.07	0.74	1.01	0.86
Skewness	1.73	1.47	2.55	1.53	2.41	2.37
Mean log of spacing	−0.18	−0.04	−0.09	−0.33	−0.12	−0.20
Std dev of logs	0.70	0.72	0.81	0.76	0.77	0.75
Distributions[1]	None	L	L,E	L,E	None	None
Best fit	L	L	E	E	L	L

[1] Acceptable fit at the 5-pct significance level (L = lognormal, E = exponential).

FIGURE 48.—San Manuel Mine scanline mapping, individual sites 21 to 24, pooled sites 1 to 10, and pooled sites 11 to 24. GDIST analyses of the spacing between successive fractures as measured along scanlines. Relative frequency (spacings in each class ÷ total spacings) is plotted at the midpoint of the corresponding class interval; the numeral corresponding to the second digit of the site number is centered on the plotted point. Below the histograms are listed the parameters of the distributions.

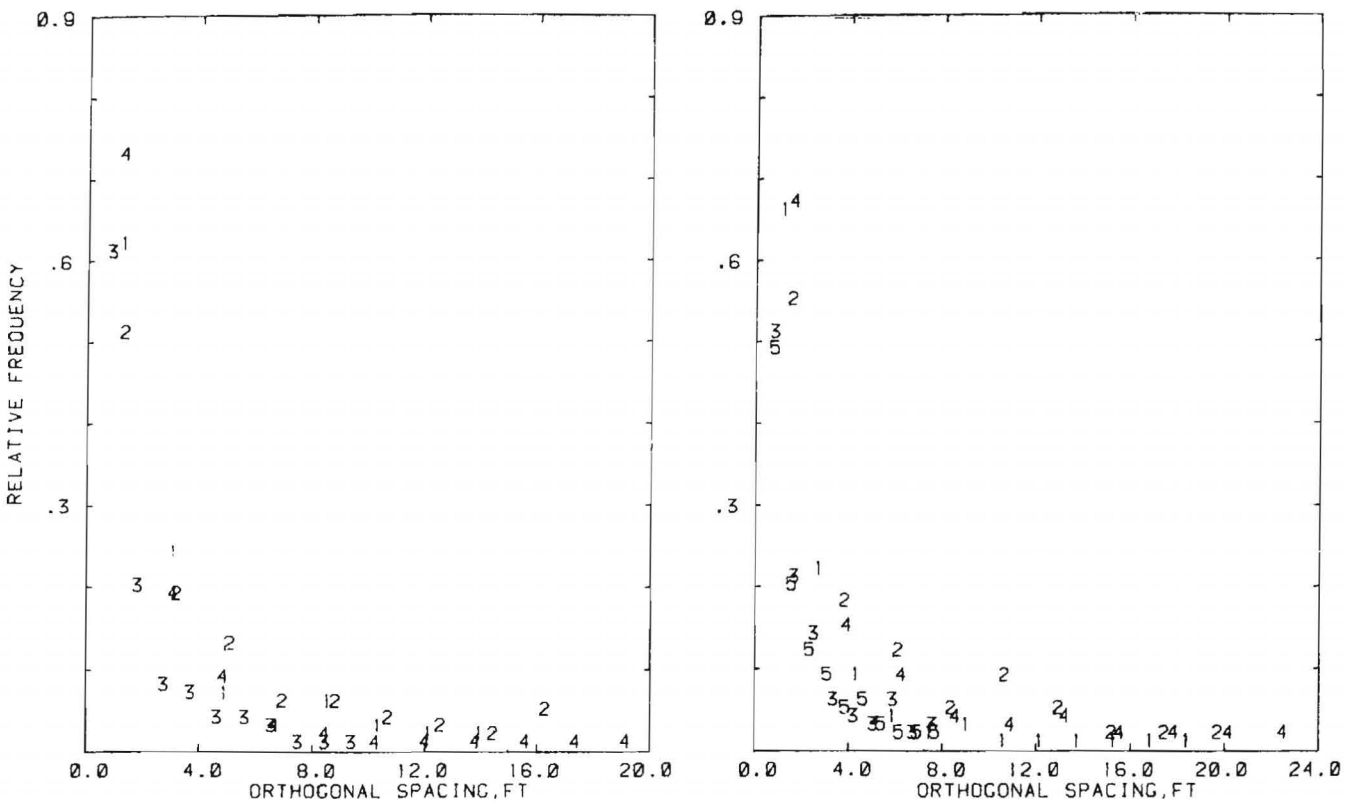

	Pooled sites 1 to 10				Pooled sites 11 to 24				
Cluster	1	2	3	4	1	2	3	4	5
Spacings observed	104	138	354	813	1,192	141	132	355	271
Maximum ft	14.66	17.05	9.67	19.88	18.97	20.63	7.81	23.41	7.86
Minimum ft	0.22	0.23	0.22	0.21	0.21	0.24	0.20	0.25	0.22
Arithmetic mean ft	2.50	3.71	1.48	1.75	1.89	3.77	1.59	3.27	1.65
Median ft	1.56	2.09	0.93	1.20	1.30	1.76	1.05	1.57	1.13
Mode ft	ND	0.29	0.37	0.83	0.60	0.47	0.20	0.88	0.28
Std dev ft	2.67	4.09	1.44	1.72	1.89	4.19	1.60	4.29	1.59
Skewness	2.13	1.63	1.99	3.88	2.68	1.53	1.77	2.60	1.65
Mean log of spacing	0.45	0.70	0.02	0.23	0.27	0.69	0.01	0.59	0.07
Std dev of logs	0.97	1.17	0.85	0.80	0.84	1.18	0.97	1.07	0.94
Distributions[1]	L	L,E	χ	χ,E	None	None	χ	L	L,E,χ
Best fit	L	L	χ	χ	χ	E	χ	L	χ

ND No appropriate value was determinable.
[1] Acceptable fit at the 5-pct significance level (L = lognormal, E = exponential, χ = chi squared).

FIGURE 49.—San Manuel Mine scanline mapping, GDIST analyses of orthogonal fracture spacing within fracture families. Left, Pooled sites 1 to 10; right, pooled sites 11 to 24. Relative frequency (spacings in each class ÷ total spacings) is plotted at the midpoint of the corresponding class interval; the numeral indicating the cluster number is centered on the plotted point.

HENDERSON MINE DATA

The Henderson Mine is a molybdenite deposit located about 50 miles west of Denver, CO, in mountainous terrain. The ore body is a stockwork within and adjacent to multiple rhyolitic-granitic Tertiary intrusions into the Precambrian Silver Plume Granite. The major host rocks are Urad Porphyry, Primos Porphyry, and Henderson Granite. This igneous complex, which consists of a number of closely related rocks, mineralogically and chemically similar, lies in the structurally complex acute angle between two regional faults, the Berthoud Pass Fault (strike N30°E, steep dip) about 9,000 ft to the southeast, and the Vasquez Pass Fault (strike N24°E, dip 67°NW) about 2,000 ft to the west. The deposit, shaped like an inverted cup tilted downward to the southeast, measures in plan about 3,000 ft NE-SW by 2,300 ft (*34*).

When the present data acquisition began, the mine had been in production less than 4 years. The first production level is 8,100 ft above sea level; the depth of cover ranges from about 3,400 to 4,200 ft. The first lift, up to 500 ft thick, is being mined by mass caving. The ore is undercut on the 8,155-ft level by blasting successive vertical rings of drill holes on the boundary of the undercutting excavation. This procedure resulted in a single large caved zone that progressed steadily southward. The caved ore falls by gravity to the draw points on the 8100 level, where it is transferred by load-haul-dump vehicles to ore passes. Figure 50 shows the southerly half of the active cave in May 1979.

Two sites were selected for core drilling 3-in-diam holes. The west drilling site was expected to be in typical ore; the east drilling site was near a contact between the Urad and Primos Porphyries. Diamond drilling to produce oriented core from holes 1 to 4 was completed by a contract drilling crew April 5, 1979; a total of 570 ft of upward-inclined hole was drilled at an average rate of 15 ft per work shift in this very hard rock, including time for core orienting and other related tasks. Diamond drilling of holes 5 to 8, each 100 ft long, was performed by Bureau of Mines personnel in May and June 1979. (Drill cores are shown in figure 51.) By that time the southward-progressing ring drilling on the 8155 level had reached overhead our drilling site, and hence we reversed the hole directions, drilling them below the horizontal in order to avoid interfering with the ring drilling. Ordinarily in a deposit of this size, a difference of 100 ft as to the drill hole location would not noticeably change the characteristics of the sample; because of the proximity of the geological contact at this site, however, a few feet change of location might have a substantial influence.

The 5-ft-long, split-inner-tube core barrel was used for all eight drill holes, along with the impression method of core orienting. Core recovery was essentially 100 pct in this strong rock, which facilitated the matching of core fracture surfaces for core orienting.

Fracture mapping along multiple scanlines, using the five-scanline scheme at eight sections on the 8100 level, was performed intermittently from February to June 1979, as a low-priority task. Sites 1, 2, 5, and 7 in the N-S production drifts were 50-ft-long sections; sites 3, 4, 6, and 8, which were inside future draw points to obtain E-W orientation, were limited to exposures 35 to 36 ft long.

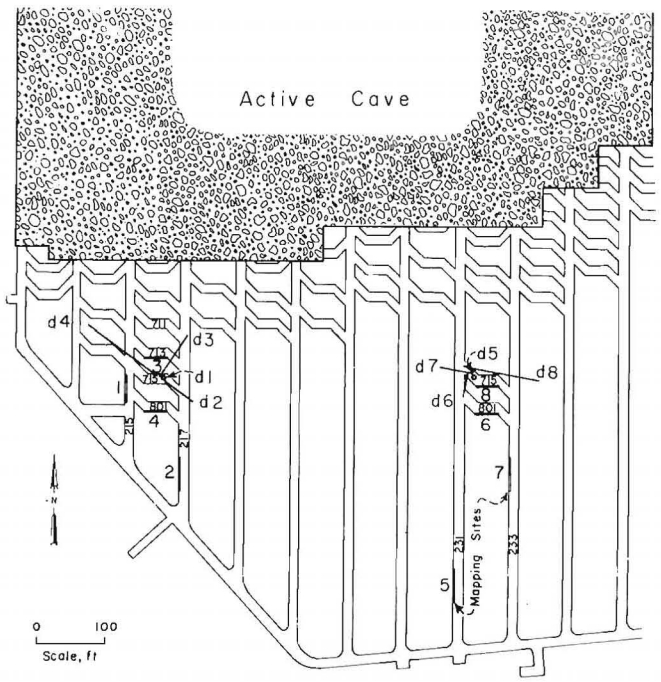

FIGURE 50.—Henderson Mine: Plan view of 8100 level showing scanline mapping sites 1 to 8 and diamond drill holes d1 to d8 for oriented core.

HOLE 1, 97 TO 116 FT

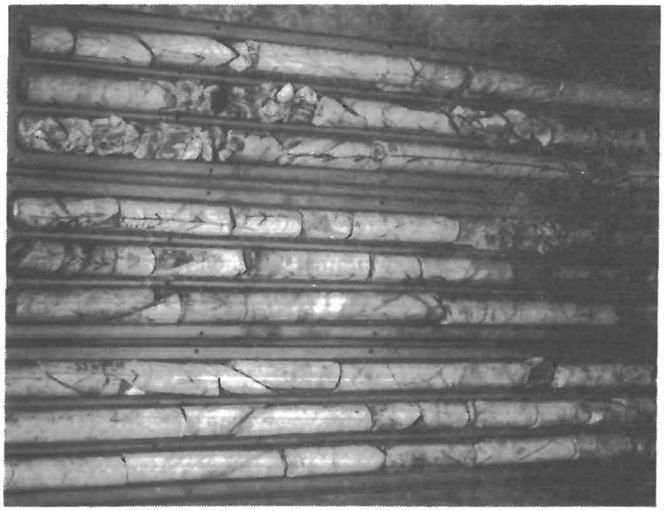

HOLE 5, 34 TO 69 FT

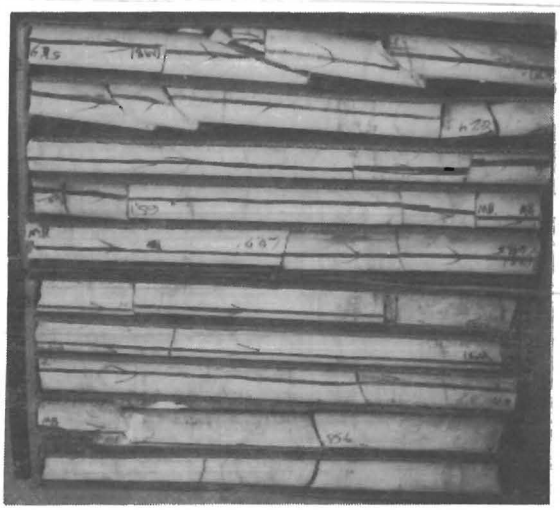

HOLE 2, 58 TO 78 FT

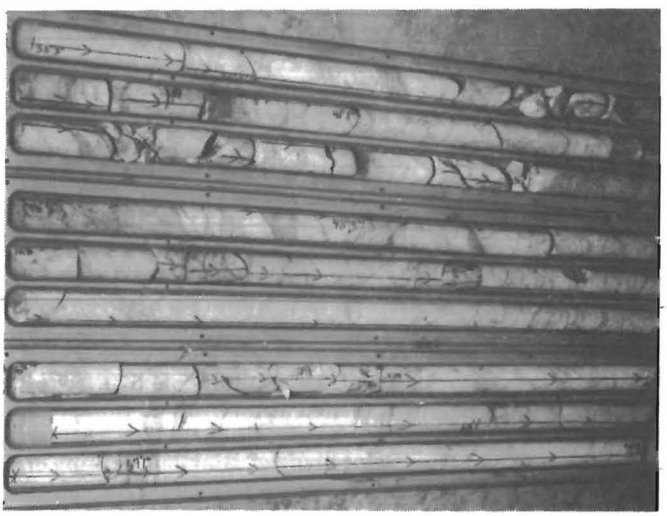

HOLE 6, 35 TO 70 FT

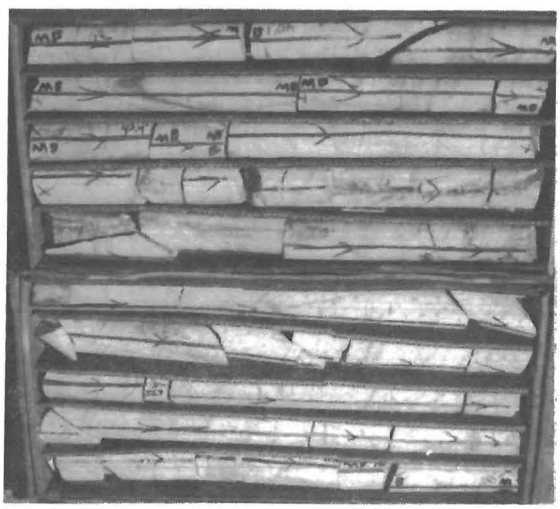

HOLE 3, 39 TO 58 FT

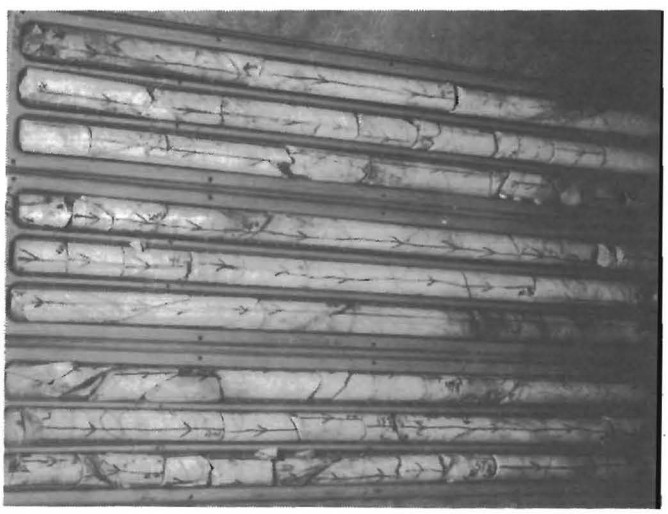

HOLE 7, 23 TO 59 FT

FIGURE 51.—Henderson Mine oriented diamond drill cores.

HENDERSON ORIENTED CORE

Fracture Orientation

The FRACTAN cluster solutions selected in accordance with the criteria stated (figs. 52 to 55) show that, for individual drill holes, the fracture-plane normals are concentrated within 60° of the drill hole axis. The best interpretation appears to be obtained by combining the fractures from all the drill holes at each site, thus compensating for the underrepresentation of fractures whose poles deviate by more than 60° from the respective drill hole axes. The apparent absence of a particular fracture family in a particular drill hole is more easily understood by comparing the angular zones of coverage achieved by the four-drill-hole configurations (figs. 54*B* and 55*B*).

Arranging the fracture families as in table 11, to exhibit coinciding orientations among drill holes, one finds three orientations that appear in at least two of the four drill holes at both sites; on the average an individual drill hole exhibits two of these three orientations. One of these three families is flat dipping; the others dip steeply ENE and moderately to steeply W to NW, respectively. In addition, there is indication of the presence of the following three fracture families, mainly in holes 5 to 8:

1. A family that dips moderately N is indicated in holes 2, 5, 6, and 7. Although it is not identified in the pooled-holes analysis at either site, evidence of this cluster appears in the PEA plots for pooled holes 5 to 8.

2. A family that dips moderately SE is indicated in holes 5 and 7, approximating the family that dips steeply SE in pooled holes 1 to 4, which, however, is not indicated in any of the individual holes 1 to 4.

3. A family that dips steeply SW is indicated by the FRACTAN solutions for hole 8 and for pooled holes 5 to 8; evidence of this cluster appears in the PEA plots for holes 5 and 7.

Cluster 6 of pooled holes 5 to 8 is a poor result from the FRACTAN analysis, as it encompasses 722 of the 979 fractures, with excessively scattered orientations. A much better partition, considering the clusters identified in the individual holes 5 to 8 and the PEA plot of pooled holes 5 to 8, would be to partition this cluster into four parts, one going with the ENE-dipping family, one going with the W-dipping family, one representing the N-dipping family, and one representing the flat-dipping family; the last two parts are not identified by the solution.

Fracture Spacing

The spacings from fracture to fracture along the drill cores, without regard to fracture orientation, are shown in figure 56. The best fitting distributions of the spacings are most often exponential; lognormal and chi-squared distributions are frequently also acceptable. The median spacings range from 0.25 to 0.67 ft. The median spacing at the west drilling site is greater than that at the east drilling site, 0.50 versus 0.33 ft.

The orthogonal spacings between successive fractures of similar orientation are shown in figure 57 for holes 1 to 4 and in figure 58 for holes 5 to 8. These results were obtained from the pooled data at each of the two sites, as follows: The FRACTAN cluster analyses (figs. 54-55), partitioned the fractures from four pooled holes into seven and six clusters, respectively. For each drill hole the orthogonal fracture spacings within a given cluster were computed by equation 1, using the appropriate angle δ

TABLE 11.—Henderson oriented core: Mean dip and dip azimuth (dipaz) of clusters as determined by FRACTAN analysis

(Fracture families grouped to show correlations; below each dip, dipaz pair is given the corresponding W3/n)

Drill hole	Dip direction, deg						
	0-360 Flat	358-14 N	60-94 ENE	116-147 SE	220-247 SW	261-328 W to NW	Not correlated
1	11, 10 141/210	—	73, 72 13/15	—	—	—	—
2	13, 90 131/183	46, 12 8/9	—	—	—	—	—
3	22, 63 114/156	—	—	—	—	58, 328 39/44	—
4	—	—	86, 72 43/48 85, 88 13/13	—	—	67, 311 176/198	28,265 17/18
1+2+3+4	23, 83 260/331 8, 191 15/15 8, 251 12/12	—	87, 74 86/97	89, 141 21/22	—	48, 316 311/400	45, 186 16/17
5	[2]5, 244 103/118	51, 358 34/39	53, 60 49/53	40, 117 24/27	(1)	61, 261 47/55	52, 183 27/30
6	23, 69 23/24 9, 194 9/10	[2]41, 6 67/85	58, 94 6/7	—	—	40, 282 9/10	89, 3 7/7
7	11, 86 4/4 26, 230 25/30	38, 14 20/22	[2]41, 72 60/69	59, 147 22/25	(1)	—	64, 109 10/10
8	—	—	—	—	57, 223 30/32	[2]72, 283 225/303	85, 46 18/19
5+6+7+8	(1)	(1)	54, 75 24/25	57, 116 58/64 32, 122 45/49	65, 220 64/73 54, 247 44/46	30, 314 368/722	—

— No appropriate cluster identified.
[1]Polar equal-area plot indicates a possible cluster having this orientation.
[2]Orthogonal spacings were analyzed within this cluster, to obtain a more realistic estimate for this orientation.

corresponding to the mean orientation of that cluster with respect to the specified drill hole. The orthogonal spacings for a given cluster were pooled for the four drill holes at each site and analyzed by GDIST. In addition, because of the poor partitioning provided by the FRACTAN cluster analysis for pooled holes 5 to 8, GDIST analyses were made of the orthogonal spacings within four clusters that were selected to represent four major fracture orientations at the east drilling site, in order to obtain more realistic estimates for these four families.

Within the clusters identified for the pooling of holes 1 to 4, the best fitting distribution of orthogonal spacings is usually the lognormal (five of seven clusters). The GDIST analyses for the four selected clusters from holes 5 to 8 replace the results for clusters 3 and 6 identified in the pooled data and provide estimates for two additional fracture families; with these substitutions the most common distributions of orthogonal spacings are the chi squared, the exponential, and the lognormal.

The orthogonal spacings exhibit large differences among families. Neglecting clusters that contain fewer than 20 observed values, median spacings range from 0.61 to 2.44 ft for holes 1 to 4 and from 0.33 to 2.23 ft for holes 5 to 8, as modified by the four additional selected clusters. The smallest median spacing at both sites is that of the NW-dipping family identified in the pooled data at both sites.

Summary, Henderson Oriented Core

Analyses of the eight drill holes indicate the presence of the same three prominent fracture families at both sites, one flat lying, one dipping moderately to steeply ENE, and one dipping moderately to steeply W to NW. These three families are also the ones that exhibit the smallest median values of orthogonal fracture spacing, 0.91, 0.88, and 0.61 ft respectively, in holes 1 to 4. The fracture pattern at the east drilling site is different from that at the west site, exhibiting three additional fracture families, apparently because of the proximity of the contact between two major rock bodies. Nevertheless, the above-named three prominent fracture families, which exhibit mean orthogonal spacings of 0.58, 0.70, and 0.33 ft respectively, comprise three of the four clusters having the smallest spacings at the east drilling site.

HENDERSON MULTIPLE SCANLINE MAPPING

Fracture Orientation

All the fracture orientations determined by the scanline mapping are presented in PEA diagrams, one for each mapping site, in figures 59 and 60, which also show the best FRACTAN partitioning into clusters. To increase the sample size and obtain a more balanced representation of all clusters, analyses were also made for pooled data, sites 1 to 4 and sites 5 to 8, in figure 61, reflecting a simple geographic subdivision similar to that of the two drilling sites.

FRACTAN analyses of individual sites and of the pooled sites suggest that either the flat-lying fractures are few in number or there is a minor bias against identifying fractures of slight dip on a vertical exposure. Evidence for a bias with respect to fracture azimuth is not persuasive.

Comparisons of the mean orientations of the fracture families reveal approximate correspondences at four orientations, listed by column in table 12. A family of slight dip is identified at only three of eight sites; the three steeply dipping families are identified at seven of eight sites. The NW-dipping family is the most numerous and most consistent. A fifth family, dipping steeply SE, is indicated at sites 1, 3, and 4. The families listed as "not correlated" represent in every instance clusters that are small relative to the total number of fractures mapped at the respective sites.

Fracture Spacing

The distributions of spacings between successive fractures along the scanlines A, B, C, D, and E, without regard for fracture families, shown in figure 62, were obtained by code GDIST for the individual mapping sites 1 to 8 and for the pooled data sets, sites 1 to 4 and sites 5 to 8. The spacings are most often describable by a lognormal distribution, with medians ranging from 0.7 to 1.0 ft.

The spacings between successive fractures of similar orientation were obtained from the two sets of pooled data as follows: The FRACTAN cluster analyses, figure 61, partitioned the pooled fractures of sites 1 to 4 into four clusters and the pooled fractures of sites 5 to 8 into three clusters. The orthogonal spacings between successive fractures of a given cluster were computed by equation 1, using the value of δ corresponding to the mean orientation of that cluster with respect to the scanline. The orthogonal spacings for a given cluster were pooled for sites 1 to 4 (and 5 to 8) and analyzed by GDIST, figure 63. A lognormal distribution is the most common, when an acceptable fit exists. Median orthogonal spacing ranges from 0.77 to 1.32 ft, with relatively little variation among the clusters.

Fracture Trace Length

The distribution of the observed fracture trace lengths into 15 classes is given in table 13 for the clusters identified by the FRACTAN analysis for pooled sites 1 to 4 and 5 to 8 (fig. 61). For each of these clusters the N_i provide six estimates of $\hat{\theta}'$ via equations 13 to 18. Since mapping sites 1 and 2 have the same orientation and thus the same α for any given cluster, each value of N_i substituted in equations 13 to 18 is the sum, for sites 1 and 2, of the number of observations in the corresponding trace length class. The N_i were similarly pooled for sites 3 and 4, 5 and 7, and 6 and 8. The six calculated $\hat{\theta}'$ values for each of the poolings are shown in table 13, along with the averages of the separate estimates. The mean trace lengths range from 2.5 to 17.1 ft at sites 1 to 4, and from 1.9 to 18.4 ft at sites 5 to 8.

Considering the variability among the six estimates for any given cluster, the trace lengths for clusters 1, 2, and 3 of pooled sites 1 to 4 do not differ substantially, comparing sites 1 and 2 with sites 3 and 4. The widely differing trace length estimates, 17.1 and 2.6 ft, for cluster 4 are attributed to their poor accuracy, which is caused by their being calculated from an inadequate data base, most of the N_i being zeros in table 13; the 11° dip of this family produced relatively few crossings of the horizontal scanlines.

Large variability also exists with respect to clusters 2 and 3 of pooled sites 5 to 8. Cluster 2 estimates are

TABLE 12.—Henderson scanline mapping: Mean dip and dip azimuth (dipaz) of clusters as determined by FRACTAN analysis

(Fracture families grouped to show correlations: dip given in two opposite directions (e.g., SE-NW) implies approximately vertical orientation; below each dip, dipaz pair is given the corresponding W3/n)

Mapping site	Dip direction, deg					
	0-360 Flat	55-62 222-251 NE-SW	111-130 SE	187-188 S	305-318 NW	Not correlated
1	27, 126 6/6	76, 61 28/30 78, 251 8/8	60, 115 16/17	—	59, 305 29/33	48, 82 6/6
2	12, 267 10.11	84, 238 46/57	—	—	73, 305 59/65	32, 329 6/6
3	—	79, 62 11/11	70, 111 7/7	66, 187 9/10	59, 318 23/26	32, 57 8/8 35, 112 6/6 66, 152 13/14
4	—	85, 222 19/21	67, 126 12/13	48, 188 13/15	73, 311 22/25	42, 297 10/10
1+2+3+4	11, 260 23/25	89, 55 18/155	60, 130 63/76	—	65, 308 135/149	—
	Dip direction, deg					
	350 Flat	73-88 ENE		187-217 SSW	293-317 NW	Not correlated
5	—	(1)	—	81, 187 48/65	51, 306 39/47	—
6	28, 350 13/15	88, 88 10/11	—	69, 187 5/5	67, 299 24/26 50, 317 5/5	30, 154 10/11
7	—	48, 73 9/9	—	72, 217 51/54	56, 293 33/35	—
8	—	86, 87 44/50	—	65, 195 18/20 89, 212 10/10	51, 306 30/34	34, 67 7/7
5+6+7+8	—	47, 74 34/39	—	72, 202 125/152	60, 294 164/213	—

— No appropriate cluster identified.
[1]Polar equal area plot indicates a possible cluster having this orientation.

TABLE 13.—Henderson scanline mapping: Mean trace length analyses, clusters as defined in figure 61

	Clusters of pooled sites 1 to 4								Clusters of pooled sites 5 to 8					
	Site 1 + Site 2				Site 3 + Site 4				Site 5 + Site 7			Site 6 + Site 8		
Cluster	1	2	3	4	1	2	3	4	1	2	3	1	2	3
N_1	3	5	4	4	2	5	7	1	3	0	1	5	4	11
N_2	1	2	7	0	1	1	0	0	6	2	1	2	1	5
N_3	0	4	0	0	0	2	0	0	3	0	2	3	2	3
N_4	1	2	2	0	3	0	2	0	3	0	2	1	1	1
N_5	0	5	2	0	1	4	4	0	4	3	1	2	0	5
N_6	3	6	9	0	1	5	2	0	8	0	4	2	2	5
N_7	1	2	5	0	2	2	3	0	1	2	0	1	0	4
N_8	4	8	2	0	1	3	2	0	6	1	3	1	1	11
N_9	5	8	9	0	12	10	8	0	27	3	25	5	0	13
N_{10}	2	11	10	1	8	6	10	1	7	0	3	5	4	17
N_{11}	3	10	12	1	3	2	6	0	13	1	9	4	4	13
N_{12}	3	10	11	4	1	4	0	2	7	0	10	2	0	12
N_{13}	2	9	9	0	3	4	2	0	12	2	12	5	0	10
N_{14}	1	9	4	3	2	4	2	1	6	0	6	3	3	9
N_{15}	1	7	7	4	6	4	7	2	3	1	3	2	1	11
sin α	0.73	1.00	0.80	0.03	0.79	1.00	0.87	0.19	0.95	0.28	0.59	0.77	0.72	0.85
Eq 13	5.4	2.4	3.4	28.7	6.1	4.3	3.3	2.6	5.4	30.8	12.1	4.0	2.1	3.4
Eq 14	4.2	2.1	2.9	14.3	5.2	3.6	3.2	2.6	3.8	22.0	7.8	3.4	1.7	2.8
Eq 15	6.6	3.1	3.6	14.3	5.3	3.4	2.7	2.6	5.2	7.0	17.4	2.6	2.3	3.3
Eq 16	2.7	2.1	2.9	14.3	6.2	2.8	3.6	2.6	3.4	24.8	8.4	2.5	1.1	2.6
Eq 17	8.0	2.7	3.0	14.3	6.0	3.7	4.5	2.6	4.4	10.3	7.8	3.1	2.4	3.8
Eq 18	6.4	2.7	3.6	16.7	11.3	4.6	7.1	2.6	6.3	15.3	9.3	4.8	n.a	3.8
Av	5.6	2.5	3.2	17.1	6.7	3.7	4.1	2.6	4.8	18.4	10.5	3.4	1.9	3.3

NOTE.— Top: The number of fractures observed in trace length classes 1 to 15 defined in figure 12. Bottom: The values of mean trace length $\hat{\theta}'$ (ft) calculated from the appropriate equation in table 1 (s = 1 ft).

handicapped by insufficient data (the large number of zero N_i). On the other hand, the consistently larger estimates for sites 5 and 7 indicate that the trace lengths are substantially greater on the N-S exposures than on the E-W exposures.

Summary, Henderson Scanline Mapping

Analyses of the eight sets of scanline mapping data indicate the presence of five prominent orientations. On the average four of these five are identified at any individual site 1 to 4, and three of these five at any one of sites 5 to 8. Only the NW-dipping family is indicated by FRACTAN at every site. This family has the smallest orthogonal fracture spacing, although not by a wide margin, as the median fracture spacing for all families has a small range, from 0.8 to 1.3 ft. The next most prominent families dip northeasterly and southerly. Four of the five have moderate to steep dips. The flat-dipping family is the least prominent. The grand means of the trace lengths for the most prominent families range from 3 to 11 ft.

HENDERSON FRACTURES—SUMMARY

The orientation and spacing characteristics of the most prominent fracture families are summarized in table 14. Analyses of the oriented core indicate six orientations, one of which, north dipping, is not identified in the scanline mapping data. Of these six, on the average only two appear in any single drill hole at the west drilling site, whereas four appear in any single drill hole at the east drilling site, which is near a geologically important contact. Of the five orientations identified by scanline mapping, four appear at any one of the west mapping sites, and three appear at any one of the east mapping sites.

Orthogonal spacing between fractures of a given family is smaller along oriented core than along scanlines, but the relationship is not systematic, probably because it is influenced by the particular partitionings of fractures that were selected. However, the spacing between fractures irrespective of their orientation is about half as great in the oriented cores as along the scanlines.

TABLE 14.—Henderson Mine: Fracture families indicated by the two methods

WEST STUDY AREA: ORIENTED CORE, POOLED DRILL HOLES 1 to 4[1]						
Dip, dip azimuth	23, 83	—	87, 74	89, 141	—	48, 316.
W3/n	260/331	—	86/97	21/22	—	311/400.
Dip	Flat	Moderate	Steep	Steep	—	Moderate.
Dip azimuth	—	N	ENE	SE	—	NW.
Cluster	4	—	2	1	—	7.
Orthogonal spacing	0.91 ft	[2]	0.88 ft	2.44 ft	—	0.61 ft.
WEST STUDY AREA: SCANLINE MAPPING, POOLED SITES 1 to 4[3]						
Dip, dip azimuth	—	—	89, 55	60, 130	—	65, 308.
W3/n	—	—	118/155	63/76	—	135/149.
Dip	Flat	—	Vertical	Steep	Moderate	Steep.
Dip azimuth	—	—	NE-SW	SE	S	NW.
Cluster	4	—	2	1	—	3.
Orthogonal spacing	[2]	—	1.09 ft	0.98 ft	[2]	1.01 ft.
EAST STUDY AREA: ORIENTED CORE, POOLED DRILL HOLES 5 to 8[4]						
Dip, dip azimuth	5, 244	41, 6	41, 72	32, 122	65, 220	72, 283.
W3/n	103/118	67/85	60/69	45/49	64/73	225/303.
Dip	Flat	Moderate	Moderate	Moderate	Steep	Steep.
Dip azimuth	—	N	ENE	SE	SW	W.
Cluster	[5]6	[5]4	[5]4	5	1	[5]3.
Orthogonal spacing	0.58 ft[5]	0.57 ft[5]	0.70 ft[5]	1.30 ft	0.91 ft	0.33 ft[5].
EAST STUDY AREA: SCANLINE MAPPING, POOLED SITES 5 to 8[3]						
Dip, dip azimuth	—	—	47, 74	—	72, 202	60, 294.
W3/n	—	—	34/39	—	125/152	164/213.
Dip	Flat	—	Moderate	—	Steep	Steep.
Dip azimuth	—	—	ENE	—	SSW	NW.
Cluster	—	—	2	—	1	3.
Orthogonal spacing	[2]	—	1.32 ft	—	0.79 ft	0.77 ft.

— No appropriate cluster identified.
[1]Fracture spacing, irrespective of fracture orientation, median = 0.50 ft.
[2]Weak cluster inferred from individual hole or site, not included in pooled-sites calculations.
[3]Fracture spacing, irrespective of fracture orientation, median = 0.80 ft.
[4]Fracture spacing, irrespective of fracture orientation, median = 0.33 ft.
[5]Calculated from the 4 selected clusters, figure 58.

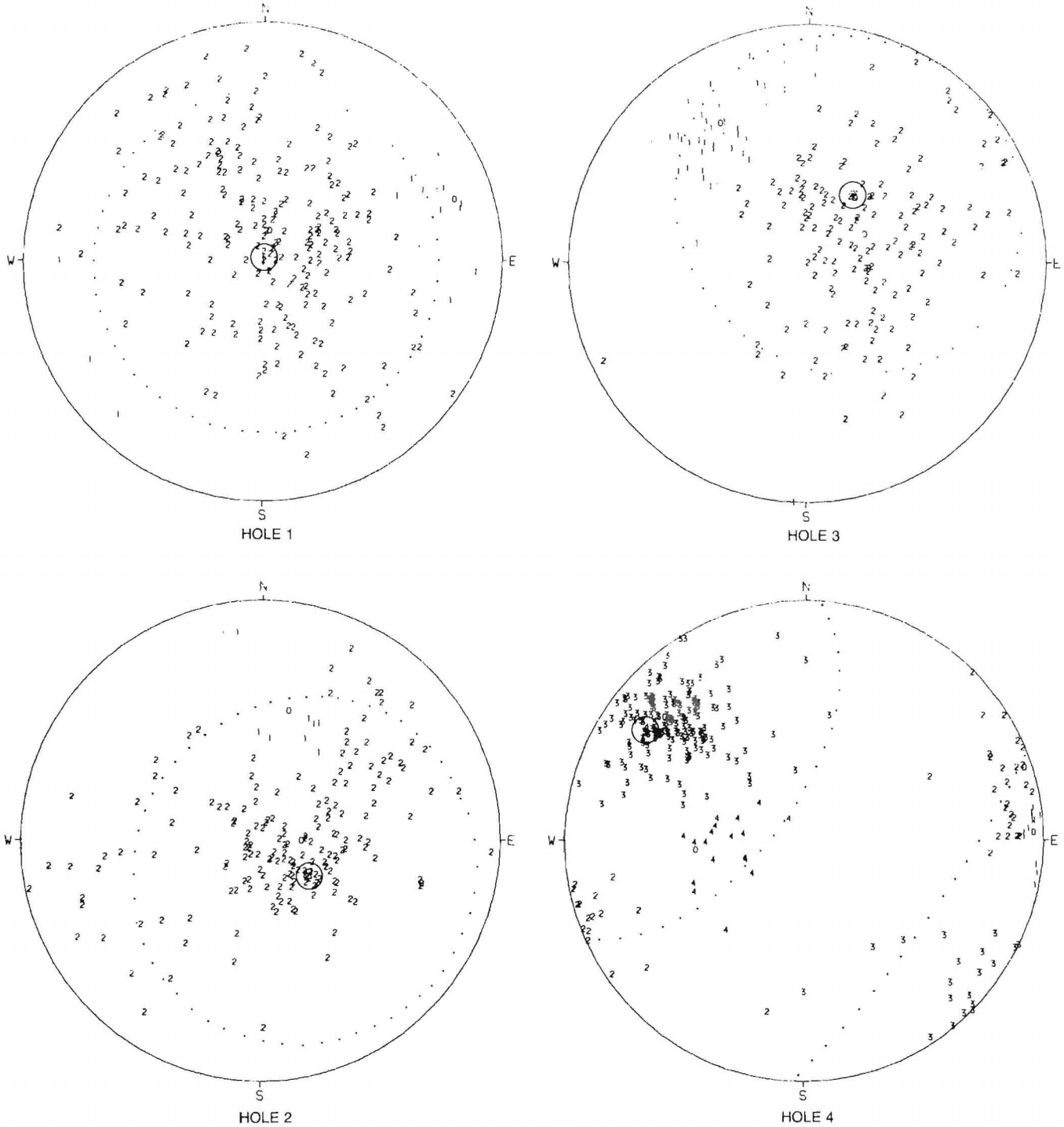

FRACTAN r	Clusters					Eigenvalues		
	No.	Obs	Est	Dip	Az	W1	W2	W3
HOLE 1 (INCL +90)								
11.00	1	15	51	73	72	1	1	13
	2	210	214	11	10	23	46	141
HOLE 2 (INCL +70, AZ 125)								
9.00	1	9	16	46	12	0	1	8
	2	183	188	13	90	15	37	131

FRACTAN r	Clusters					Eigenvalues		
	No.	Obs	Est	Dip	Az	W1	W2	W3
HOLE 3 (INCL +62, AZ 35)								
11.00	1	44	70	58	328	1	4	39
	2	156	160	22	63	17	25	114
HOLE 4 (INCL +20, AZ 305)								
10.50	1	13	18	85	88	0	0	13
	2	48	91	86	72	1	3	43
	3	198	200	67	311	6	16	176
	4	18	28	28	265	0	1	17

FIGURE 52.—Henderson Mine oriented core, holes 1, 2, 3, and 4, polar equal-area plots, upper hemisphere.

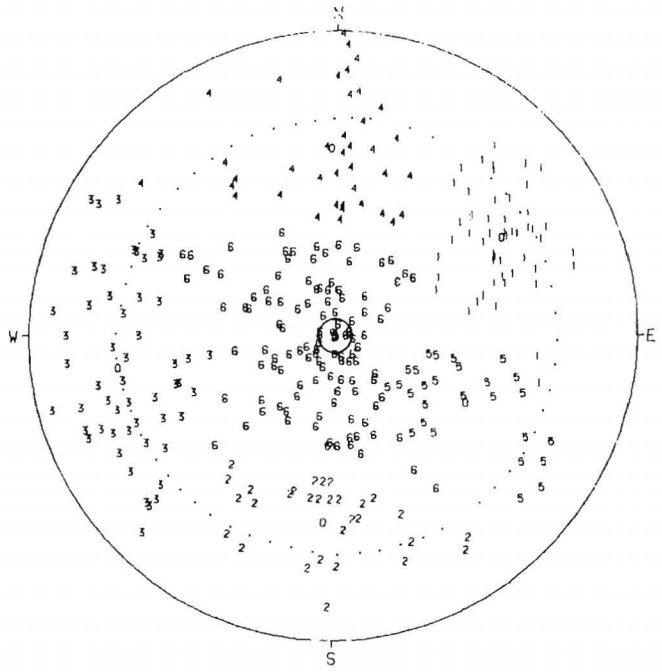

HOLE 5

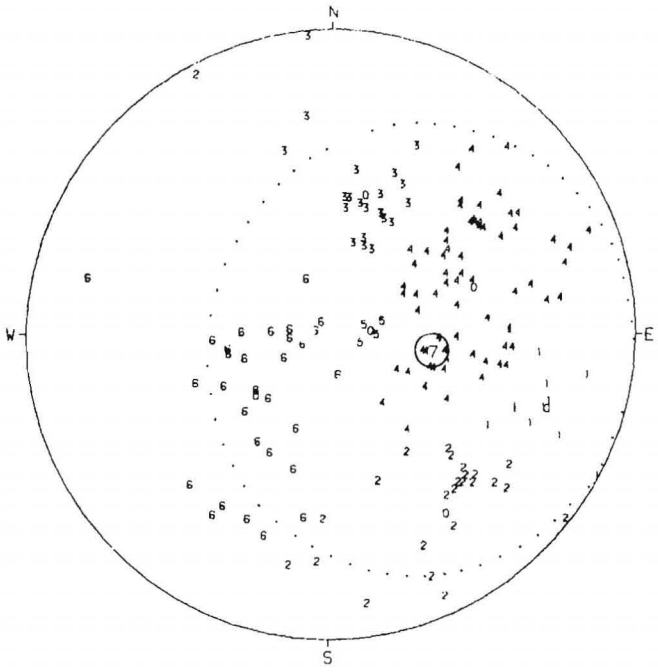

HOLE 7

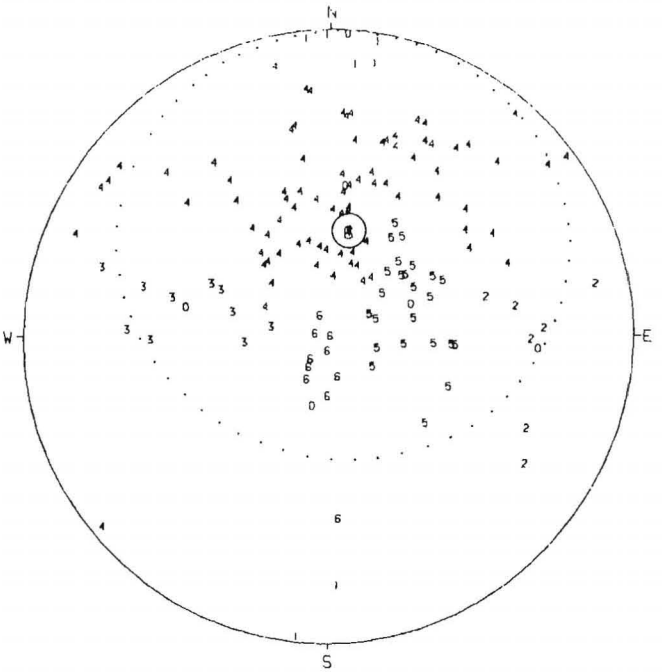

HOLE 6

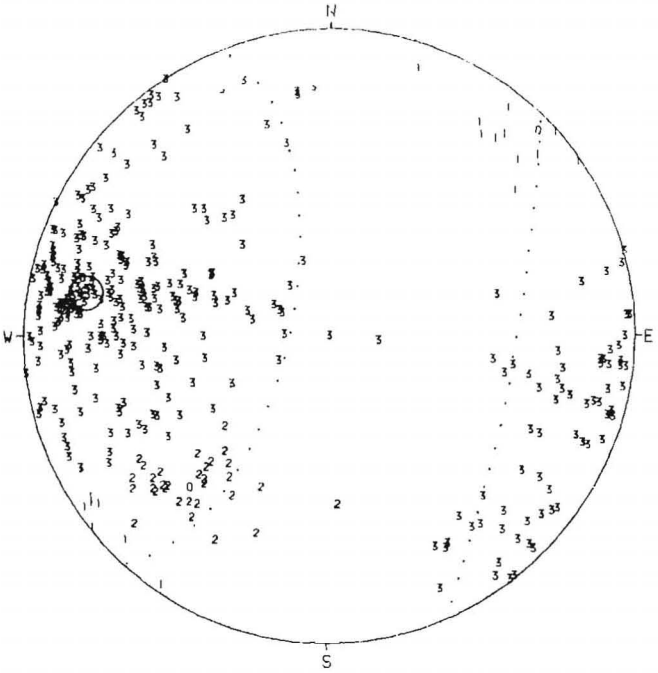

HOLE 8

FRACTAN r	Clusters					Eigenvalues		
	No.	Obs	Est	Dip	Az	W1	W2	W3
HOLE 5 (INCL –90)								
10.00	1	53	88	53	60	2	2	49
	2	30	49	52	183	1	2	27
	3	55	113	61	261	2	6	47
	4	39	62	51	358	2	3	34
	5	27	35	40	117	1	2	24
	6	118	119	5	244	5	10	103
HOLE 6 (INCL –62, AZ 190)								
10.50	1	7	14	89	3	0	0	7
	2	7	14	58	94	0	1	6
	3	10	15	40	282	0	1	9
	4	85	87	41	6	6	12	67
	5	24	27	23	69	0	1	23
	6	10	13	9	194	0	1	9

FRACTAN r	Clusters					Eigenvalues		
	No.	Obs	Est	Dip	Az	W1	W2	W3
HOLE 7 (INCL –62, AZ 280)								
10.00	1	10	12	64	109	0	0	10
	2	25	34	59	147	1	2	22
	3	22	31	38	14	0	1	20
	4	69	74	41	72	2	6	60
	5	4	4	11	86	0	0	4
	6	30	43	26	230	2	3	25
HOLE 8 (INCL –20, AZ 100)								
11.00	1	19	37	85	46	0	1	18
	2	32	52	57	223	0	1	30
	3	303	304	72	283	30	48	225

FIGURE 53.—Henderson Mine oriented core, holes 5, 6, 7, and 8, polar equal-area plots, upper hemisphere.

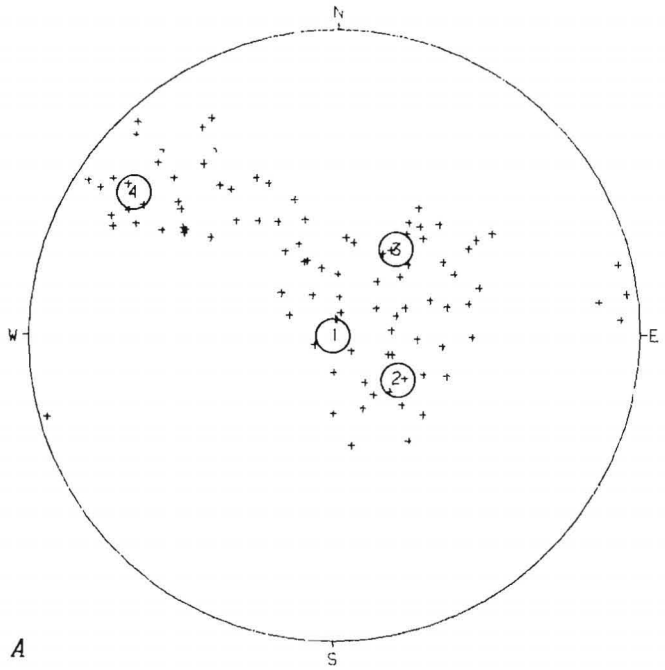

A

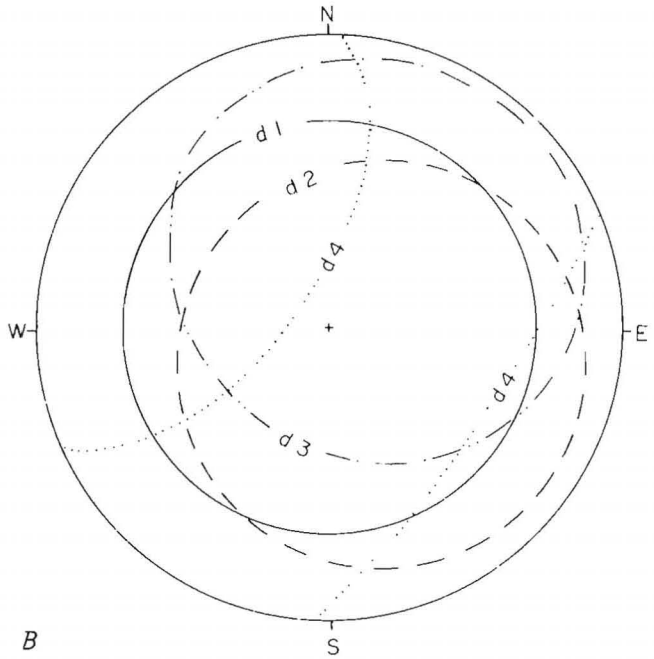

B

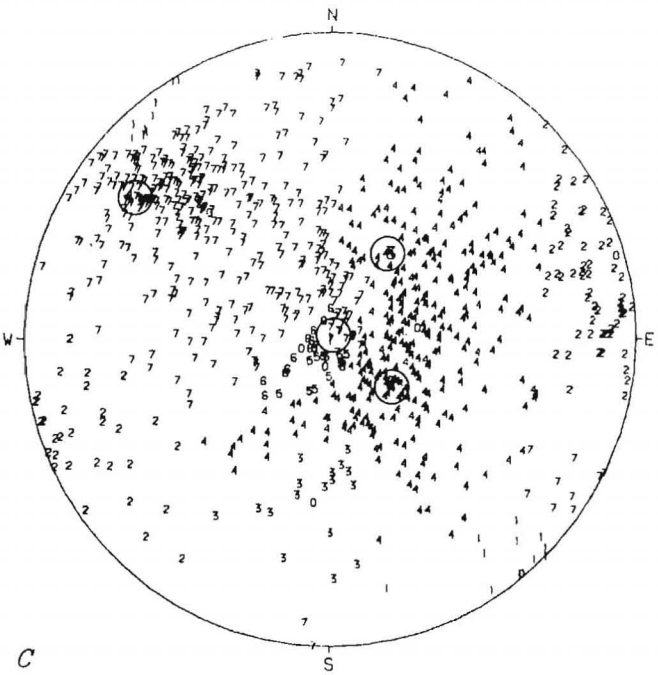

C

FRACTAN r	Clusters				Eigenvalues		
	No.	Obs	Dip	Az	W1	W2	W3
HOLES 1+2+3+4 POOLED							
8.50	1	22	89	141	0	1	21
	2	97	87	74	3	7	86
	3	17	45	186	0	1	16
	4	331	23	83	18	53	260
	5	15	8	191	0	0	15
	6	12	8	251	0	0	12
	7	400	48	316	25	64	311

FIGURE 54.—Henderson Mine oriented core, pooled holes 1 + 2 + 3 + 4, polar equal-area plots, upper hemisphere. *A*, Dense points determined by FRACTAN cluster solution; *B*, 60° cones about the four drill hole axes; *C*, numerals corresponding to the cluster numbers denote the poles of the joint planes.

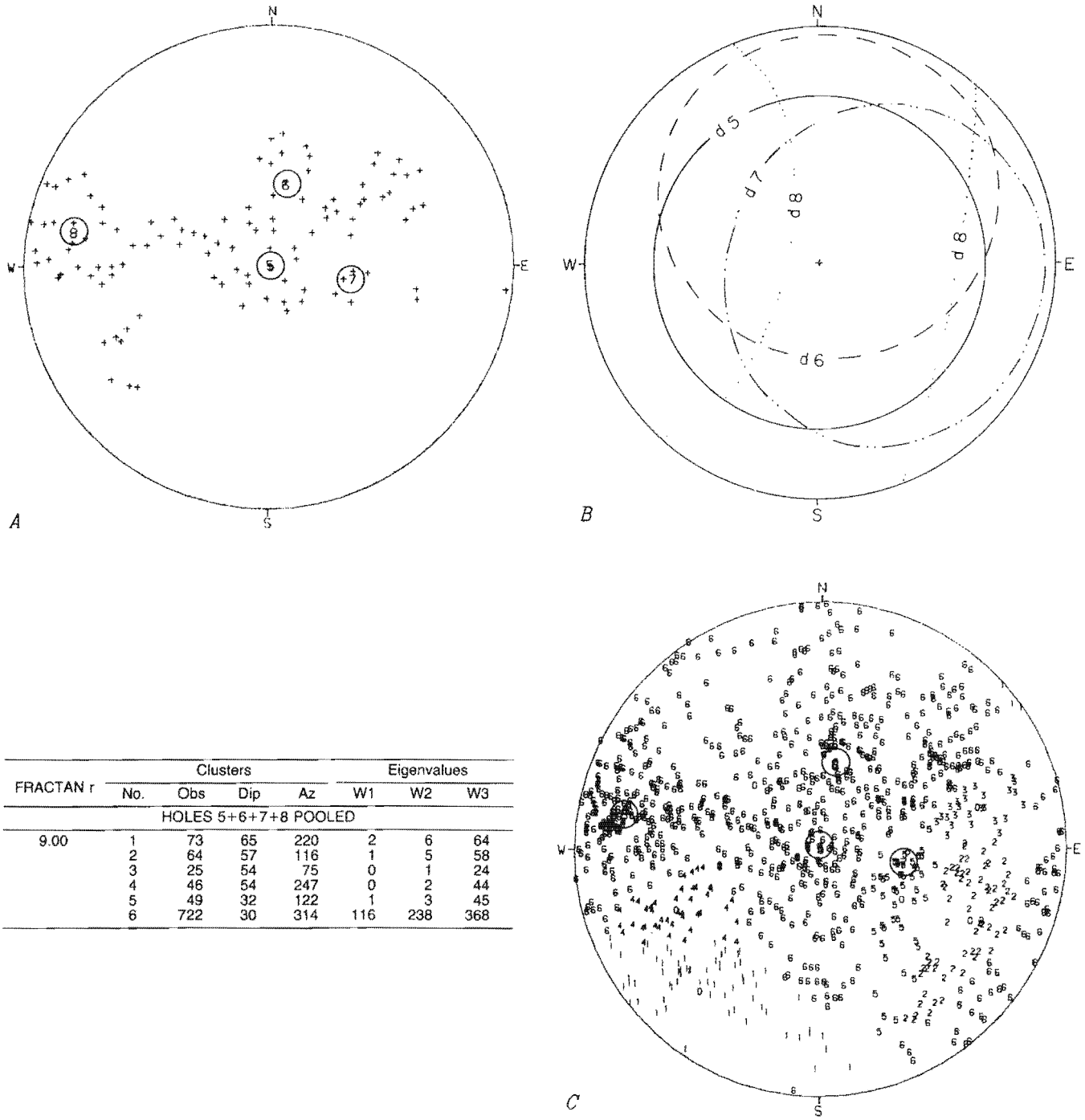

FRACTAN r	Clusters				Eigenvalues		
	No.	Obs	Dip	Az	W1	W2	W3
HOLES 5+6+7+8 POOLED							
9.00	1	73	65	220	2	6	64
	2	64	57	116	1	5	58
	3	25	54	75	0	1	24
	4	46	54	247	0	2	44
	5	49	32	122	1	3	45
	6	722	30	314	116	238	368

FIGURE 55.—Henderson Mine oriented core, pooled holes 5 + 6 + 7 + 8, polar equal-area plots, upper hemisphere. *A*, Dense points determined by FRACTAN cluster solution; *B*, 60° cones about the four drill hole axes; *C*, numerals corresponding to the cluster numbers denote the poles of the joint planes.

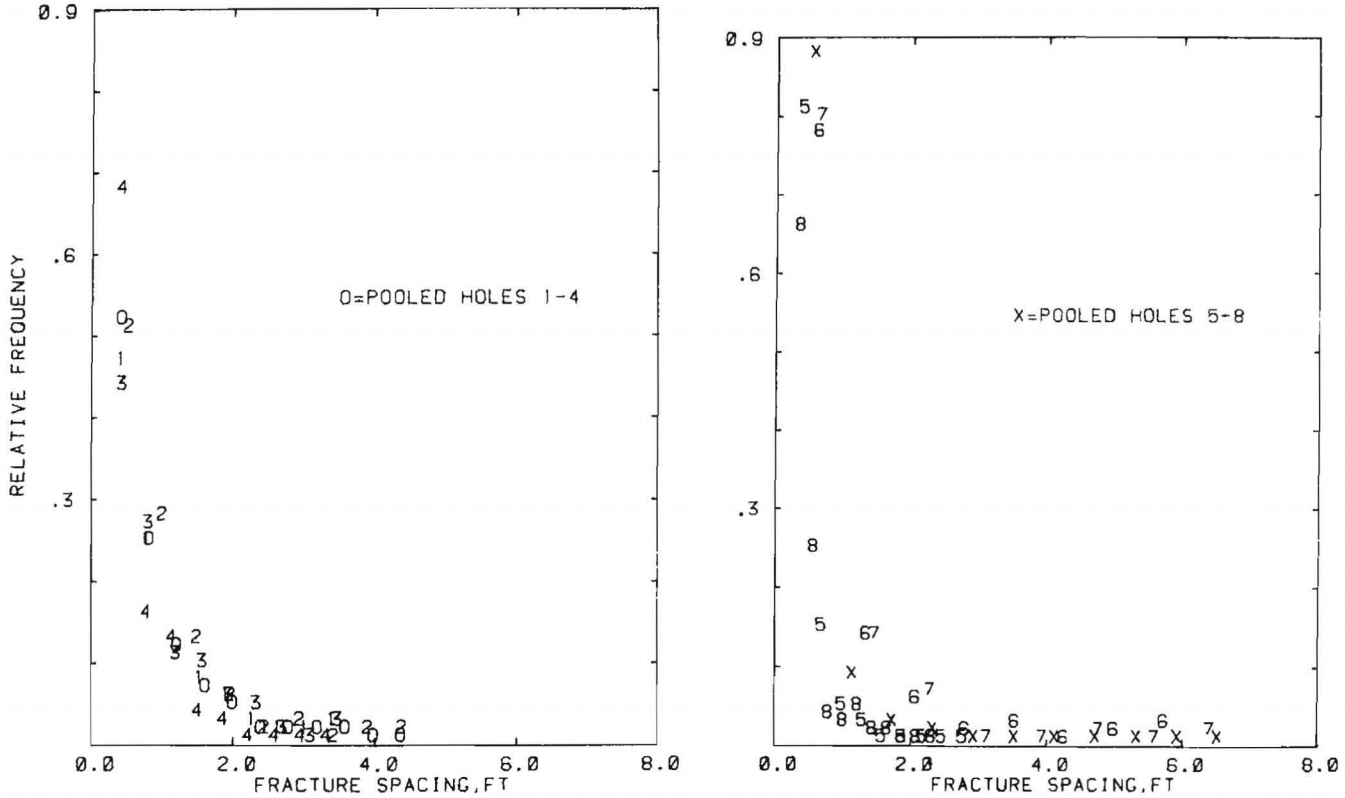

Drill hole	1	2	3	4	Pooled 1 to 4	Pooled 5 to 8	5	6	7	8
Spacings observed	187	178	175	233	773	740	249	118	116	257
Maximum ft	3.50	4.50	3.58	3.42	4.50	6.75	2.83	6.00	6.75	2.33
Minimum ft	0.17	0.17	0.17	0.17	0.17	0.17	0.17	0.17	0.17	0.17
Arithmetic mean ft	0.80	0.84	0.85	0.54	0.74	0.48	0.36	0.76	0.69	0.38
Median ft	0.58	0.63	0.67	0.42	0.50	0.33	0.25	0.42	0.42	0.25
Mode ft	ND	0.25	0.25	0.25	0.25	0.25	0.25	0.17	ND	0.25
Std dev ft	0.66	0.75	0.71	0.44	0.65	0.59	0.28	1.00	0.84	0.29
Skewness	1.74	2.32	1.61	2.40	2.13	5.74	3.92	3.51	4.37	2.77
Mean log of spacing	−0.51	−0.49	−0.47	−0.88	−0.61	−1.03	−1.20	−0.72	−0.74	−1.15
Std dev of logs	0.77	0.79	0.81	0.68	0.78	0.69	0.55	0.86	0.79	0.57
Distributions[1]	L,E	L,E	L,E	None	L	None	E	χ	L,E,χ	None
Best fit	E	L	E	E	L	χ	E	χ	χ	E

ND No appropriate value was determinable.
[1]Acceptable fit at the 5-pct significance level (L = lognormal, E = exponential, χ = chi squared).

FIGURE 56.—Henderson Mine oriented core, GDIST analyses of the spacing between successive fractures as measured along drill core. Relative frequency (spacings in each class ÷ total spacings) is plotted at the midpoint of the corresponding class interval; the numeral indicating the drill hole number is centered on the plotted point. Below the histograms are listed the parameters of the distributions.

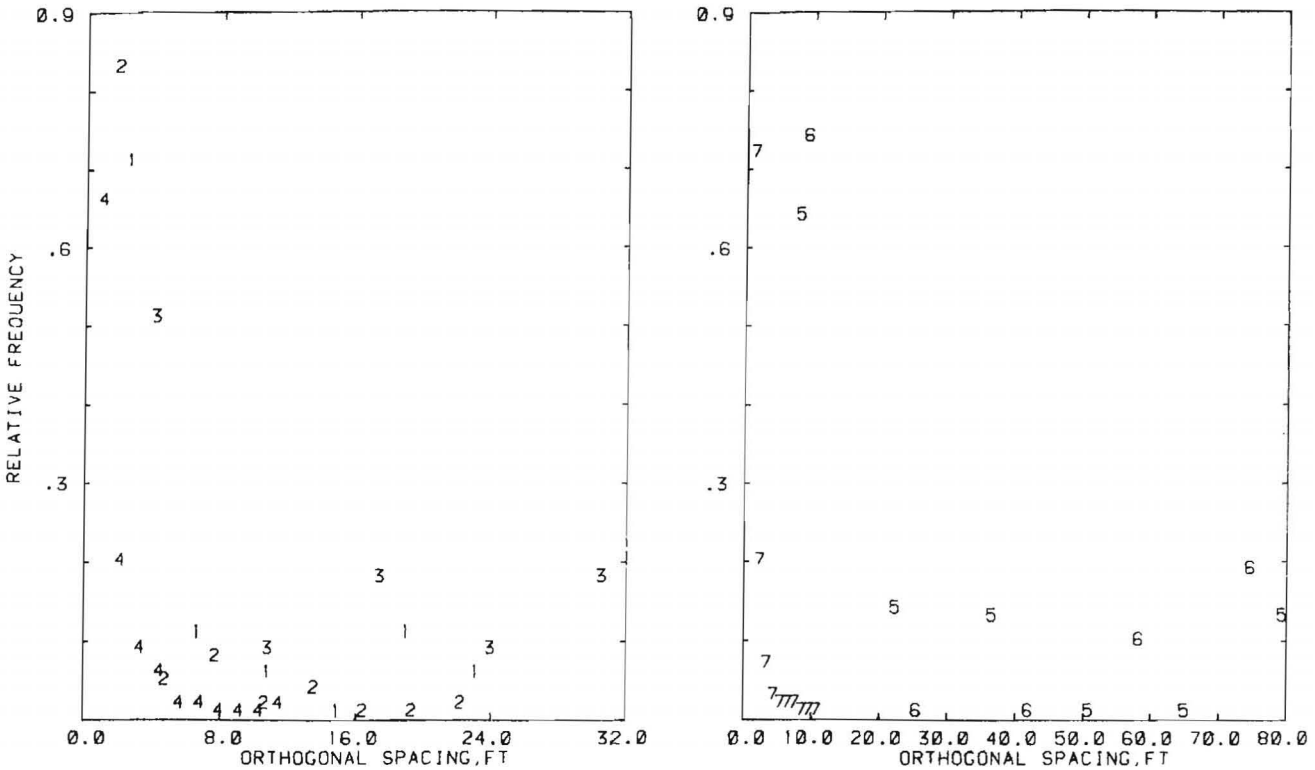

	Pooled holes 1+2+3+4						
Cluster	1	2	3	4	5	6	7
Spacings observed	20	67	12	306	16	11	330
Maximum ft	24.86	23.38	33.55	11.74	85.58	81.99	10.60
Minimum ft	0.24	0.18	0.64	0.15	0.31	0.30	0.16
Arithmetic mean ft	5.09	2.36	12.18	1.37	20.71	22.75	1.09
Median ft	2.44	0.88	7.21	0.91	11.61	5.86	0.61
Mode ft	ND	0.18	ND	0.16	ND	ND	0.16
Std dev ft	7.02	3.95	11.95	1.46	26.49	30.94	1.28
Skewness	1.72	3.26	0.68	3.00	1.68	1.10	3.20
Mean log of spacing	0.73	0.01	1.80	–0.11	2.10	1.93	–0.39
Std dev of logs	1.44	1.25	1.44	0.93	1.68	1.84	0.94
Distributions[1]	None	None	E	L,E,χ	L	None	L,χ
Best fit	L	L	E	χ	L	L	L

ND No appropriate value was determinable.
[1]Acceptable fit at the 5-pct significance level (L = lognormal, E = exponential, χ = chi squared).

FIGURE 57.—Henderson Mine oriented core, GDIST analyses of orthogonal fracture spacing within fracture families, pooled drill holes 1 + 2 + 3 + 4. Relative frequency (spacings in each class ÷ total spacings) is plotted at the midpoint of the corresponding class interval; the numeral indicating the cluster number is centered on the plotted point. Below the histograms are listed the parameters of the distributions.

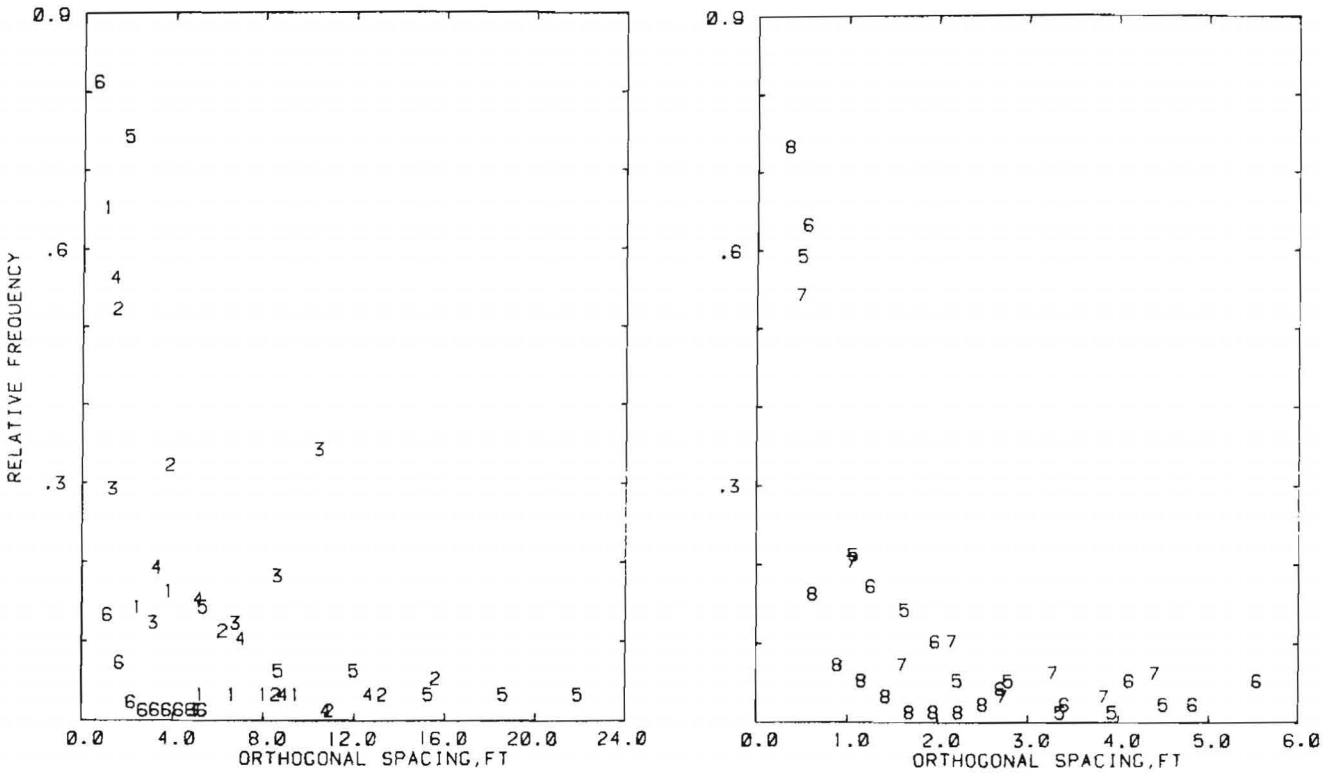

	Pooled holes 5+6+7+8						Hole 5	Hole 6	Hole 7	Hole 8
Cluster	1	2	3	4	5	6	6	4	4	3
Spacings observed	53	51	18	44	63	466	104	76	64	217
Maximum ft	9.89	16.53	11.11	13.34	23.32	5.39	4.73	5.85	4.62	2.58
Minimum ft	0.16	0.18	0.22	0.29	0.17	0.15	0.16	0.16	0.16	0.16
Arithmetic mean ft	1.79	3.24	6.24	2.84	3.22	0.54	0.84	1.14	1.15	0.42
Median ft	0.91	2.23	7.59	1.58	1.30	0.35	0.58	0.57	0.70	0.33
Mode ft	0.24	0.22	ND	ND	1.55	0.22	0.25	0.17	0.39	0.25
Std dev ft	2.05	3.52	4.10	2.72	4.59	0.58	0.77	1.38	1.16	0.34
Skewness	1.88	2.13	–0.33	1.69	2.37	4.42	2.01	2.10	1.66	2.95
Mean log of spacing	–0.03	0.60	1.38	0.60	0.36	–0.92	–0.53	–0.41	–0.29	–1.07
Std dev of logs	1.15	1.19	1.23	0.99	1.28	0.69	0.85	1.01	0.92	0.60
Distributions[1]	L,E,χ	L,E,χ	U	N,L,E,χ	L	None	L,E	L,χ	L,E,χ	None
Best fit	χ	χ	U	E	L	χ	E	χ	χ	E

ND = No appropriate value was determinable.
[1]Acceptable fit at the 5-pct significance level (N = normal, L = lognormal, E = exponential, χ = chi squared, U = uniform).

FIGURE 58.—Henderson Mine oriented core, GDIST analyses of orthogonal fracture spacing within fracture families, drill holes 5 to 8. Relative frequency (spacings in each class ÷ total spacings) is plotted at the midpoint of the corresponding class interval. Left, Pooled holes 5 to 8; the numeral indicating the cluster number is centered on the plotted point. Right, Selected clusters in individual holes; the plotted numeral is the hole number. Below the histograms are listed the parameters of the distributions.

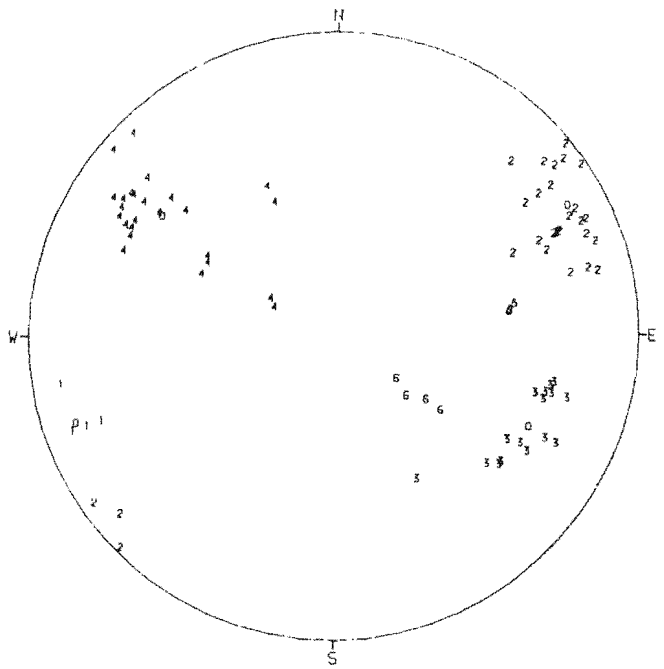

SITE 1

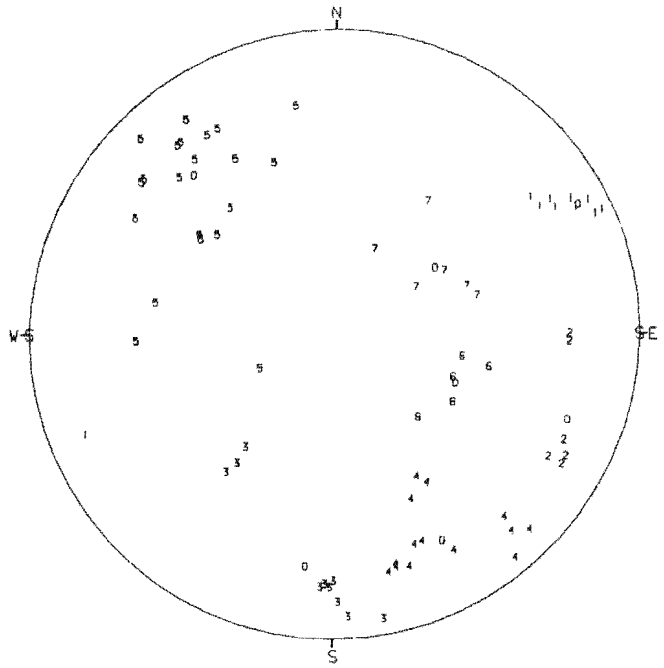

SITE 3

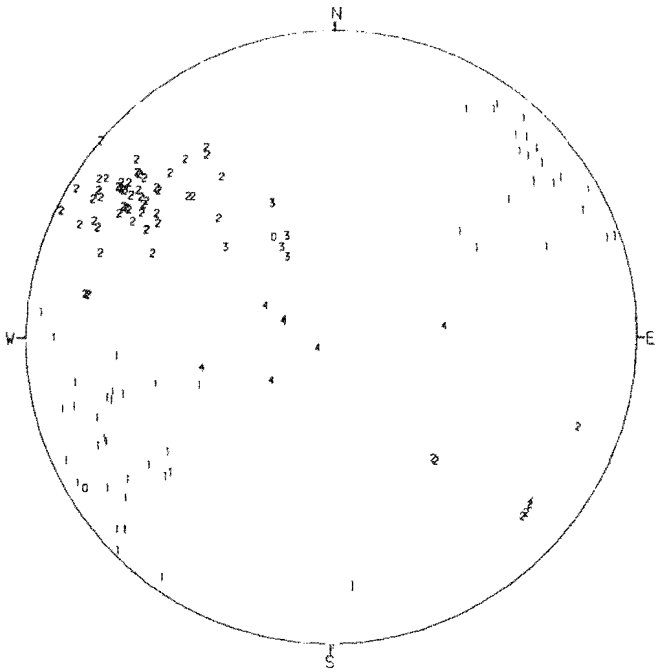

SITE 2

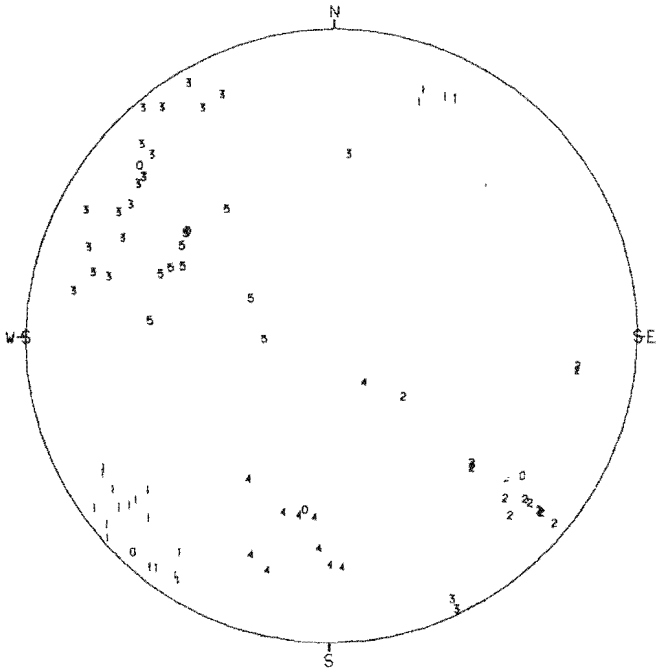

SITE 4

FRACTAN r	Clusters				Eigenvalues		
	No.	Obs	Dip	Az	W1	W2	W3
			SITE 1				
12.50	1	8	78	251	0	0	8
	2	30	76	61	1	1	28
	3	17	60	115	0	1	16
	4	33	59	305	1	3	29
	5	6	48	82	0	0	6
	6	6	27	126	0	0	6
			SITE 2				
11.00	1	57	84	238	3	8	46
	2	65	73	305	1	5	59
	3	6	32	329	0	0	6
	4	11	12	267	0	1	10

FRACTAN r	Clusters				Eigenvalues		
	No.	Obs	Dip	Az	W1	W2	W3
			SITE 3				
14.50	1	11	79	62	0	0	11
	2	7	70	111	0	0	7
	3	10	66	187	0	1	9
	4	14	66	152	0	1	13
	5	26	59	318	1	2	23
	6	6	35	112	0	0	6
	7	8	32	57	0	0	8
			SITE 4				
15.00	1	21	85	222	0	2	19
	2	13	67	126	0	1	12
	3	25	73	311	1	2	22
	4	15	48	188	0	2	13
	5	10	42	297	0	0	10

FIGURE 59.—Henderson Mine scanline mapping, sites 1, 2, 3, and 4, polar equal-area plots, upper hemisphere.

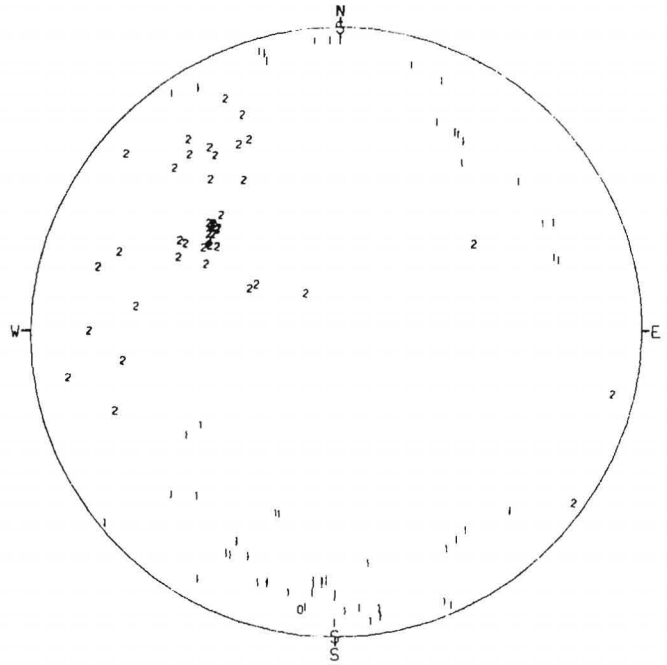

SITE 5

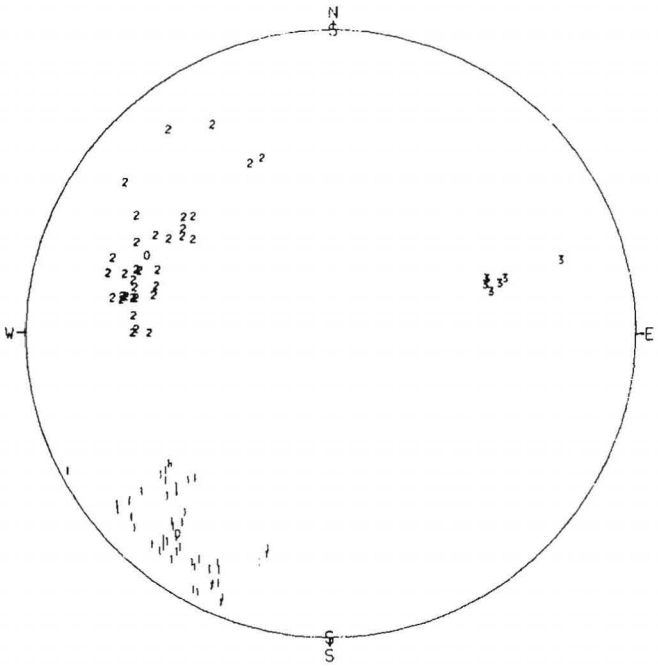

SITE 7

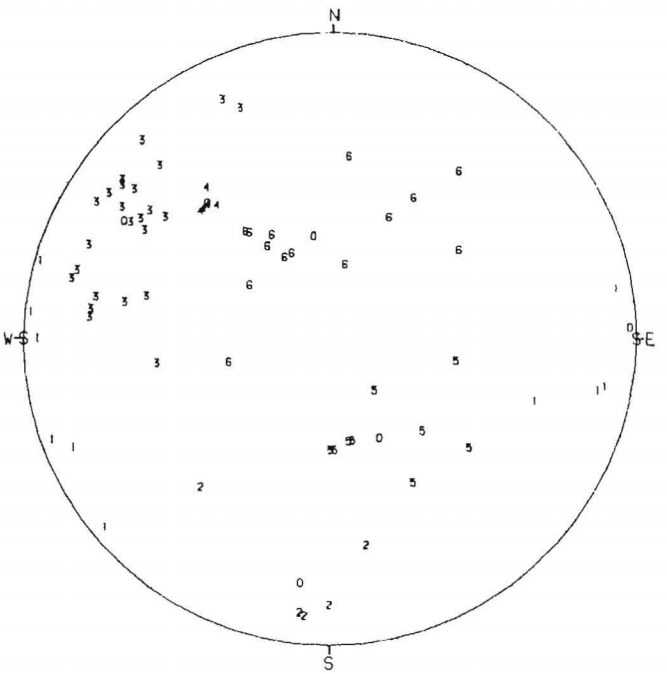

SITE 6

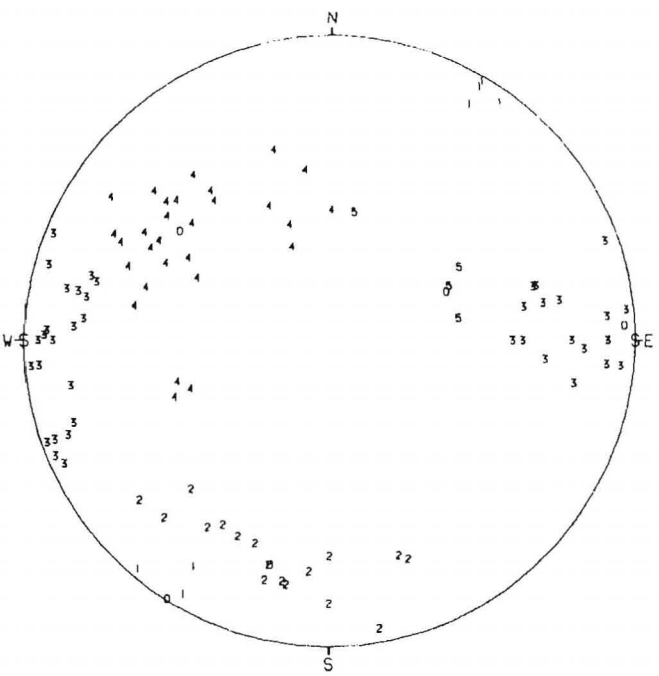

SITE 8

FRACTAN r	Clusters				Eigenvalues		
	No.	Obs	Dip	Az	W1	W2	W3
			SITE 5				
12.50	1	65	81	187	6	11	48
	2	47	51	306	3	5	39
			SITE 6				
11.00	1	11	88	88	0	1	10
	2	5	69	187	0	0	5
	3	26	67	299	0	2	24
	4	5	50	317	0	0	5
	5	11	30	154	0	1	10
	6	15	28	350	0	2	13

FRACTAN r	Clusters				Eigenvalues		
	No.	Obs	Dip	Az	W1	W2	W3
			SITE 7				
12.50	1	54	72	217	1	2	51
	2	35	56	293	0	2	33
	3	9	48	73	0	0	9
			SITE 8				
13.00	1	10	89	212	0	0	10
	2	20	65	195	0	2	18
	3	50	86	87	2	4	44
	4	34	51	306	2	3	30
	5	7	34	67	0	0	7

FIGURE 60.—Henderson Mine scanline mapping, sites 5, 6, 7, and 8, polar equal-area plots, upper hemisphere.

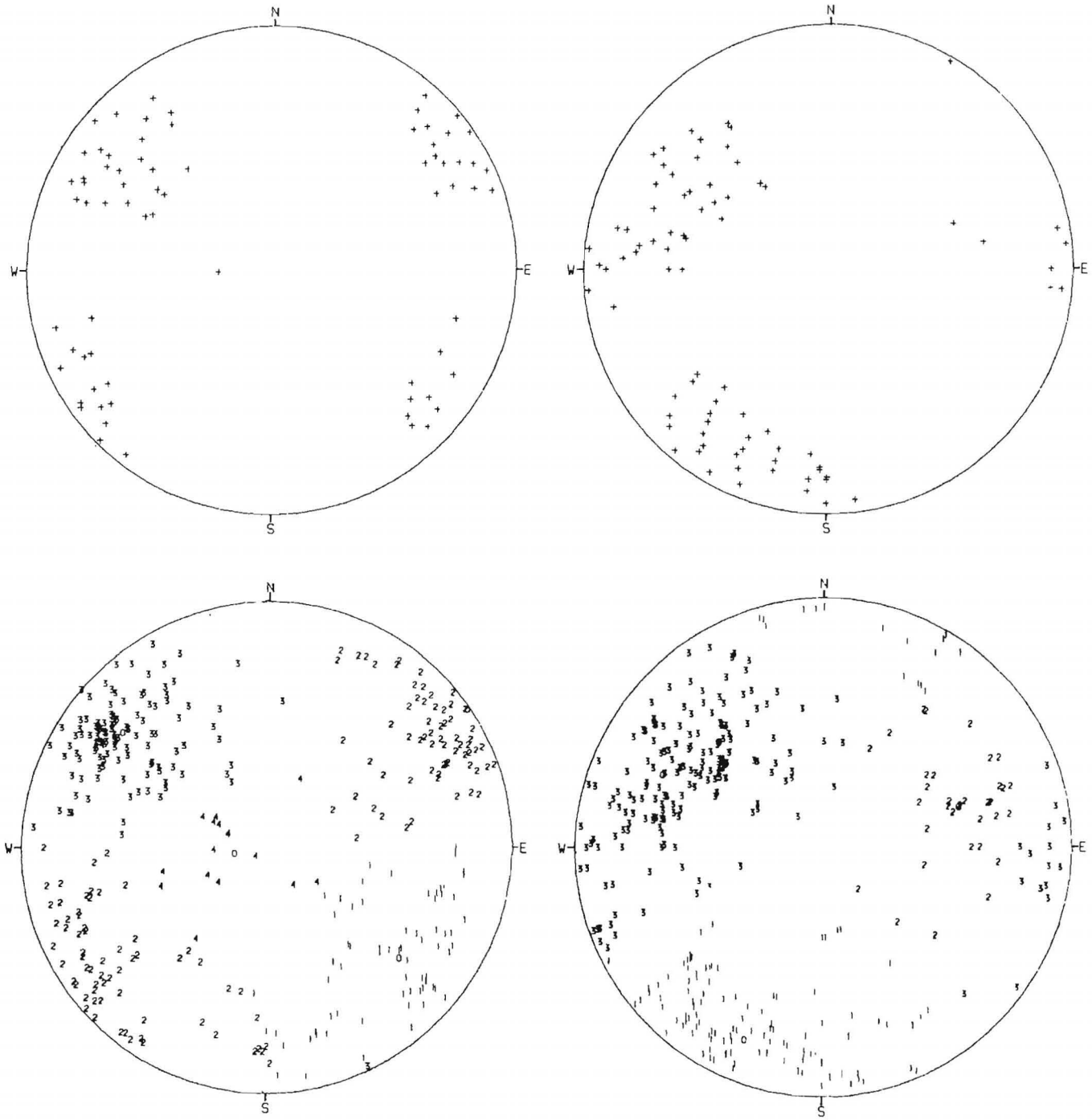

FRACTAN r	Clusters				Eigenvalues		
	No.	Obs	Dip	Az	W1	W2	W3
	POOLED SITES 1+2+3+4						
11.50	1	76	60	130	5	8	63
	2	155	89	55	12	25	118
	3	149	65	308	6	8	135
	4	25	11	260	1	1	23

FRACTAN r	Clusters				Eigenvalues		
	No.	Obs	Dip	Az	W1	W2	W3
	POOLED SITES 5+6+7+8						
13.00	1	152	72	202	11	16	125
	2	39	47	74	2	3	34
	3	213	60	294	13	36	164

FIGURE 61.—Henderson Mine scanline mapping, pooled sites 1 + 2 + 3 + 4 (left) and 5 + 6 + 7 + 8 (right), polar equal-area plots, upper hemisphere. Top, Dense points determined by FRACTAN cluster solution; bottom, numerals corresponding to the cluster numbers denote the poles of the joint planes.

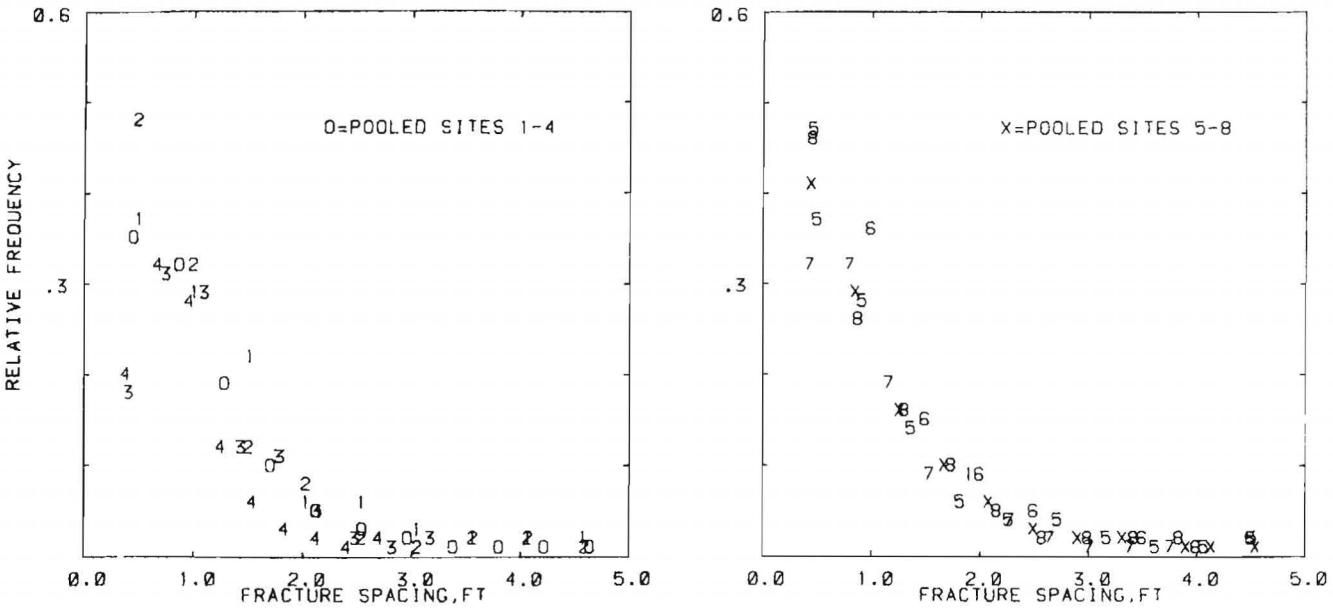

Scanline mapping site	1	2	3	4	Pooled 1 to 4	Pooled 5 to 8	5	6	7	8
Spacings observed	166	247	166	201	780	887	261	162	265	199
Maximum ft	4.80	4.80	3.30	2.80	4.80	4.70	4.70	4.70	3.90	4.00
Minimum ft	0.20	0.20	0.20	0.20	0.20	0.20	0.20	0.20	0.20	0.20
Arithmetic mean ft	1.14	0.96	0.98	0.82	0.97	0.93	0.91	1.07	0.91	0.88
Median ft	1.00	0.80	0.90	0.70	0.80	0.80	0.70	0.90	0.80	0.70
Mode ft	0.70	0.60	1.10	0.50	0.70	0.70	0.20	0.80	0.70	0.30
Std dev ft	0.76	0.68	0.51	0.47	0.63	0.66	0.73	0.68	0.58	0.61
Skewness	1.56	2.19	0.98	1.44	1.89	1.76	2.06	1.67	1.26	1.67
Mean log of spacing	−0.09	−0.24	−0.16	−0.35	−0.22	−0.30	−0.37	−0.13	−0.30	−0.35
Std dev of logs	0.69	0.64	0.58	0.58	0.63	0.70	0.75	0.64	0.67	0.68
Distributions[1]	L,E	L,E	L	L	L	L	L,E	L,E	L,E	L
Best fit	L	L	L	L	L	L	L	L	E	L

[1] Acceptable fit at the 5-pct significance level (L = lognormal, E = exponential).

FIGURE 62.—Henderson Mine scanline mapping, GDIST analyses of the spacing between successive fractures as measured along scanlines. Relative frequency (spacings in each class ÷ total spacings) is plotted at the midpoint of the corresponding class interval; the numeral indicating the site number is centered on the plotted point. Below the histograms are listed the parameters of the distributions.

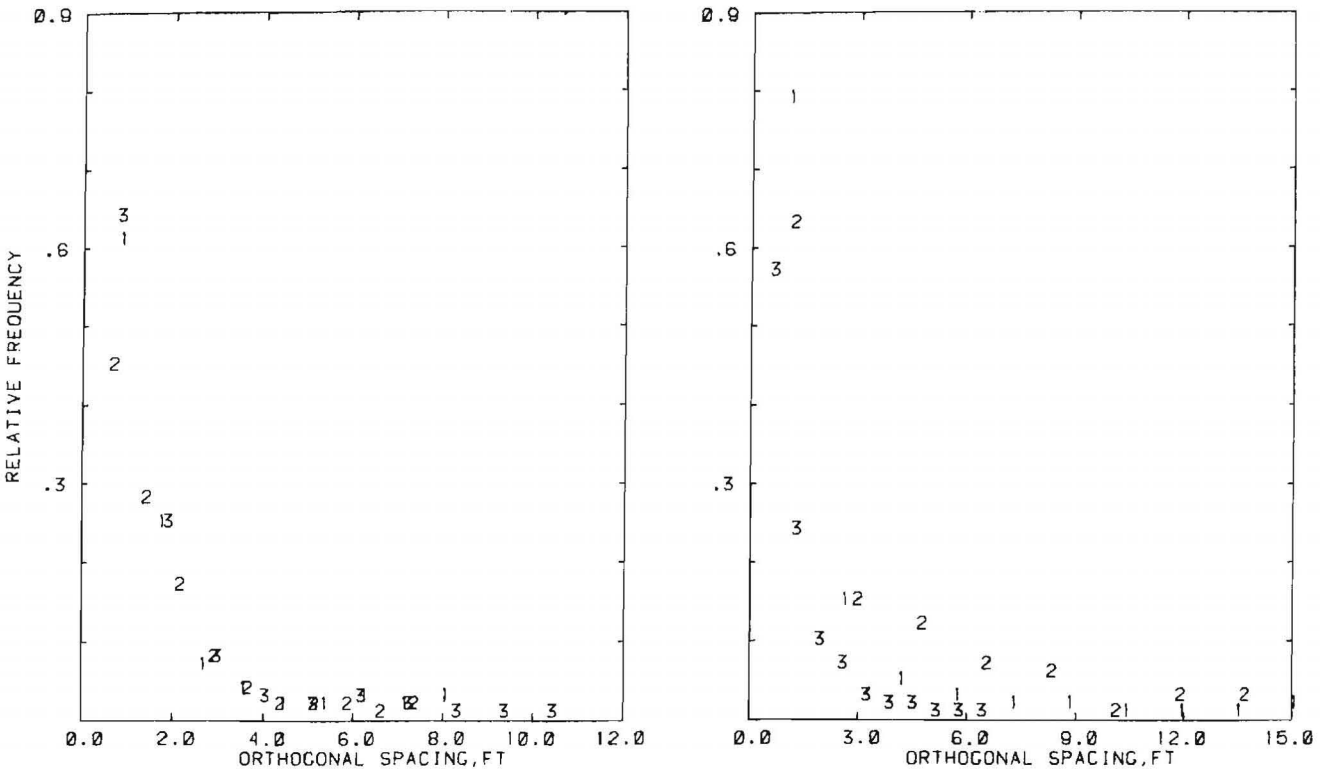

Cluster	Pooled sites 1 to 4			Pooled sites 5 to 8		
	1	2	3	1	2	3
Spacings observed	176	305	298	320	65	434
Maximum ft	8.40	7.62	10.86	15.72	14.45	6.63
Minimum ft	0.33	0.23	0.22	0.21	0.21	0.22
Arithmetic mean ft	1.49	1.43	1.40	1.38	2.58	1.05
Median ft	0.98	1.09	1.01	0.79	1.32	0.77
Mode ft	0.66	0.57	ND	0.62	ND	0.32
Std dev ft	1.50	1.17	1.39	1.82	2.89	0.91
Skewness	2.65	2.26	2.89	4.27	1.97	2.18
Mean log of spacing	0.09	0.09	0.01	−0.14	0.41	−0.25
Std dev of logs	0.72	0.72	0.79	0.90	1.06	0.77
Distributions[1]	None	L,E	None	L,χ	L,E,χ	L,E
Best fit	χ	L	χ	L	E	L

ND = No appropriate value was determinable.
[1] Acceptable fit at the 5-pct significance level (L = lognormal, E = exponential, χ = chi squared).

FIGURE 63.—Henderson Mine scanline mapping, GDIST analyses of orthogonal fracture spacing within fracture families. Left, Pooled sites 1 to 4; right, pooled sites 5 to 8. Relative frequency (spacings in each class ÷ total spacings) is plotted at the midpoint of the corresponding class interval; the numeral indicating the cluster number is centered on the plotted point. Cluster with fewer than 10 observations is omitted. Below the histograms are listed the parameters of the distributions.

DISCUSSION

Acquisition of fracture data by the two methods, oriented core logging and scanline mapping on exposures, facilitates the interpretation and validation of the results achieved by both methods, including the procedures for data analysis. After attempting to identify cluster orientations from the polar equal-area plots of data from individual drill holes or mapping sites, and comparing such estimates with the computed results, one quickly becomes aware of the advantages of processing orientation data by a computer code such as FRACTAN. This is particularly true for the three study mines, where the fracture families are so numerous and the scatter within each family so great that a numerical procedure for finding the mean axes of the fracture plane clusters is not merely desirable for convenience, reliability, and objectivity, but is indispensable for detecting the subtle differences in densities of the pole points. One may nevertheless retain some reservations as to the real existence of some of the fracture families. One's confidence increases when the same analysis procedures indicate the presence of essentially the same cluster orientations in oriented core as in scanline mapping in the same areas, which is found herein for the three study mines.

To include the fracture measurements from more areas of a mine can be expected to increase the number of fracture families that are identified in a given pooling of data, but since the ultimate objective of these studies is to predict the caving of an undercut rock mass, which is assured if each unit volume is sufficiently weak, the more important parameter is the number of fracture families that exist within each increment of volume. The present study indicates that at each of the three mines either three or four (on the average) of the correlatable fracture families are identified in every drill hole and at every scanline mapping site, which represent volume increments on the order of 50 to 100 ft in diameter.

One can, to a degree, judge the prominence of a fracture family by the number of observations of members of that family relative to those of other families in the same set of data. A more exact approach is to compare orthogonal spacings. The median values of the orthogonal spacings over all fracture families are about 1.1, 1.2, and 0.9 ft respectively for Lakeshore, San Manuel, and Henderson, considering all results from core logging and scanline mapping. The orthogonal spacings depend on the selected fracture partitions, which are nonuniform in that no limit is imposed on the angular disperson for inclusion of a fracture in any given family, and hence a systematic relationship is not observed between the magnitude of orthogonal spacing for drill core and that for scanline mapping.

The spacing between successive fractures along a reference line, however, which is not subject to the influence of the partition boundaries, is only half as great in the drill cores as along the scanlines, which indicates that a large proportion of the breaks in drill core are the result of the drilling process, i.e., are not preexisting fractures. The spacing of fractures along a drill core apparently depends therefore on the strength of the rock mass, the core diameter, and the drilling conditions, as well as on the preexisting fractures. Median values of fracture spacing are 0.28, 0.32, and 0.41 ft respectively for the Lakeshore, San Manuel, and Henderson Mines; median values of fracture trace length, by cluster, are 1.1, 3.8, and 3.8 ft respectively.

The two methods, logging of oriented core and mapping along scanlines, produce essentially the same results as to fracture orientations. Fracture spacing in drill cores appears to be a complex factor, not a direct index of preexisting fractures in the rock mass. The multiple-scanline scheme, utilized in 20- to 50-ft sections, produces viable results for characterizing the orientation, spacing, and trace length of fractures.

REFERENCES

1. Alldredge, J. R., and D. D. Bolstad. GDIST: A Computer Code for Analysis of Statistical Distributions of Physical Data. BuMines IC 8731, 1977, 57 pp.

2. Baecher, G. B., and N. A. Lanney. Trace Length Biases in Joint Surveys. Paper in Proceedings 19th U.S. Symposium on Rock Mechanics. Conferences & Institutes, Extended Programs and Continuing Education, 1978, pp. 56-65.

3. Barton, N., R. Lien, and J. Lunde. Engineering Classification of Rock Masses for the Design of Tunnel Support. Rock Mech., v. 6, No. 4, 1974, pp. 189-236.

4. Bieniawski, Z. T. Engineering Classifications of Jointed Rock Masses. Trans. S. Afr. Inst. Civil Eng., v. 15, No. 12, 1973, pp. 335-344.

5. Bolstad, D. D., and M. A. Mahtab. A Bureau of Mines Direct-Reading Azimuth Protractor. BuMines IC 8617, 1974, 7 pp.

6. Cohen, A. C. Progressively Censored Samples in Life Testing. Technometrics, v. 5, No. 3, Aug. 1963, p. 333.

7. Commission on Classification of Rocks and Rock Masses, International Society for Rock Mechanics. Basic Geotechnical Description of Rock Masses. Int. J. Rock Mech. and Min. Sci. & Geomech. Abstr., v. 18, 1981, pp. 85-110.

8. Dienes, J. K. On the Inference of Crack Statistics From Observations on an Outcropping. Paper in Proceedings 20th U.S. Symposium on Rock Mechanics. Center for Earth Sciences and Engineering, Univ. TX at Austin, 1979, pp. 259-263.

9. Einstein, H. H., G. B. Baecher, D. Veneziano, H. C. Chan, W. D. Dershowitz, E. F. Glynn, J. L. Galzi, N. A. Lanney, K. O'Reilly, W. S. Scull, and P. Yip. Risk Analysis for Rock Slopes in Open Pit Mines. Part I. Distributions of Rock Mass Properties (contract JO275015, MIT). BuMines OFR 46(1)-81, 1979, 200 pp.; NTIS PB 81-201592.

10. ———. Risk Analysis for Rock Slopes in Open Pit Mines. Part II. Limit Equilibrium Analysis for Rock Wedge Stability (contract JO275015, MIT). BuMines OFR 46(2)-81, 1979, 182 pp.; NTIS PB 81-201600.

11. ———. Risk Analysis for Rock Slopes in Open Pit Mines. Part III. Reliability Analysis of Rock Slope Stability (contract JO275015, MIT). BuMines OFR 46(3)-81, 1979, 354 pp.; NTIS PB 81-201618.

12. ———. Risk Analysis for Rock Slopes in Open Pit Mines. Part IV. Field Exploration To Determine Rock Mass Properties (contract JO275015, MIT). BuMines OFR 46(4)-81, 1979, 176 pp.; NTIS PB 81-201626.

13. ———. Risk Analysis for Rock Slopes in Open Pit Mines. Part V. Probabilistic Models of Jointed Rock Mass Deformation and Their Implications (contract JO275015, MIT). BuMines OFR 46(5)-81, 1979, 113 pp.; NTIS PB 81-201634.

14. ———. Risk Analysis for Rock Slopes in Open Pit Mines. Part VI. Executive Summary, Introduction and Technical Summary, Bibliography (contract JO275015, MIT). BuMines OFR 46(6)-81, 1979, 63 pp.; NTIS PB 81-201642.

15. ———. Risk Analysis for Rock Slopes in Open Pit Mines. Part VII. Appendices A Through M, Detailed Geologic Data Underlying Developments (contract JO275015, MIT). BuMines OFR 46(7)-81, 1979, 394 pp.; NTIS PB 81-201659.

16. ———. Risk Analysis for Rock Slopes in Open Pit Mines. Part VIII. Appendix UM, User's Manuals for Computer Programs (contract JO275015, MIT). BuMines OFR 46(8)-81, 1979, 453 pp.; NTIS PB 81-201667.

17. Epstein, B. Tests for the Validity of the Assumption That the Underlying Distribution of Life Is Exponential. Technometrics, v. 2, No. 1, Feb. 1960, p. 84.

18. Ewan, V. J., G. West, and J. Temporal. Reproducibility of Joint Spacing Measurements in Rock. Transport and Road Res. Lab., Crowthorne (England), 1981, 29 pp.; NTIS PB 82-135344.

19. Harper, H. E., and J. R. Reynolds. The Lakeshore Copper Deposit. Min. Congr. J., v. 55, No. 11, 1969, pp. 26-30.

20. Hudson, J. A., and S. D. Priest. Discontinuities and Rock Mass Geometry. Int. J. Rock Mech. and Min. Sci. & Geomech. Abstr., v. 16, 1979, pp. 339-362.

21. Jennings, J. E. A Mathematical Theory for the Calculation of the Stability of Slopes in Open Cast Mines. Ch. in Planning Open Pit Mines. A. A. Balkema, Amsterdam, 1970, pp. 87-102.

22. Kendorski, F. S., and M. A. Mahtab. Fracture Patterns and Anisotropy of San Manuel Quartz Monzonite. Bull. Assoc. Eng. Geol., v. 13, No. 1, 1976, pp. 23-52.

23. Kulhawy, F. H. Geomechanical Model for Rock Foundation Settlement. ASCE J., v. 104 (GT2), 1978, pp. 211-227.

24. Laubscher, D. H. Geomechanics Classification of Jointed Rock Masses—Mining Applications. Trans. IMM, sec. A, v. 86, 1977, pp. A1-A7.

25. Mahtab, M. A., D. D. Bolstad, and R. R. Pulse. Determination of Attitudes of Joints Surveyed With a Borescope in Inclined Boreholes. BuMines IC 8615, 1973, 12 pp.

26. Mahtab, M. A., and T. M. Yegulalp. A Rejection Criterion for Definition of Clusters in Orientation Data. Paper in Proceedings 23rd U.S. Symposium on Rock Mechanics, ed. by R. E. Goodman and F. E. Heuze. SME-AIME, 1982, pp. 116-123.

27. Panek, L. A. Comparative Cavability Studies at Three Mines. Ch. in Design and Operation of Caving and Sublevel Stoping Mines, ed. by D. R. Stewart. SME-AIME, 1981, pp. 99-106.

28. Panek, L. A., and W. J. Tesch. Monitoring Ground Movements Near Caving Stopes—Methods and Measurements. BuMines RI 8585, 1981, 108 pp.

29. Priest, S. D., and J. A. Hudson. Estimation of Discontinuity Spacing and Trace Length Using Scanline Surveys. Int. J. Rock Mech. and Min. Sci & Geomech. Abstr., v. 18, 1981, pp. 183-197.

30. Shanley, R. J., and M. A. Mahtab. FRACTAN: A Computer Code for Analysis of Clusters Defined on the Unit Hemisphere. BuMines IC 8671, 1975, 49 pp.

31. Terzaghi, R. D. Sources of Error in Joint Surveys. Geotechnique, v. 15, 1965, pp. 287-304.

32. Thomas, L. A. Geology of the San Manuel Ore Body. Ch. in Geology of the Porphyry Copper Deposits—Southwestern North America, ed. by S. R. Titley and C. L. Hicks. Univ. AZ Press, 1966, pp. 133-142.

33. Turner, F. J., and L. E. Weiss. Structural Analysis of Metamorphic Tectonites. McGraw-Hill, 1963, 545 pp.

34. Wallace, S. R., W. B. MacKenzie, R. G. Blair, and N. K. Muncaster. Geology of the Urad and Henderson Molybdenite Deposits, Clear Creek County, Colorado. Econ. Geol., v. 73, No. 3, 1978, pp. 325-368.

35. Watson, G. S. The Statistics of Orientation Data. J. Geol., v. 74, No. 5, pt. 2, 1966, pp. 786-797.

36. Wilson, E. D. Geologic Factors Related to Block Caving at San Manuel Copper Mine, Pinal County, Ariz. Progress Report, April 1954-March 1956. BuMines RI 5336, 1957, 78 pp.

37. ———. Geologic Factors Related to Block Caving at San Manuel Copper Mine, Pinal County, Ariz. Progress Report. April 1956-March 1958. BuMines RI 5561, 1960, 43 pp.

INT.-BU.OF MINES,PGH.,PA. 28426

U.S. GOVERNMENT PRINTING OFFICE: 1987 - 605-017 60020